

Sulfur on Mars from the Atmosphere to the Core

Heather B. Franz¹, Penelope L. King², and Fabrice Gaillard³

¹NASA Goddard Space Flight Center, Greenbelt, MD 20771, USA

²Research School of Earth Sciences, Australian National University, Canberra ACT 2601, Australia

³CNRS-Université d'Orléans, ISTO, la rue de la Ferrollerie, 45071 Orléans, France

Abstract

Observations of the martian surface from orbiting spacecraft and *in situ* landers and rovers, as well as analyses of martian meteorites in terrestrial laboratories, have consistently indicated that Mars is a sulfur-rich planet. The global inventory of sulfur, from the atmosphere to the core, carries widespread implications of potential geophysical, geochemical, climatological, and astrobiological significance. For example, the sulfur content of the core carries implications for core density; the speciation of igneous sulfur minerals reflects the oxidation state of the magma from which they formed; sulfur-bearing gases may have exerted control on the temperatures at the surface of early Mars; and the widespread availability of sulfur on Mars would have provided an abundant source for energy and nutrients to fuel sulfur-metabolizing microbes, such as those that arose during the emergence of primitive life on Earth. Here we provide an overview of martian sulfur and its relevance to these areas of interest, including a discussion of analytical techniques and results acquired by space missions and meteorite analyses to date. We review current studies modeling the potential effects of sulfur-bearing gases on the past martian climate and possible constraints on atmospheric composition implied by sulfur isotopic data. We also explore the importance of sulfur to the search for extinct or extant life on Mars. Finally, we summarize a few areas of interest to future work, including advances in space exploration technology and preparation for Mars sample return.

1. Introduction

1.1. The prevalence of sulfur on Mars

The widespread occurrence of sulfur on Mars was first noted by the Viking mission (Baird et al., 1976; Clark et al., 1976; Clark et al., 1977; Toulmin et al., 1977). Since that time, the ubiquitous nature of martian sulfur has been confirmed through *in situ* measurements by subsequent rovers and landers, remote sensing observations by orbiting spacecraft, and analyses of martian meteorites in terrestrial laboratories. These observations all point to a higher abundance of sulfur on the surface of Mars than on present-day Earth, leading to suggestions that the geochemical history of the martian surface may have been dominated by the sulfur cycle, analogous to the manner in which the carbon cycle dominates surficial processes on Earth (Gaillard et al., 2013; Halevy et al., 2007; King et al., 2004; King and McLennan, 2010; McLennan and Grotzinger, 2008). The martian sulfur cycle includes sulfur output from the deep interior to the surface and atmosphere through magmatism and volcanism as well as assimilation of sulfur-bearing phases from the surface or shallow subsurface into rising magmas (Farquhar et al., 2000b; Franz et al., 2014a; Jones, 1989; King et al., 2004). Nonetheless, experimental

constraints suggest that on Mars as on Earth, the abundance of sulfur in the core is a critical parameter in modeling the physical state of the core and its ability to sustain a global magnetic field (Stewart et al., 2007).

1.2. Sulfur geochemistry and isotopes

Sulfur is a versatile element that is found in a wide range of organic and inorganic compounds, in valence states from -2 to +6, and in solid, aqueous and gas phases. It has four stable isotopes, ^{32}S , ^{33}S , ^{34}S and ^{36}S , with abundances of approximately 95.04%, 0.75%, 4.20% and 0.015%, respectively (Ding et al., 2001). Because these isotopes fractionate during processing of sulfur-bearing compounds, analysis of sulfur isotopes has emerged as a vital tool for understanding numerous processes, both geological and biological in nature. Most commonly, mass-dependent fractionation occurs, in which isotopes of a given element partition differentially between chemical compounds or phases based on the small differences in their masses (Urey, 1947). In other cases, the partitioning of isotopes is controlled by additional factors and cannot be predicted simply from isotopic masses. For example, on Mars UV photochemistry is an important mechanism to partition isotopes of certain elements, including oxygen and sulfur, in ways that are not proportional to the difference in isotopic masses (Clayton and Mayeda, 1983; Farquhar et al., 2001; Thiemens, 1999). This type of behavior, commonly known as mass-independent fractionation (MIF), presents an additional means to track processes in elements with more than two stable isotopes through deviation of the minor isotopes from mass-dependent compositions. Anomalies in abundances of both ^{33}S and ^{36}S compared to the other isotopes produce distinctive patterns that differ with the processes responsible for the fractionation (Farquhar et al., 2000a; Farquhar et al., 2001; Gao and Thiemens, 1991, 1993a, b; Hulston and Thode, 1965; Ono et al., 2006). MIF is portrayed conceptually in Fig. 1.

Isotope ratios are usually reported in terms of delta (δ) values, representing per mil (‰) deviations from established reference standards. For sulfur, the original reference standard was Fe-sulfide from the Cañon Diablo iron meteorite, or Cañon Diablo Troilite (CDT) (Jensen and Nakai, 1962). Due to dwindling supply of material from the meteorite as well as heterogeneity observed in isotopic composition of CDT samples (Beaudoin et al., 1994), the International Atomic Energy Agency (IAEA) established a modern sulfur isotope scale (Robinson, 1993). This scale, known as V-CDT, is closely linked to CDT but utilizes a set of synthetic Ag-sulfide mixtures spanning the range in sulfur isotopic compositions typically observed in natural samples as reference materials (Ding et al., 2001). The sulfur isotopic composition measured for a sample is then reported as the deviation from the reference composition for each ratio of minor isotope to ^{32}S :

$$\delta^{33}\text{S} = [({}^{33}\text{S}/{}^{32}\text{S})_{\text{meas}}/({}^{33}\text{S}/{}^{32}\text{S})_{\text{ref}} - 1] \cdot 1000 \quad (1)$$

$$\delta^{34}\text{S} = [({}^{34}\text{S}/{}^{32}\text{S})_{\text{meas}}/({}^{34}\text{S}/{}^{32}\text{S})_{\text{ref}} - 1] \cdot 1000 \quad (2)$$

$$\delta^{36}\text{S} = [({}^{36}\text{S}/{}^{32}\text{S})_{\text{meas}}/({}^{36}\text{S}/{}^{32}\text{S})_{\text{ref}} - 1] \cdot 1000 \quad (3)$$

where the subscript “meas” denotes the measured ratio and “ref” denotes the isotopic ratio of the reference standard. “Capital delta” notation is used to report mass-independent fractionation:

$$\Delta^{33}\text{S} = \delta^{33}\text{S} - 1000 \cdot [(1 + \delta^{34}\text{S}/1000)^{0.515} - 1] \quad (4)$$

$$\Delta^{36}\text{S} = \delta^{36}\text{S} - 1000 \cdot [(1 + \delta^{34}\text{S}/1000)^{1.90} - 1] \quad (5)$$

where values of zero indicate mass-dependent behavior and non-zero values indicate MIF.

1.3. Clues to Mars' past

Studying sulfur compounds on Mars can provide clues to numerous facets of martian history, which will be explored in the sections that follow. The abundance and redox state of sulfur-bearing minerals in the igneous rocks comprising our collection of martian meteorites informs estimates of the planet's total inventory of sulfur and the oxidation state of magmas. These parameters are also linked to the quantity and identity of sulfurous gases that would have been released into the atmosphere due to volcanic activity. Since SO_2 in particular has the potential to act as a greenhouse gas, the atmospheric mixing ratio of sulfur, in conjunction with that of water, is critical in attempts to model the martian climate and to address the question of whether the surface was ever sufficiently warm that liquid water could have existed even transiently.

The past climate and water activity also bear directly on the question of whether ancient Mars was habitable – in other words, whether it could have supported a biosphere with any resemblance to that of Earth. The terrestrial sulfur cycle is heavily dominated by biological processes, which are intimately tied to the sulfur isotopic compositions observed in all types of environments. The presence of sulfur-metabolizing microorganisms near the root of the phylogenetic tree (e.g., Edmonds et al., 1991; Gregersen et al., 2011; Shooner et al., 1996; Stetter, 1996; Woese et al., 1991) has sparked interest in whether such primitive metabolisms could also have arisen on Mars, with its rich abundance of sulfur. Sulfur isotope ratios also provide evidence suggesting that a UV photochemical cycle, distinct from that of Earth, operated in the martian atmosphere in the past. Deciphering this isotopic fingerprint to reveal the nature of photochemical processes that produced it may yield clues to the composition of the atmosphere at the time, which affects climate scenarios as well as potential means for providing UV shielding to protect past martian life.

2. Martian sulfur reservoirs

2.1. Sulfur abundance and core formation

It is informative first to assess martian sulfur abundance in a solar system context. Sulfur was the most abundant moderately volatile element in the solar nebula, present as H_2S that condensed out of the nebula by temperature-dependent reactions with solid phases (Ebel, 2011; Lodders et al., 2009). For example, highly refractory CaS condenses ~ 1200 K (Pasek et al., 2005), while Fe-sulfides form in the range ~ 500 -710 K (Lauretta et al., 1997; Lodders et al., 2009; Pasek et al., 2005). Variations observed among classes of chondrites in volatile element abundances relative to solar composition reflect fractionation by gas-solid reaction processes during condensation. The CI chondrites have sulfur abundances similar to the solar value (2 – 10 wt%) (Palme and Jones, 2003), while other types of chondrites exhibit relative depletions (Lodders et al., 2009). Volatile element depletions are also observed in differentiated solar system bodies, including the Earth, Moon, and eucrites (Palme et al., 1988). In comparison to Earth, analyses of martian meteorites suggest that Mars contains more volatile and moderately volatile elements, except for chalcophile elements (Zn, Tl, In) (Dreibus and Wanke, 1985). The

sulfur content of bulk Mars has been modeled in various ways using elemental volatility trends in comparison to chondritic meteorites, yielding a range of results as shown in Table 1.

In the case of both Earth and Mars, most sulfur is modeled as residing in the core. These models are based on partitioning of sulfur between Fe-Ni metal (the “core”) and silicate melt (the “mantle”) during core segregation (e.g., Kargel and Lewis, 1993), although Gaillard et al. (2013) note the difficulties inherent in such modeling due to non-ideal behavior of sulfur in Fe-S melts. The sulfur content of the core is a critical parameter in models of core solidification, since its presence depresses the melting temperature compared to pure Fe or Fe-Ni metal (Fei et al., 2000; Stewart et al., 2007). At least a portion of the core must be liquid to sustain a convectively-driven magnetic field (Acuna et al., 1999; Connerney et al., 1999; Fei and Bertka, 2005; Schubert and Spohn, 1990; Stewart et al., 2007; Young and Schubert, 1974). Magnetic surveys of the martian crust by the Mars Global Surveyor provide evidence to suggest that the young Mars had an active core dynamo for as long as several hundred million years (Acuna et al., 1999; Lillis et al., 2008; Solomon et al., 2005). This dynamo could have been driven by convection due to a compositional gradient in a liquid outer core as the inner core solidified or by thermal convection due to high heat flux out of a fully liquid core (Fei and Bertka, 2005; Stevenson, 2001). The sulfur abundance of the core thus strongly influences the ability of the planet to sustain a magnetic field, which has implications for the climate and surface radiation environment (Lillis et al., 2008).

Elemental abundance estimates for Mars have been generated through analyses of martian meteorites combined with geophysical models, producing a range of results for the distribution of sulfur between Mars’ mantle and core (Table 1). Estimates of mantle sulfur abundance based directly on sulfur abundances in meteorites have yielded a wide range of values, because the ultimate sulfur abundance and distribution among mineral phases in the meteorites reflect a multitude of factors (see Section 2.3). However, it is inferred from meteorite compositional analyses that the martian mantle is roughly a factor of two richer in FeO than that of Earth (McSween, 1994; Wanke and Dreibus, 1994). As explained in Section 2.1, the amount of sulfur that can be dissolved in silicate melts is limited by its partitioning with other coexisting phases. The maximum sulfur content of a silicate melt, governed by the sulfur capacity, is expected to correlate with FeO content (Carroll and Rutherford, 1985; Gaillard et al., 2013; O’Neill and Mavrogenes, 2002; Wallace and Carmichael, 1992), so assuming that the martian mantle was once molten (i.e., magma ocean) (Elkins-Tanton, 2008), the sulfur abundance of the martian mantle is expected to be higher than that of the Earth’s mantle (Gaillard and Scaillet, 2009; Wanke and Dreibus, 1994).

Wänke and Dreibus (1988) applied general cosmochemical constraints to estimate the bulk composition of Mars by applying mass balance to elemental abundances observed in chondrites. They demonstrated that two-component mixing models originally developed to explain Earth’s mantle composition (Ringwood, 1979; Wänke, 1981) could also be applied to Mars. The model of Wänke and Dreibus required a highly reduced component A, free of elements more volatile than Na, and an oxidized component B, containing all elements in CI abundances, in proportions A:B of approximately 60:40. Sulfur, present as FeS in component B, reacted with Fe-Ni metal from component A to form a sulfur-rich Fe-Ni alloy during core segregation, extracting chalcophile elements into the core according to their sulfide-silicate partition coefficients. The core composition was estimated as 77.8% Fe, 7.6% Ni, 0.4% Co, and 14.2% S (Wanke and Dreibus, 1988).

Other compositional models for Mars have incorporated oxygen isotopes to constrain accretion from mixtures of different types of chondrites (e.g., Lodders and Fegley, 1997). It was shown by Clayton et al. (1976) that the Earth, Moon, and chondritic meteorites may be classified into several distinct groups according to their oxygen isotope systematics, specifically by variations in the relationship between $^{18}\text{O}/^{16}\text{O}$ and $^{17}\text{O}/^{16}\text{O}$ that have been interpreted to reflect heterogeneities in solar nebula composition or localized effects of photochemical processes that occurred in the nebula (Clayton, 1993, 2002, 2003; Clayton and Mayeda, 1984; Clayton et al., 1991; Thiemens and Heidenreich, 1983). Analyses of martian meteorites reveal that Mars also carries a characteristic mass-independent oxygen isotopic signature (Clayton and Mayeda, 1983, 1996), with silicates displaying $\Delta^{17}\text{O}$ of 0.32‰ on average compared to V-SMOW (Franchi et al., 1999). From mass balance calculations, Lodders and Fegley (1997) suggested that Mars accreted from about 85% H-, 11% CV-, and 4% CI-chondritic material, comprising ~80% silicates with the remaining ~20% in a metal-sulfide core containing ~10.6% sulfur. This model produced an estimate of 2.2% for the bulk sulfur content of Mars and 900 ppm sulfur in the martian mantle (Lodders and Fegley, 1997), approximately four times that of Earth (Allègre et al., 2001; Dreibus and Palme, 1996). The latter value overlaps with the range of 700-1000 ppm reported as upper limits for cold and hot martian mantle models based on a recent analysis of meteorite bulk sulfur contents, combined with a mantle partial melting model (Ding et al., 2015).

Some more recent models for the bulk chemical composition of Mars have exploited improved knowledge of martian geophysical data provided by radiometric tracking of spacecraft, such as moment of inertia (MOI), solar tidal deformation parameters, mass and size, to constrain estimates of bulk composition. For example, a higher sulfur content in the core implies lower core density (Fig. 2), requiring a larger core radius to fit a given mass and producing a larger mean MOI factor, while a lower sulfur content would have the opposite effect (Wang et al., 2013b). Bertka and Fei (1998) performed high-pressure experiments with appropriate analog mixtures to evaluate the Wänke and Dreibus (1988) model in light of MOI measurements based on tracking of the Pathfinder rover (Folkner et al., 1997; Yoder and Standish, 1997). They concluded that accretion models based solely on CI chondrites cannot match the observed moment of inertia of Mars and are insufficient to explain the variations in Fe/Si among the terrestrial planets, but that mixtures of carbonaceous chondrites with ordinary or enstatite chondrites could produce bulk planet compositions consistent with geophysical constraints (Bertka and Fei, 1998). Sanloup et al. (1999), using an oxygen isotope approach similar to that of Lodders and Fegley (1997) but further constrained by Pathfinder MOI observations (Folkner et al., 1997), invoked a mixture of H- and EH-chondrites (Wasson and Kallemeyn, 1988) in a ratio of 55:45 to produce a core containing a maximum of 16.2% sulfur (Sanloup et al., 1999).

Wang et al. (2013) used a method similar to that of Bertka and Fei (1998) with an updated Mars MOI based on measurements of Mars Reconnaissance Orbiter, Mars Global Surveyor, Mars Odyssey, Pathfinder and Viking (Konopliv et al., 2011), but assumed a liquid Fe-S core (Yoder et al., 2003) as opposed to the solid core assumed by Bertka and Fei (1998). Wang et al. (2013) used the mantle compositional model of Wänke and Dreibus (1988) and the temperature profile of Fei and Bertka (2005) to test the effects of core sulfur concentration on mantle-core density profiles, then calculated the MOI factors for each density profile and compared to observed MOI (Konopliv et al., 2011) to constrain Mars' composition. The range of compositions generated by their model indicates core sulfur content between 10.6 and 14.9 wt% (Wang et al., 2013b). Another study by Rivoldini et al. (2011) produced a model for the interior structure of Mars based on the thermoelastic properties of the mantle and core, constrained by

the MOI and tidal deformation parameters. Those authors derived a sulfur abundance of $16 \pm 2\%$ for the core (Rivoldini et al., 2011).

Stewart et al. (2007) performed experiments with Fe-S and (Fe,Ni)-S mixtures at pressures corresponding to the core-mantle boundary and the center of Mars (~23 and 40 GPa, respectively) to investigate possible core crystallization scenarios. Their experiments included sulfur abundances of 10.6 wt%, 14.2 wt%, and 16.2 wt%, which encompass the range of core sulfur abundances determined by compositional studies as well as the eutectic melt compositions at various core pressures (Table 1). By comparing liquidus intersections of the resulting pressure-temperature curves with temperature models for the martian interior, they concluded that presently the martian core is almost entirely, if not entirely, in a liquid state. Their model also examined potential mechanisms of core solidification that may ensue as Mars continues to cool. They identified two possible crystallization regimes for martian core conditions, depending on the sulfur abundance. On the iron-rich side of the eutectic composition (10 and 14 wt % sulfur), iron-rich solids would nucleate in the outer region of the core and sink toward the center in a “snowing core” model. On the sulfur-rich side of the eutectic (14-16 wt% sulfur), Fe-sulfide phases would crystallize from the center of the core outward, in a “sulfide inner-core” model (Stewart et al., 2007).

Stewart et al. (2007) note that since the martian core is currently in a liquid state, the putative magnetic field that existed during the Noachian period must have been driven by a vigorous core convection different than that of the Earth. Some major change in the liquid core convection regime, other than core solidification, must have occurred to cause the cessation of Mars’ early magnetic field. Furthermore, they suggest that when large-scale core crystallization ultimately begins on Mars, the resultant change in convection regime could reestablish a dynamo driving a second period of Mars’ history characterized by a strong global magnetic field (Stewart et al., 2007). The crystallization regimes indicated by their model suggest that the sulfur abundance in the core will largely control the nature of this dynamo.

The highest existing estimate of martian core sulfur content was obtained by Khan and Connolly (2008), who applied inversion of martian geophysical parameters to produce an estimate of > 20 wt% sulfur in the core. Khan and Connolly (2008) also calculated a bulk planet Fe/Si ratio of ~ 1.2 and suggested that this indicates accretion of Mars from different solar system materials than those that formed Earth, such as ordinary chondrites, which also have oxygen isotopic ratios similar to those in martian meteorites.

Two recent studies have resulted in lower estimates for the sulfur content of the martian core than those reported previously. Shahar et al. (2015) performed a series of experiments at high pressure and temperature designed to constrain the iron isotopic fractionation during core-mantle differentiation. Reconciliation of their experimental results with geophysical models and data for iron isotopic signatures in martian meteorites requires an upper limit of ~ 8 wt% sulfur in the martian core. Wang and Becker (2017) pointed out that the high FeO content of martian meteorites would require a higher sulfur concentration in parent magmas than have generally been measured in meteorites. They examined chalcophile element concentrations in martian meteorites and noted that limited variations in ratios of these elements in magmas with a wide range of volatility indicates little degassing loss of several volatile elements, including sulfur, during eruption. Based on limited variability in ratios of elements with different sulfide-silicate melt partition coefficients and negative correlations of chalcophile elements with MgO, they further suggested that sulfide-undersaturated magmas may have been prevalent throughout Mars’ geological history. We should note here that under reduced conditions similar to those prevailing

in the martian interior during the earliest stages of magma ocean or even for more recent magmatic activities, sulfur is not a strongly volatile element; at $fO_2 < IW+2$, sulfur tends to remain in the molten silicate (see Gaillard et al., 2013). That being said, through comparison of copper and sulfur contents in meteorites, Wang and Becker (2017) estimated a concentration of $360 \pm 120 \mu\text{g/g}$ of sulfur in the martian mantle and 5-10 wt% sulfur in the core. They state that such a low sulfur content in the interior of Mars is consistent with the low zinc content in the martian mantle, from which an estimate of ~5 wt% sulfur in the core is derived (Wang and Becker, 2017).

Another recent study examining sulfur isotopic fractionation between metal and silicate melts at high pressure suggests that the $\delta^{34}\text{S}$ of mantle sulfur may yield information about the pressure of core-mantle differentiation (Labidi et al., 2016). Sulfur in the martian mantle (Franz et al., 2014a) and in chondrites (Gao and Thiemens, 1993a, b) has an isotopic composition indistinguishable from Cañon Diablo Troilite (CDT), while sulfur in the Earth's mantle shows a small depletion in ^{34}S (Labidi et al., 2013). A series of high-pressure and temperature experiments with synthetic mixtures of metal and silicate melts revealed that the sulfur isotopic fractionation between metal and silicate phases increases linearly with aluminum and boron concentrations, which affect the structure of the melt through coordination number of bonds and lead to stronger sulfur bonds in metal alloys than in silicates (Labidi et al., 2016; Shahar et al., 2009). Because the coordination number is similarly affected by changes in pressure, the authors conclude that the occurrence of sulfur isotopic fractionation during formation of Earth's core and the absence of such fractionation on Mars suggests a lower average pressure during core-mantle equilibration on Mars compared to Earth (Labidi et al., 2016). This topic deserves further investigation.

2.2. Sulfur in melts, vapor, sulfide, sulfate and metal

How much sulfur dissolves in silicate melts, commonly called sulfur solubility in silicate melts, is limited by the ability of the coexisting phase to concentrate sulfur. In the framework of the martian cycling of sulfur and its secular evolution, the phases coexisting with a silicate melt of basaltic composition are metal, sulfide, sulfate, and vapor during the stage of core formation, mantle melting, magma fractionation, and magma degassing, respectively. Due to the tremendous range of oxidation state for sulfur (-2 to +6), the partitioning of sulfur between a silicate melt and any of the above-mentioned phases is critically controlled by oxygen fugacity, fO_2 , which is a thermodynamic measure of the oxidation state of a multiphase system (Gaillard et al., 2015).

In silicate melts, sulfur essentially dissolves as S^{2-} and S^{6+} (Jugo et al., 2010). In metals, by definition, the oxidation state of sulfur is 0. In (liquid) Fe-sulfide, FeS, we generally assume a -2 oxidation state, although non-stoichiometric sulfide, FeS_x , is common (Kiseeva and Wood, 2013). The existence of a complete solid solution between molten Fe and FeS at high temperature complicates the matter, as it implies a change in the oxidation state of both Fe and S at a composition that remains unclear (Gaillard and Scaillet, 2009; Wang et al., 1991). This continuous solid solution between metal and sulfide has introduced confusion in the literature addressing core-mantle equilibration (Gaillard et al., 2013). Sulfate is a magmatic mineral that carries sulfur with the oxidation state +6 (Jugo, 2009). Finally, in the vapor phase, the commonly considered species, H_2S , S_2 and SO_2 , carry sulfur with an oxidation state of -2, 0 and +4 (Gaillard et al., 2011). Variation of the prevalent oxidation state between phases - melt, metal,

sulfide, and vapor - for a given fO_2 implies that the partitioning of sulfur between these phases is overwhelmed by fO_2 . In turn, the transfer of sulfur between these phases is also expected to affect fO_2 (Gaillard et al., 2011).

The solubility of sulfur in silicate melts saturated in sulfide (solid or molten) has been widely studied by material scientists and geochemists (O'Neill and Mavrogenes, 2002, and references therein). The concept of sulfur capacity was introduced 70 years ago to quantify the following heterogeneous equilibrium:



Eq. (6) describes the partitioning of sulfur between gas and melt. The introduction of ionic species to a silicate melt in equilibrium, with a thermodynamic standard state difficult to define, led to the concept of sulfur capacity, representing a quantitative gauge of the ability of the silicate melt to dissolve sulfur. From Eq. (6), one can assume that the silicate melt is dominated by oxygen anions (i.e., activity of $O^{2-}=1$), which defines the dependence of sulfur capacity, C_s , on oxygen fugacity, fO_2 , and sulfur fugacity, fS_2 :

$$\ln C_S^{silicate} = \ln X_{S^{2-}}^{silicate} + \frac{1}{2} \ln f_{O_2} - \frac{1}{2} \ln f_{S_2}. \quad (7)$$

This equilibrium is critical in the modeling of sulfur degassing and can also be related to another parameter critical for petrological modeling of sulfur: the sulfur content at sulfide saturation (SCSS) that corresponds to the following equilibrium:



Eq. (8) implies that the SCSS can be calculated from the Gibbs free energy changes of Eq. (8), $\Delta G^\circ_{(8)}$, the activity of FeO in the silicate melt, $a_{(FeO)}$, and the sulfur capacity (Gaillard et al., 2013; O'Neill and Mavrogenes, 2002):

$$\ln (X_{S_2})^{ppm-basalt} = \Delta G^\circ_{(8)} / [RT] + \ln C_s - \ln a_{(FeO)}. \quad (9)$$

Several experimental studies have provided constraints on the dependence of C_s on the melt chemical composition (see O'Neill and Mavrogenes, 2002). In the framework of martian magmatism, the critical parameter is the high FeO content of basalts, which is 2 to 3 times greater than that of basalts on Earth (Ding et al., 2014; Gaillard and Scaillet, 2009; Righter et al., 2009). Several empirical formulations of the SCSS have been produced (Ding et al., 2014; Righter et al., 2009) and applied to determine the maximum sulfur content of martian basalts (see Section 2.3). It appears that martian basalts, being richer in FeO than Earth basalts, can dissolve ~4000 ppm sulfur, or 3 to 4 times the sulfur content in terrestrial mid-ocean range basalts (MORBs).

Less relevant to martian magmatism, petrological modeling of the sulfur content at anhydrite saturation (SCAS) has been performed by Jugo (2009). The SCAS exceeds 1% S in basaltic magma, which is significantly greater than the SCSS even for the FeO-rich martian basalts. However, this petrological parameter is relevant to fO_2 conditions $> \sim 1.5$ -2 log units

above the quartz- fayalite-magnetite (QFM) buffer, or at least 2 log units more oxidized than our current estimates of typical martian basalt fO_2 (Wadhwa, 2001).

2.3. Sulfur in the primitive mantle and crust

The primitive crust of Mars most likely formed following core-mantle differentiation, although their coeval formation cannot be ruled out. A widely accepted model holds that the crust formed from crystallization of a magma ocean, accompanied by substantial outgassing (Elkins-Tanton, 2008; Elkins-Tanton et al., 2005). Estimates of the quantity of volatiles released during this stage and the pressure of the resultant proto-atmosphere are difficult to constrain (Elkins-Tanton, 2008; Erkaev et al., 2014; Hirschmann and Withers, 2008), and efforts to quantify volcanic production have primarily focused on activity during the past ~4 Ga (Baratoux et al., 2013; Grott et al., 2011; Hirschmann and Withers, 2008).

Most of our knowledge of martian petrology and mineralogy has been acquired through the study of martian meteorites. At the time of publication, 107 distinct (unpaired) meteorites of martian origin have been recovered and classified on Earth (Irving, 2017; McSween, 1994; Meyer, 2015). They all derive from igneous parent rocks, with the single exception of an impact-produced breccia, NWA 7034 and its pairs (Agee et al., 2013; Humayun et al., 2013). Igneous rocks range in age from ~4.1 Ga for ALH 84001 (Lapen et al., 2010) to ~175 Ma for the youngest group of shergottites (Nyquist et al., 2001). Their primary sulfur mineralogy is dominated by Fe-sulfides, with minor sulfates, as discussed in more detail in Section 2.5. As mentioned above, the ultimate sulfur abundance and distribution among mineral phases in the meteorites reflect a complex interplay of factors, including mantle sulfur contents, degree of (partial) melting, pressure, temperature, iron and volatile contents of the magma, sulfur degassing during ascent, water activity of the melt, sulfur speciation, fO_2 , later weathering processes, and possible incorporation of crustal sulfur into magmas or impact glasses (Franz et al., 2014a; Gaillard et al., 2013; Gaillard and Scaillet, 2009; Jones, 1989; Rao et al., 1999; Rao et al., 2011; Wallace and Carmichael, 1992; Walton et al., 2010). Accurate interpretation of meteorite data requires consideration of sulfur contents with respect to the abundances of other elements. Measurements of the bulk sulfur abundances of martian meteorites have yielded a wide range of values (Table 1), sometimes even among multiple analyses of a single meteorite. These variations likely arise from a combination of sample heterogeneity and differences in measurement techniques between studies.

The most primitive martian meteorites and arguably most informative about Mars' mantle composition are shergottites. The initial oxygen fugacity (fO_2) of shergottite magmas upon partial melting of the mantle source was typically in a reducing range, ~1 to 3 log units below the QFM buffer (Herd, 2003; Herd et al., 2002; Lorand et al., 2005; McSween et al., 1996; Smith and Hervig, 1979; Stolper and McSween, 1979; Wadhwa, 2001). Since the oxidation state and solubility of sulfur in a S-saturated melt is a function of fO_2 , magmatic sulfur under these conditions would have either dissolved in the melt as S^{2-} (preserved in glass) or produced sulfide minerals (Jugo et al., 2005; Wallace and Carmichael, 1992). A limited number of shergottites record more oxidizing conditions with fO_2 near the QFM buffer (Herd, 2003). This is within the range where S^{6+} /total S becomes significant (Jugo et al., 2005) and may indicate that late-stage sulfates could have been stable (Gross et al., 2013).

Sulfides in the shergottites are commonly associated with Fe-Ti oxides (Lorand et al., 2005), reflecting the relationship between FeO content and sulfide saturation as the melts evolved. The behavior of sulfur in basaltic magma reflects the competing effects of pressure, temperature, composition, fO_2 and fS_2 (Haughton et al., 1974; O'Neill and Mavrogenes, 2002). Although each of these factors alone can result in sulfide saturation, their activities in concert control precipitation of sulfide minerals. Sulfur solubility decreases as a magma ascends from its mantle source region and cools along an adiabatic path. At conditions of emplacement, FeO content of the melt may decrease due to precipitation of Fe-Ti oxides, which may induce localized sulfide precipitation (Gaillard et al., 2013; Haughton et al., 1974; Kress and Carmichael, 1991; Li and Ripley, 2005, 2009; O'Neill and Mavrogenes, 2002; Righter et al., 2009; Wallace and Carmichael, 1992).

The sulfide abundances of shergottites have also been used in conjunction with compositional data of shergottites and chondritic meteorites to estimate the sulfur abundance of the martian mantle (Table 1 and references therein) and the quantity of sulfur that may have been introduced to the surface through volcanic outgassing (Gaillard and Scaillet, 2009; Halevy et al., 2007; Righter et al., 2009). Calculations of this type may be best undertaken with meteorites that approximate melt compositions, as the sulfur abundances in meteorites with significant cumulate fractions may underrepresent the composition of the mantle (Ding et al., 2015). Another important consideration is that the meteorites may include sulfur from crustal or hydrothermal rather than magmatic sources (Franz et al., 2014a). The maximum sulfur content of a martian magma can be estimated by assuming that it was initially sulfide saturated (Gaillard et al., 2013; Righter et al., 2009). Gaillard et al. (2013) adopted a range of 700-2000 ppm for martian mantle sulfur, although other studies have suggested that the lower end of this range from 700-1000 ppm is most realistic (Ding et al., 2015; Gaillard and Scaillet, 2009). Assuming that sulfur is perfectly incompatible during melting, more conservative estimates yield 3000 ± 500 ppm or more sulfur in martian magmas upon mantle melting (Gaillard and Scaillet, 2009; Righter et al., 2009), largely exceeding the sulfur content of primary basalts on Earth (1000 ± 500 ppm). A first critical question recently raised by Ding et al. (2015) is whether the mantle melting that produced the shergottites on Mars left a mantle residue that remained sulfide saturated. Interestingly, Ding et al. (2015) argued based on geochemical modeling that it may not always be the rule, since sulfide can be exhausted during mantle melting. This implies that sulfur content < 3000 ppm in primary shergottites can be expected. The second critical question is whether all sulfur dissolved in the shergottite melts can be degassed into the atmosphere (see Section 2.4).

In contrast to the shergottites, the nakhlites have higher fO_2 values of ΔQFM 0 to +1.5 (e.g., Chevrier et al., 2011; Dyar, 2005; Szymanski et al., 2010). Such values allow for higher sulfur contents in any melt phase, and a larger proportion of S^{6+} in the melt that could saturate the melt in sulfates. See Section 2.2 for related discussion.

Although most existing constraints on the sulfur abundance of the martian mantle have been derived from sulfur geochemistry of martian meteorites, ratios of chalcophile elements may also be used to constrain sulfur behavior in melts. As discussed in Section 2.1, Wang and Becker (2017) estimated ~ 360 ppm sulfur in the martian mantle using this method, significantly lower than most previous estimates.

2.4. Sulfur from volcanic outgassing

As a magma ascends, a fraction of its sulfur escapes due to degassing (Fig. 3), with quantity and species of sulfur-bearing gases dependent on several factors, including the overlying pressure, temperature, melt $f\text{O}_2$, $f\text{S}_2$, melt composition, and the concentration and speciation of other volatile elements present (e.g., H, C, Cl) (Gaillard and Scaillet, 2014). Models of martian volcanic degassing are discussed extensively in Gaillard and Scaillet (2009) and Gaillard et al. (2013). Besides the physical effect of pressure on gas solubility, sulfur degassing on Mars is particularly sensitive to $f\text{O}_2$ and magmatic water content, with both factors exerting positive effects of similar magnitude on quantity of sulfur released (Gaillard et al., 2013). The maximum sulfur degassing would be achieved by hydrated and oxidized melts (~0.4 wt% water and $f\text{O}_2$ ~QFM-0.5), which would release about 75% of their initial sulfur content into the atmosphere (Gaillard et al., 2013). Although H_2S would have dominated during degassing of an early magma ocean and at higher eruptive pressures (1-1000 bar), the dominant sulfur species at conditions expected for martian volcanism during the past ~4 Ga (< 0.1 bar) would be SO_2 (Gaillard et al., 2013; Zolotov, 2003). Release of SO_2 would also be favored by an increase in oxidation state of magmas due to assimilation of crustal material, a process that would have been facilitated by slow magma ascent in low gravity and high liquidus temperatures of magmas with low water content (Zolotov, 2003). An increase in $f\text{O}_2$ due to assimilation of oxidized crustal material (Franz et al., 2014a; Herd et al., 2002; Jones, 1989; Wadhwa, 2001) would be offset by a decrease in $f\text{O}_2$ due to outgassing of SO_2 from the magma (Gaillard et al., 2013). A synthesis of the tradeoff between sulfur content in primary magma (during mantle melting) and the degassing process that transfers this magmatic sulfur into the atmosphere is summarized in Fig. 4. Here, different cases simulate the degassing of sulfur-rich and sulfur-poor magma. The conclusion is clear: the amount of sulfur degassing is affected by the amount of sulfur present in the primary melt, but a decrease of a factor of 4 in the sulfur melt content translates into a decrease by a factor of 2 in the quantity of sulfur degassed. Furthermore, the sulfur content and its speciation in the volcanic gases are only moderately affected by the sulfur content of the primary melt, with the highest mole fraction of SO_2 produced by the most sulfur-poor melts. This illustrates that degassing is the key factor in the transfer of sulfur from the mantle to the atmosphere.

Gaillard and Scaillet (2009) calculated the amount of sulfur that could have been introduced to the martian surface during formation of the Tharsis volcanic province, assuming associated basalt production of $3 \times 10^8 \text{ km}^3$ (Phillips et al., 2001). We revise their estimate here based on the amount of sulfur outgassed for sulfur-rich and sulfur-poor martian melts as defined in Fig. 4. If all outgassed sulfur were ultimately deposited on the ground, we estimate that volcanic sulfur could have delivered a global equivalent layer of sulfates 7 – 35 m thick. Volcanic outgassing thus presents a feasible mechanism for generating the abundant sulfate minerals now observed and redistributed at the surface (Gaillard and Scaillet, 2009).

A substantial quantity of sulfur has likely been cycled through the martian atmosphere due to volcanic outgassing. The timing of past activity is based on application of crater size-frequency distribution models to volcanic landforms (Hartmann and Neukum, 2001). Studies by Werner (2009) and Robbins et al. (2011) using images acquired with the Mars Express High Resolution Stereo Camera (HRSC) and the Mars Reconnaissance Orbiter ConTeXt Camera (CTX), respectively, concluded that volcanic activity in the Tharsis province ended between 100 and 200 million years ago. However, the unusually long and episodic lifetimes of volcanoes on Mars (Frankel, 1996) have led to suggestions that there may still be active regions on the planet today. A study of plain-style volcanoes with CTX indicated extended areas in Tharsis that have been resurfaced by basaltic lava flows in the past few tens of millions of years (Hauber et al.,

2011). Neukum et al. (2004) examined HRSC images of the Tharsis and Elysium provinces and reported evidence for repeated activation and resurfacing of 5 volcanoes during the last 20 percent of martian history. Citing phases of activity that occurred as recently as 2 million years ago, they suggested that Tharsis volcanoes may be currently active (Neukum et al., 2004). In addition, they reported evidence for glacial activity at the base of the Olympus Mons escarpment as recently as 4 million years ago (Neukum et al., 2004). Further HRSC images of Olympus Mons revealed evidence for very recent geological activity, $\leq 25\text{-}40$ Ma, on the volcano's eastern flank, including fluvial networks, emplacement of lava flows and dikes, and wrinkle ridges and troughs due to tectonic processes (Basilevsky et al., 2006).

2.5. Sulfur at the martian surface

Our knowledge of sulfur abundance and mineralogy at the surface of Mars is based on a combination of data acquired through remote sensing from Earth and by spacecraft orbiting Mars, *in situ* measurements by instruments on rovers and landers, and studies of martian meteorites. As indicated in Fig. 5 and discussed in the following sections, sulfur may be found on Mars in a range of oxidation states, dependent on reactions with iron, oxygen, hydrogen, carbon, and sulfur or interactions with radiation. Common sulfur oxidation states are: S^{2-} (e.g., in pyrrhotite, FeS_{1-x}), S^{-1} (e.g., pyrite FeS_2), S^{4+} ($SO_2(g)$, SO_2^{2-} bisulfine, SO_3^{2-} bisulfite) and S^{6+} ($SO_3(g)$, SO_4^{2-} sulfate, SO_3^{2-} sulfone), and S^+ , S^{2+} , S^{3+} and S^{5+} may also exist.

In the following sections, we briefly describe some of the measurement techniques that have provided existing data on sulfur chemistry and mineralogy from (A) the martian surface; (B) martian meteorites and (C) orbiters.

A. In situ observations

A.1. Measurement techniques

A.1.1. X-ray fluorescence (XRF) and alpha-particle/proton X-ray spectrometry (APXS)

A range of sulfur contents has been measured *in situ* with rover and lander missions on Mars (Table 1; Fig. 6). X-ray fluorescence analyses from the Viking missions revealed that Mars has sulfur-rich surface regolith or soil (Baird et al., 1976; Clark et al., 1976; Clark et al., 1982; Toulmin et al., 1977). We use the term “soil” in a general sense to imply loose, unconsolidated material at the planet's surface, as applied by previous authors (e.g., Blake et al., 2013; Morris et al., 2000; Vaniman et al., 2014). Subsequent rover missions confirmed high sulfur contents using two different APXS instruments: an alpha-*proton* X-ray spectrometer on the Pathfinder mission (Bell et al., 2000; Bruckner et al., 2001; Foley et al., 2001; McSween and Keil, 2000) and an alpha-*particle* X-ray spectrometer on each of the Mars Exploration Rovers (MER) Spirit and Opportunity (Gellert et al., 2006; McLennan and Grotzinger, 2008; Ming et al., 2008; Ming et al., 2006; Rieder et al., 2004) and the Mars Science Laboratory Curiosity rover (Berger et al., 2014; Berger et al., 2015; Campbell et al., 2012; McLennan et al., 2014). The results of these studies are examined in more detail below.

Dust, by which we generally mean weathered grains usually less than a few micrometers in size that remain suspended in the atmosphere for prolonged periods of time, is ubiquitous on Mars' surface and in its atmosphere; therefore, dust or regolith is included as a coating on underlying rocks or sediments reported by XRF and many APXS analyses. APXS analysis of

airfall dust on the observation tray of the Curiosity rover revealed the highest concentrations of SO₃ and Cl yet measured in martian dust (8.3 wt% SO₃, or 3.3 wt% S, and 1.1 wt% Cl) (Berger et al., 2016). The surface of Mars is reported to have an average SO₃ content of 6.8 wt% (2.7 wt% S), with soil having an average SO₃ content of ~6.2 wt% (2.5 wt% S) (Taylor and McLennan, 2009; Yen et al., 2005). Our compilation in Fig. 6 suggests that the median value for most MER and MSL APXS analyses is ~5-6 wt%. Sulfur-rich veins and infill are common (Fig. 7) and these have higher sulfur contents (Fig. 6).

Using data from the Mars Pathfinder mission, Foley et al. (2003) calculated a soil-free rock composition using linear regression of rock and coating compositions to subtract a soil component (Foley et al., 2003). Similar approaches or ratios of raw data to global soil or dust compositions have been applied in the MER mission (e.g., Gellert et al., 2006; Yen et al., 2005). Alternately, authors have examined samples that have been brushed or abraded (RAT – rock abrasion tool) to minimize the contribution from surface material. Such studies show that the coatings on rocks contribute to the analysis of untouched (as is) rocks and that if rocks have not been brushed or abraded, the interpretation of their bulk sulfur contents is challenging. For example, Fig. 8 shows Cl versus SO₃ for rocks from the MER-A (Spirit rover) at Gusev Crater, indicating that rocks that have been abraded have lower Cl and SO₃ than those that are brushed or untouched. These data indicate mixing between the rock and either, or both, soil and Ca- and/or Mg-sulfate minerals (Ming et al., 2006). For instance, the samples with higher SO₃ content are inferred to contain sulfate minerals. Within the soil, sulfur is commonly correlated with Cl, Ca, Mg (Fig. 9-11) and/or Na and Br, as well as oxidized Fe³⁺ (Morris et al., 2006) (Fig. 12).

A.1.2. Wet chemistry titration

The Phoenix Lander included a Wet Chemical Laboratory (WCL) with four cells designed to analyze chemical properties of martian soil samples (Kounaves et al., 2009). After mixing a soil sample with a leaching solution, sulfate detection was facilitated by titration with BaCl₂ powder, in which Ba²⁺ ions released by dissolution reacted with sulfate ions in solution. A Ba²⁺ ion-selective electrode allowed detection and quantification of sulfate present in the sample (Kounaves et al., 2010). The WCL carried three aliquots of BaCl₂ powder, each allowing detection of up to 5 wt% SO₃ (Kounaves et al., 2010).

A.1.3. Laser Induced Breakdown Spectroscopy (LIBS)

Laser Induced Breakdown Spectroscopy (LIBS) is one of the techniques used by ChemCam on the MSL Curiosity rover (Wiens et al., 2013). Sulfur is typically challenging to identify with LIBS because it tends to generate weak spectral lines (Dyar et al., 2011; Salle et al., 2004; Sobron et al., 2012; Vaniman et al., 2012). Nonetheless, sulfur has been detected by LIBS in veins, nodules and bowls (subspherical mm-sized nodules); the sulfur-rich nature of some of these targets is confirmed through APXS analyses. For example, S lines have been detected in many targets at Yellowknife Bay, generally in combination with high Ca lines and H detection (Nachon et al., 2014). Sulfur has also been detected at Reddick Bight (#5 and #8) and Denault (#4) in the Shaler unit of Gale crater (Anderson et al., 2015).

A.1.4. Evolved Gas Analysis (EGA)

Both the Thermal and Evolved Gas Analyzer (TEGA) instrument on the Phoenix lander (Boynton et al., 2001) and the Sample Analysis at Mars (SAM) instrument on the Curiosity rover

(Mahaffy et al., 2012) include a pyrolysis oven coupled with a mass spectrometer that enables evolved gas analysis (EGA) of solid samples. In this technique, powdered rock or soil samples are heated in the pyrolysis oven, while evolved gases are sampled by the mass spectrometer. Sulfur-bearing gases may be identified by their characteristic mass spectra. EGA cannot definitively identify mineral phases, but comparison of the temperature at which a gas evolves with EGA libraries of known compounds can indicate possible mineral candidates. For example, under SAM operating conditions, Fe-sulfates release SO₂ around 600 °C, while Mg- and Ca-sulfates typically do not release SO₂ until temperatures of 900 °C or higher (McAdam et al., 2014), although lower evolution temperatures are possible through catalysis by HCl derived from oxychlorine compounds in the samples (McAdam et al., 2016). See Section A.2.5 and Fig. 16 below for further details.

A.2. Results from surface missions

A.2.1. Viking landers

Analyses from the Viking x-ray fluorescence spectrometer (XRFS) showed that the sulfur concentration in martian fines is 10 to 100 times higher than that in common terrestrial and lunar rocks and soils, but similar to that in many chondritic meteorites (Clark et al., 1976). Abundances of volatile sulfur compounds, including elemental S and organic sulfur, were found to be low based on Viking molecular analysis experiment results (Biemann et al., 1976). XRFS analyses indicated that salts inferred to be on the martian surface are Mg-S-rich with significant Na and Cl (Baird et al., 1976; Clark et al., 1976; Clark and Van Hart, 1981) and that sulfur is predominantly present as S⁶⁺ (Toulmin et al., 1977). Relative abundances of sulfur and available cations suggested that Na-, Mg, and Ca-sulfates and Fe-sulfides were the only reasonable possibilities for sulfur host minerals (Clark et al., 1976). Later refinement of these results showed that Ca, Fe and Al were either uncorrelated or negatively correlated with S, and only Mg showed a positive correlation, although the precision was insufficient for strong conclusions to be drawn from these observations (Clark et al., 1982).

The two Viking landers analyzed a total of 21 samples (Clark et al., 1982). Bulk fines from both Viking lander sites were similar in composition. Sulfur contents of all samples ranged from 5.9 to 9.5 (+6/-2) wt% at Chryse Planitia and from 7.6 to 9 wt% (+6/-2) wt% at Utopia Planitia (Clark et al., 1982). “Duricrust” fragments, possibly indicating Mg-sulfate, contained ~50% higher sulfur concentrations than fines (Clark et al., 1977; Clark et al., 1982). Gooding (1978) proposed that with a scarcity of liquid water on Mars, weathering reactions may have been dominated by gas-solid interactions between atmospheric O₂, H₂O and CO₂ and primary basaltic minerals. Such reactions would have transformed igneous pyrrhotite to sulfates (Gooding, 1978). Alternative formation mechanisms for surface sulfate include deposition of atmospheric aerosols (Settle, 1979) and low-temperature saline groundwater (Burns, 1988, 1993). Because sulfate salts are relatively soluble, if dissolved in water they would form high salinity brines stable as liquid on the surface of Mars (e.g., on grain boundaries) at temperatures as low as ~210 K with appropriate concentrations of water and Cl (Brass, 1980).

A.2.2. Pathfinder rover

Pathfinder APXS analyses were more extensive than those of Viking and showed that Mg-S-rich materials are found in soils, cements, rocks and dust in the atmosphere (Bell et al., 2000; Bruckner et al., 2001; Foley et al., 2001; McSween and Keil, 2000; Morris et al., 2000;

Rieder, 1997). Morris et al. (2000) showed that Pathfinder rocks and soils are consistent with two-component mixtures of andesitic rock with low MgO and SO₃ concentrations and a global soil of basaltic composition with high MgO and SO₃.

Endmember models proposed to explain the S-rich nature of Mars' surface as seen by both Viking and Pathfinder include high-temperature volcanic gases (“acid fog”) and hydrothermal fluids (Banin et al., 1997; Catling, 1999; Morris et al., 2000; Newsom et al., 1999). Newsom et al. (1999) proposed that hydrothermal systems on Mars could be described by two endmember fluid types: (1) neutral chloride fluids with high Cl and Na contents but low S/Cl ratios, and (2) acid-sulfate fluids with high S/Cl ratios and significant vapor transport, consistent with the low water abundance on Mars. A model combining these two types of fluids can account for the abundances of S, Cl, and other mobile elements in martian soil (Newsom et al., 1999).

A.2.3. MER rovers

The MER rovers did not deploy a single instrument for definitive mineralogy, but the combined instrument suite provides appropriate information to identify mineral groups. Data from both Spirit and Opportunity indicate several types of sulfate minerals, but have not detected sulfides. Sulfate minerals are inferred by correlating APXS-derived SO₃ and major cation contents (accounting for silicates and oxides), Mössbauer spectroscopy (definitive peak intensities and peak velocity splitting), visible and near-infrared (VNIR, Pancam) spectra and/or thermal emission infrared (Mini-TES) spectra. In the near-infrared, sulfates are detected based on a range of features (e.g., polyhydrated sulfates with broad bands at 1.9–2.0 μm and 2.4 μm; monohydrated sulfates with a broad ~2.1 μm band; Bishop et al., 2009; Gendrin et al., 2005; Murchie et al., 2009a). In the thermal infrared, sulfate minerals exhibit a range of diagnostic absorption features (Lane, 2007; Lane et al., 2007) with the main ν₃ stretch of SO₄²⁻ near ~8.8–8.9 μm (~1120–1140 cm⁻¹) and a range of ~8.2–9.3 μm (~ 1070–1220 cm⁻¹).

Meridiani Planum – Jarosite was the first sulfate mineral detected with the Opportunity rover, in iron oxide-rich sedimentary rocks at Meridiani Planum (Fig. 13). Identification of jarosite was made using both Mössbauer spectrometry (Fig. 13b) in combination with high sulfur contents determined from APXS (Klingelhofer et al., 2004; Morris et al., 2006) and Mini-TES spectra (Christensen et al., 2004c). Jarosite provides evidence for low-pH aqueous conditions or low water:rock during deposition (King and McSween, 2005; Madden et al., 2004). This suggestion is supported by the laminar nature of the sedimentary layering and crystal casts suggesting subsequent dissolution and precipitation of concretions/nodules (Fig. 13c). Zolotov and Shock (2005) proposed that the assemblage of jarosite-goethite-hematite at Meridiani Planum was formed by hydrothermal pyrite precipitation followed by oxidation of pyrite to form jarosite and goethite. Hematite formation would have been promoted by later heating and dehydration of goethite (Zolotov and Shock, 2005).

The nearby Burns Formation in Endurance Crater contains eolian sandstones (Fig. 14) with a suite of sulfate minerals that are thought to have formed through evaporation of brines and then modified diagenetically by periodic recharge (Grotzinger et al., 2005; McLennan et al., 2005). Chemical data (APXS) and spectral evidence indicate jarosite (~10% based on Mössbauer spectrometry), Mg-sulfate and Ca-sulfate (~18% and 10% respectively from Mini-TES) and possibly Na-bearing sulfates (Clark et al., 2005; McLennan and Grotzinger, 2008). The hydration states of the sulfates are unknown.

More recently, thick veins of Ca-sulfate (Fig. 7a) were identified at Endeavour Crater by the Opportunity rover (Squyres et al., 2012). A strong correlation is observed between Ca and S using APXS and PanCam spectra, which are most consistent with the hydrated Ca-sulfate, gypsum.

Gusev Crater – The most S-rich soils identified at Gusev Crater are the “Paso Robles class” soils (Fig. 15) that are inferred to contain Fe³⁺-, Mg-, and Ca-sulfates. The Fe³⁺-sulfates dominate, based on studies using Mössbauer, VNIR (with two different data-processing methods), Mini-TES, and APXS spectroscopies (Johnson et al., 2007; Lane et al., 2008). Ferricopiapite [Fe³⁺_{4.6}(SO₄)₆(OH)₂·20H₂O], (para)coquimbite [Fe³⁺₂(SO₄)₃·9H₂O] and fibroferrite [Fe³⁺SO₄(OH)·5H₂O] are proposed based on at least four spectral methods, and parabutlerite [Fe³⁺(SO₄)(OH)·2H₂O] and rhomboclase [(H₃O)Fe³⁺(SO₄)₂·3H₂O] are identified based on at least three methods (Johnson et al., 2007; Lane et al., 2008). Other possible minerals include hydronium jarosite [H₃O⁺Fe³⁺₆(SO₄)₄(OH)₁₂], bilinite [Fe²⁺Fe³⁺₂(SO₄)₄·22H₂O], butlerite [Fe³⁺(SO₄)(OH)·2H₂O], and metahohmannite [Fe³⁺₂(SO₄)₂O·4H₂O].

The Mini-TES instrument has also detected sulfates, most likely Ca-sulfates based on correlations between CaO and SO₃ (Ming et al., 2006), in the dust and in the classes of rocks called Clovis, Watchtower, and Wishstone at Gusev (Christensen et al., 2004b; Glotch et al., 2006; Ruff et al., 2006). The nearby Peace rocks are cemented by sulfates as evidenced from imaging, APXS chemistry and Mini-TES spectra (Ruff et al., 2006; Squyres et al., 2006).

A.2.4. Phoenix Lander

The Phoenix WCL detected soluble sulfate equivalent to $\sim 1.3 \pm 0.5$ wt% SO₄ in the soil (Kounaves et al., 2010). Fe-sulfates were ruled out at this site because cyclic voltammetry and pH data did not indicate their presence. K and Na concentrations were low and Mg-sulfates (and some Ca-sulfates) were most favored based on geochemical models and measured cation abundances (Kounaves et al., 2010). EGA measurements by TEGA revealed no SO₂ release up to 1000 °C, suggesting that the sulfate was present as Ca-sulfate, most likely anhydrite, rather than Mg-sulfate (Golden et al., 2009)

A.2.5. Curiosity Rover

Unambiguous identification of sulfur-bearing minerals *in situ* on Mars has only been achieved using the CheMin X-ray diffraction instrument aboard the MSL Curiosity rover (Blake et al., 2012). Prior to this mission, sulfates were strongly suggested based on bulk chemistry (XRF and APXS) and spectral evidence (Mössbauer and near- to mid-infrared spectroscopy). Based on the CheMin analyses from Gale Crater, anhydrite is the most common sulfate (Table 2). It is found in the Rocknest eolian sands (Blake et al., 2013). Anhydrite, bassanite and pyrrhotite were found at the John Klein and Cumberland sites (Table 2) in the Sheepbed mudstone at Yellowknife Bay (Vaniman et al., 2014) as well as the Windjana drill site in the Dillinger sandstone at Kimberley (Treiman et al., 2016). Several phases are at the limits of CheMin detection, including pyrite at John Klein (Vaniman et al., 2014) and bassanite at Windjana (Rampe et al., 2015). Possible jarosite (near the detection limit) is the only sulfur-bearing phase at the Confidence Hills, Telegraph Hills and Mojave2 drill sites in the Pahrump Hills member of the Murray Formation (Rampe et al., 2016) and may be present in trace abundance at Windjana (Treiman et al., 2016). The Buckskin drillhole in a mudstone member of the Murray Formation contains anhydrite (Morris et al., 2016). The Big Sky drill hole is located

outside an altered fracture zone in the Stimson unit (a cross-bedded sandstone) and contains anhydrite, while the Greenhorn drillhole is within the fracture zone and yields anhydrite and bassanite (Yen et al., 2016). A sulfur-rich X-ray amorphous material – that is, with either a grain size too small to produce X-ray diffraction peaks in the detected energy range or without any crystalline structure such as a glass – is detected in all solid materials analyzed (e.g., Bish et al., 2013; Blake et al., 2013; Morris et al., 2015; Morris et al., 2016; Vaniman et al., 2014).

Although the SAM instrument on Curiosity is unable to provide definitive detection of specific minerals, SAM is a valuable complement to CheMin through its ability to observe sulfur-bearing phases in solid samples that may be present below the CheMin detection limit (McAdam et al., 2014; Sutter et al., this volume). SAM uses evolved gas analysis (EGA) protocols in which volatiles released through heating of solid samples in a pyrolysis oven are continuously sampled by SAM's quadrupole mass spectrometer. The temperature at which gases evolve provides information about possible mineral sources within the sample (Fig. 16). SAM has identified evidence supporting both oxidized and reduced forms of sulfur in Gale crater (Fig. 16), with possible sources including Fe-sulfides as well as Fe-, Mg- and Ca-sulfates (McAdam et al., 2014; Ming et al., 2014). Sulfite salts (S^{4+}) such as Ca-sulfite are also consistent with SO_2 evolution temperatures in some SAM experiments (McAdam et al., 2014). Sulfites have been proposed as potential sulfur-bearing phases at the martian surface (Halevy et al., 2007) but have not yet been definitively identified by mineralogical instruments. See Sutter et al. in this volume for more detailed discussion of SAM results.

B. Sulfur minerals in martian meteorites

B.1. Sulfides in martian meteorites

Sulfides constitute up to 1 wt% of the martian meteorites and include troilite (FeS), pyrrhotite (FeS_{1-x}), pyrite (FeS_2), rare chalcopyrite and/or cubanite, pentlandite, troilite-pentlandite-chalcopyrite intergrowths or pyrrhotite-pentlandite blebs (Fig. 17). In some cases, marcasite occurs as an alteration mineral. Most sulfides are located near rims of pyroxene, in interstitial mesostasis, or in melt inclusions (Fig. 17 a-b) indicating that sulfur is enriched in the late-stage magmatic liquids. Sulfides are also present as blebs in shock glasses or as veins in minerals associated with shock (Fig. 17 c-f) and these are discussed separately below.

The shergottites range from the least evolved Iherzolites (highest Mg#) through picritic basalt and basalt (lowest Mg#), where $Mg\# = 100Mg/(Mg+Fe)$ on a molecular basis. As the rocks become more evolved, the sulfides have lower pentlandite/pyrrhotite, and Ni content decreases in pyrrhotite (Balta et al., 2015; Grott et al., 2013; Lorand et al., 2005). These findings are interpreted to indicate that the sulfides are co-magmatic and that sulfide melts segregated as the silicate melt differentiated (Grott et al., 2013; Lorand et al., 2005). In the LAR 06319 olivine-phyric shergottite, Ni and Co contents increase from troilite to pyrrhotite to pyrite, which provides evidence for pyrite formation from late-stage oxidation and/or sulfurization of pyrrhotite (Basu Sarbadhikari et al., 2009).

NWA 7533 and its pairs represent a singular example of a meteorite derived from martian regolith breccia (Agee et al., 2013; Humayun et al., 2013; Lorand et al., 2015). NWA 7533 is also unique in containing accessory pyrite of up to 1 wt%, in contrast to the dominance of pyrrhotite in most martian meteorites (Lorand et al., 2015). This pyrite has unusually high Ni contents of up to 4.5 wt%, which Lorand et al. (2015) interpret to indicate crystallization of

pyrite from S-rich hydrothermal fluids that percolated through the breccia billions of years after breccia formation.

The nakhlites and chassignites, which have similar magmatic ages of ~1.3 Ga (Nyquist et al., 2001), are depleted in sulfur relative to the shergottites (Burgess et al., 1989; Chevrier et al., 2011; Ding et al., 2015; Franz et al., 2014a; Gibson, 1983; Gibson et al., 1985; Lorand et al., 2012; Mikouchi et al., 2003; Mikouchi et al., 2006). In the phase-specific extractions by Franz et al. (2014), sulfur was recovered predominantly as sulfate from these meteorites, despite observations of pyrrhotite or pyrite in petrographic sections of nakhlites (Imae and Ikeda, 2007; Imae et al., 2005; Mikouchi et al., 2003; Rochette et al., 2005) and Chassigny (Floran and Prinz, 1978). Some magmatic sulfides may have been oxidized to sulfate during weathering on Mars, in terrestrial environments prior to meteorite recovery, or even in curation. Observation of S-MIF signatures in magmatic pyrrhotite of nakhlites as well as some shergottites indicates that these sulfides formed from sulfur that had been processed in the martian atmosphere and incorporated into magmas after surface deposition (Farquhar et al., 2000; Franz et al., 2014: Sections 2.6 and 2.7). Pyrites in the ALH 84001 and Chassigny meteorites are interpreted as secondary alteration products (Franz et al., 2014a; Greenwood et al., 2000).

Several martian meteorites contain regions with unusually high sulfur contents in shock glass pockets and veins (Fig. 17 c-f). The Tissint meteorite has significant concentrations of sulfide blebs in shock glass (Fig. 17 c-d), with up to 6000 ppm S (Aoudjehane et al., 2012). The Elephant Moraine A (EETA) 79001 lithology C (EETA 79001C) contains <22 wt% SO₃ as small vesicular pyrrhotite blebs, veins of mobilized pyrrhotite in shocked minerals, and sulfur dissolved in shock glasses (Fig. 17 e-f) (Barrat et al., 2014; Schrader et al., 2011; Walton et al., 2010). Interestingly, shock glasses in Shergotty glasses (a meteorite “find”) may have pyrrhotite blebs, but some S-bearing glasses with the highest SO₃ (~3 wt%) contain Ca-sulfate crystals (Rao et al., 2008). In the case of all three meteorites, the sulfur in the shock glasses may be derived from preferential mobilization of Fe-sulfide from the target rock into the impact glass (Barrat et al., 2014; Walton et al., 2010), incorporation of secondary sulfates from the Martian regolith into the impact melt (Rao et al., 2012; Rao et al., 2008), or, in the case of Tissint, desert weathering (Barrat et al., 2014).

The shock imparted by impact may also have resulted in sulfur devolatilization that converted pyrrhotite to troilite and metal alloys and may have eliminated Ca-sulfate in some meteorites (Lorand et al., 2012). For example, the chassignite NWA 2737 contains metal-saturated Fe-Ni sulfides with Fe/S of 1.0 ± 0.01 , suggesting modification of primary magmatic pyrrhotites (Lorand et al., 2012). Changes in sulfide structures accompanying shock-induced sulfur degassing may also have resulted in loss of original magnetic properties in some meteorites (Lorand et al., 2012), analogous to the demagnetization of the martian crust in regions with high impact crater densities (Louzada et al., 2007; Rochette et al., 2005).

B.2. Sulfates in martian meteorites

Sulfides are readily weathered by fluids (even at low fluid/rock ratios), and they may form alteration products such as pyrite (FeS₂ – cubic) at higher temperatures, or marcasite (FeS₂ – orthorhombic) and sulfate minerals at lower temperature (e.g., King and McSween, 2005). Sulfate minerals may also form at high temperature from volcanic gas (Gooding, 1978; Settle, 1979) or reactions of SO₂ gases with minerals and glasses (Henley et al., 2015).

The martian meteorites “falls” (Shergotty, Zagami, Nakhla, Chassigny, and Tissint) are widely accepted to provide the best evidence for the primary sulfur mineralogy of the martian

crust because they are the least affected by terrestrial processes. Because Tissint is a recent fall, the other four falls have been studied much more extensively (Leshin and Vicenzi, 2006). The best characterized sulfate-bearing minerals from Mars are Ca-sulfates (Fig. 18 a-c), Mg-sulfates (Fig. 18d), jarosite (Fig. 18e) and K-(Na)-Fe-(phosphate)-sulfates (Fig. 18f). Calcium- and Mg-sulfates have been observed in the interiors of some martian meteorites (i.e. inside fusion crusts), suggesting that these secondary minerals formed on Mars (e.g., Bridges and Grady, 2000; Gooding et al., 1991; Treiman et al., 1993; Wentworth and Gooding, 1994). Iron-bearing sulfates (some with Na, K, or P) have been identified in Martian meteorites (Gooding et al., 1991; Wentworth and Gooding, 1994), including jarosite [$\text{KFe}_3(\text{SO}_4)_2(\text{OH})_6$] trapped in a melt inclusion (Fig.18e, McCubbin et al., 2009).

Mass spectrometry combined with thermal analysis of the interior portions of the Nakhla meteorite as well as shergottites ALH 77005 and EET 79001 indicate that a significant fraction of SO_2 is evolved at high temperatures ($>\sim 800^\circ\text{C}$), which is consistent with sulfates (Gooding et al., 1990) and the observation of anhydrite in Shergotty shock glass (Rao et al., 2008). We note that Walton et al. (2010) only found reduced sulfur in EET 79001 samples that they analyzed. Oxidized sulfur was detected in other aliquots of EET 79001 glass (Sutton et al., 2008), but beam damage cannot be ruled out (cf. Metrich et al., 2009). More investigations of these shock glasses should better resolve the oxidation state of the dissolved sulfur.

Sulfates are especially labile due to their high solubility and the sensitivity of phase transitions to relative humidity and temperature (e.g., Hogenboom et al., 1995; Vaniman et al., 2004; Wang et al., 2011; Wang et al., 2009); therefore, it is necessary to document textural features, age, and isotopic signatures, which can provide evidence in support of a martian origin (e.g., Leshin and Vicenzi, 2006). Unfortunately, the original hydration state of most of these sulfates (except jarosite) is unknown. For this reason, particular care must be made in analyzing many sulfate minerals (e.g., Hyde et al., 2011). In the case of the martian meteorites, it is possible that primary sulfates are hydrated on Earth, which would result in ambiguous, disrupted textures (cf. Orgueil meteorite; Gounelle and Zolensky, 2001) because the hydrated forms of sulfate tend to have higher molar volumes.

B.3. Other sulfur-bearing minerals detected in martian meteorites

Sulfur-rich aluminosilicates were observed in shergottite sample EET 79001 (Fig. 18g) by Gooding and Muenow (1986). The aluminosilicates were tentatively identified as amphiboles, but they contain up to 3 wt% SO_3 , making it more likely that the beam volume overlapped glass underlying a sulfate mineral.

Alteration minerals rich in sulfur were identified in the Lafayette meteorite, a nakhlite (Treiman et al., 1993). Again, the exact host of the sulfur is unknown: sulfur may be adsorbed to phyllosilicates, present as a substituent in smectite or ferrihydrite, or perhaps present as gypsum. Similarly, sulfur is found in association with iddingsite (<0.69 wt% SO_3) and carbonate (<0.26 wt% SO_3) alteration minerals in Shergotty, although the exact host is unknown (Rao et al., 2008). More analyses, preferably with higher lateral resolution techniques such as transmission electron microscopy, would help determine the host phase for the sulfur.

C. Remote sensing observations

C.1. Gamma Ray Spectrometry

The Mars Odyssey Gamma Ray Spectrometer (GRS) detects element abundances in approximately the upper few decimeters of the martian surface (Boynton et al., 2004). The average GRS sulfur abundance is 1.76 wt% ($\text{SO}_3 = 4.4$ wt%) (McLennan et al., 2010), although the values vary widely (Fig. 19a) due to the variable nature of the surface materials (e.g., dust vs. bed rock). Hot spots in sulfur content (~ 3 wt%) are observed in the region surrounding Gale Crater, an area near Nakong Vallis and the western Vallis Marineris catchment (Fig. 19a). As noted above, S-rich veins and infill have been detected at Gale Crater with ~ 40 wt% SO_3 (Fig. 6, 9-11), and such materials would undoubtedly contribute to the detected GRS sulfur content.

The lower average sulfur abundance determined by the GRS, compared to average soils measured in situ, constrains the relative distributions of soil and igneous bedrock exposed at the surface. Overall, these findings are consistent with the observation that sulfur has been extensively transported, deposited and remobilized across the martian surface in dust, veins and infill.

C.2. Spectral detection of sulfate minerals from Earth

The first remote measurements suggesting sulfates were present on Mars were made of dust in the atmosphere using Earth-based telescopes (Bell et al., 1994; Blaney and McCord, 1995). These studies examined infrared spectra of Mars at wavelength ranges encompassing absorption features characteristic of certain minerals, including sulfates, carbonates, and hydrated silicates. Comparison with terrestrial infrared spectral libraries indicated the presence of sulfates, carbonates (or bicarbonates) and oxides on the martian surface and/or in atmospheric dust, providing confirmation that the bulk sulfur chemistry measured by Viking was best explained by oxidized sulfur.

C.3. Spectral detection of sulfate minerals from orbit around Mars

Infrared spectrometers deployed on orbiters around Mars provide information in both the thermal and visible to near-infrared parts of the electromagnetic spectrum. Note that spectra at the wavelength range employed by these instruments are typically sensitive to surficial composition to depths of a few tens of micrometers at most, as opposed to gamma ray spectrometer instruments capable of detecting elemental abundances to depths of a few decimeters (Boynton et al., 2004). Inferred mineralogy of stratigraphic sections, such as Candor Mensa shown in Fig. 20, are thus based on the spectra of phases on exposed surfaces of the section and may reflect weathering that affected the uppermost layer of minerals but not the entire stratigraphic layer. Below, we summarize the primary results from each of the remote sensing instruments in sequence of the satellite's launch date.

C.3.1. Thermal infrared imaging spectrometers

(a) Thermal Emission Spectrometer (TES)

The Mars Global Surveyor was launched in 1996 and contains the Thermal Emission Spectrometer (TES) that detects signals in the thermal IR part of the spectrum (Christensen et al., 2001). This instrument collects spectra from known 3×6 km areas over the ~ 6 - 50 μm wavelength range. Data from TES confirmed that sulfates are present in the martian dust (Bandfield et al., 2003; Christensen et al., 2004b). Also, the 7.27 μm band was tentatively assigned to sulfate with TES and the relative band intensity has been mapped as shown in Fig. 19 (USGS, 2000). Interestingly, this work shows that 7.27 μm band is not related to large volcanic

provinces on Mars (Tharsis, Olympus Mons, Elysium), perhaps suggesting that any sulfur that was derived from volcanoes has been remobilised (Hoefen et al., 2003; Hoefen et al., 2000).

(b) Thermal Emission Imaging System (THEMIS)

Mars Odyssey, launched in 2001, carries the Thermal Emission Imaging System (THEMIS), which has primarily been used to identify minerals and to determine thermal inertia (Christensen et al., 2004a). The instrument collects images over seven bands in the 6.7 – 14.8 μm wavelength range and 100 x 100 m areas. The THEMIS spectrometer should be capable of detecting sulfates, but an intensive survey of putative martian paleolakes found no evidence for them, which suggested either high detection limits or that they are obscured by dust (Stockstill et al., 2005). In 2009, the Mars Odyssey moved to an earlier orbit time, to provide better detection of sulfates at warmer temperatures. The warmer, post-2009 THEMIS data do indicate sulfate minerals (Baldrige et al., 2013), although not always in the same location that has been identified by the Compact Reconnaissance Imaging Spectrometer for Mars (CRISM, below), possibly due to the spectral and lateral resolution of THEMIS, uncertainty in the diurnal temperature, and scattering effects from induration and particle size variations at the surface (Baldrige et al., 2013).

C.3.2. Visible/near infrared imaging spectrometers

In the last decade or so, visible/near-infrared spectrometers have collected a large volume of information on the location of sulfates on Mars. Sulfates have been identified in the Valles Marineris canyon system, Meridiani Planum, Terra Meridiani, Mawrth Valles, Gale Crater, Aram Chaos (Figs. 19C, 20, 21) and in the northern circumpolar dune fields and deposits (Fig. 21e). The majority of sulfate-rich rocks are coincident with areas rich in phyllosilicate-bearing rocks (Fig. 21e) (Bibring et al., 2007; Bibring et al., 2005; Bibring et al., 2006; Ehlmann and Edwards, 2014) and, in common with the TES data, the sulfate-rich areas are adjacent to volcanic provinces rather than closely associated with them (Michalski and Bleacher, 2013).

(a) Observatoire pour la Minéralogie, l'Eau, les Glaces et l'Activité (OMEGA)

The Mars Express satellite was launched in 2003 and it includes the Observatoire pour la Minéralogie, l'Eau, les Glaces et l'Activité (OMEGA) spectrometer. This instrument collects spectral images with resolution of 200-2000 m/pixel over the 0.4-5 μm wavelength range. OMEGA has been used to identify extensive deposits of kieserite, gypsum and an unidentified "polyhydrated sulfate" (Bibring et al., 2005; Gendrin et al., 2005; Roach et al., 2010) in Valles Marineris and surrounds. Also, elevated sulfate concentrations were identified in Aureum and Iani Chaos (Gendrin et al., 2005; Noe Dobrea et al., 2006a; Noe Dobrea et al., 2006b). In Candor Chasma (Fig. 20), kieserite occurs on steep, heavily eroded scarps overlying polyhydrated sulfates that formed on less eroded slopes. Iron oxides are typically associated with the sulfate-rich scarps and at the base of layered deposit scarps (Fig. 20b) (Bibring et al., 2007; Mangold et al., 2008). At Meridiani Planum and locations elsewhere, Hesperian sedimentary rocks have been identified with hematite and both polyhydrated and monohydrated sulfates, overlying clay-bearing, highly cratered Noachian units (Arvidson et al., 2005; Arvidson et al., 2006; Bibring et al., 2007; Gendrin et al., 2005; Roach et al., 2010; Wiseman et al., 2010). Jarosite and polyhydrated sulfate minerals are identified on the NE flank of Syrtis Major (Fig. 19c) and are interpreted to indicate hydrothermally altered basaltic flows (Mustard and Ehlmann, 2010), and jarosite and alunite have been proposed in the Terra Sirenum basins

(Swayze et al., 2008; Wray et al., 2011). An unusual $\text{Fe}^{3+}\text{SO}_4(\text{OH})$ is proposed to occur at Aram Chaos (Lichtenberg et al., 2010).

(b) Compact Reconnaissance Imaging Spectrometer for Mars (CRISM)

The Mars Reconnaissance Orbiter satellite, launched in 2005, contains the Compact Reconnaissance Imaging Spectrometer for Mars (CRISM) instrument (Murchie et al., 2009b). This instrument collects spectral images with resolution of 18-200 m/pixel over the 0.4-4 μm wavelength range. Murchie et al. (2009b) summarize an extensive inventory of sulfate minerals in different settings as follows: (1) *Meridiani-type layered deposits* host monohydrated or polyhydrated sulfates on top of cratered terrain, with common hematite-rich layers (e.g. Terra Meridiani and Aram Chaos; Fig. 19). (2) *Valles-type layered deposits* are dominated by polyhydrated sulfates overlying monohydrated sulfates and commonly form mounds or deeply eroded plateaus or infill chasmata. Some of these deposits include ferric oxides, oxyhydroxides, or hydrated sulfates (e.g., Valles Marineris, Juvente Chasma) (Bishop et al., 2009). (3) *Intracrater clay-sulfate deposits* have sulfate layers (e.g., gypsum, polyhydrated and monohydrated Mg/Fe-sulfates, jarosite, alunite, and szomolnokite) that are interbedded with phyllosilicate layers and exposed on crater walls (e.g. craters in Terra Sirenum) (Wray et al., 2011; Wray et al., 2009). The sulfates make up about 10% of the minerals present and are considered to have formed in lakes fed by groundwater, although the alunite may have a hydrothermal origin. (4) *Gypsum plains* are made of sandy material including gypsum and they are reworked into dunes, probably with other hydrated minerals (e.g., north polar erg and layered deposits) (Fishbaugh et al., 2007). (5) *Siliceous layered deposits* consist of jarosite associated with amorphous silica layers (e.g., plains surrounding Valles Marineris, Mawrth Vallis) (Farrand et al., 2009). The Nili Fossae region (Fig. 19c) also contains a range of sulfate minerals (Ehlmann et al., 2009).

2.6. Surface processes for sulfur

Although impactors may have provided some sulfur to the martian surface, most sulfur is ultimately derived from the martian mantle and transported to the surface at high temperatures through magmatic and hydrothermal processes (e.g., magmatic degassing, acid sulfate fumaroles, hot springs; King and McLennan, 2010). Redistribution at high temperatures can also occur via impact and possibly metamorphic processes (Fig. 22).

Geomorphic evidence indicates that sulfates are extensively remobilized through the sedimentary processes with water at low temperature on Mars' (near-)surface (Fig. 22; King and McLennan, 2010; McLennan and Grotzinger, 2008; Ming et al., 2008). Mechanical (or physical) plus chemical transport of sulfur occurs through sedimentary, hydrologic, glacial, eolian, impact and diagenetic processes with sulfur in solids (sulfate, sulfide, amorphous S-bearing material and possibly sulfur), gas phase (e.g., species in Fig. 5), or in solution. In these processes, sulfate minerals may undergo changes in grain size, density sorting, deliquescence, dissolution, evaporation, reaction, and crystallization. These surface processes produce the “basin type” assemblages of sulfates, including Ca- and Mg-sulfates and possibly Na- and Fe-sulfates.

Geochemical evidence from the laboratory, Earth and theoretical models indicates that sulfate minerals on Mars may vary, dependent on the starting composition of any solution, temperature, the other phases present, whether the system remains open or closed, adsorption and desorption reactions, and cation-exchange reactions. This area of research has received a huge

amount of attention that is well beyond the scope of this review, and the reader is referred to the following key publications: (Altheide et al., 2009; Arvidson et al., 2010; Bridges et al., 2001; Bridges and Grady, 2000; Bruckner et al., 2008; Burns, 1987, 1988; Burns and Fisher, 1990; Catling, 1999; Chevrier and Mathé, 2007; Chevrier and Altheide, 2008; Clark et al., 2005; Dehouck et al., 2012; King et al., 2004; King and McSween, 2005; Liu and Wang, 2015; Marion et al., 2008; McLennan et al., 2005; McLennan and Grotzinger, 2008; Ming et al., 2008; Ming et al., 2006; Rampe et al., 2016; Tosca and McLennan, 2006; Tosca et al., 2005; Wang et al., 2013a; Wang et al., 2011; Wang et al., 2006a; Wang et al., 2009; Wang et al., 2016; Wang and Ling, 2011; Wang and Zhou, 2014; Wilson and Bish, 2011; Xu and Parise, 2009; Xu et al., 2008).

The terrestrial sulfur cycle is dominated by biological processes that introduce large isotopic fractionations between sulfur phases (Canfield, 2001a). Due to the early emergence of sulfur-metabolizing microbes on Earth (Shen et al., 2001; Wacey et al., 2011) and the high abundance of sulfur on Mars, sulfur isotopes provide a key target in the search for martian biomarkers.

2.6.1. Importance of sulfates for hydrogen on Mars

Most sulfates contain H₂O and/or OH⁻ and may have total H₂O contents as high as 62 wt% (Wang et al., 2009), rendering them potentially some of the most water-rich minerals on Mars. Therefore, there is a strong link between water and sulfur transport on Mars (Fig. 22). Furthermore, sulfates serve to substantially decrease the freezing temperature of any solutions (Brass, 1980; Fairen et al., 2009; King et al., 2004), which allows liquid brines and films of liquid on grain boundaries to be stable to much lower temperatures than liquid water (<-60 °C). To understand the transfer of water on Mars, it is necessary to account for dehydration/hydration reactions among sulfates. Such reactions are common (Cloutis et al., 2007; Janchen et al., 2005), and hydration can be associated with large increases in molar volume (Peterson and Wang, 2006). Sulfate hydration reactions, such as those due to interlayer H₂O-loss from clays (Bish et al., 2003), may produce either higher-hydrate sulfates or amorphous gel-like materials (e.g., Chipera and Vaniman, 2007). Also, sulfates may dissolve if sufficient water is present (e.g., Elwood Madden et al., 2004 and Fig. 13c), or they may undergo cation exchange with clay minerals, even in relatively dry environments (Wilson and Bish, 2011). Sulfate stability depends on temperature, relative humidity, composition, and, for the Fe-bearing sulfates, the partial pressure of oxygen and pH (Brass, 1980; Chipera and Vaniman, 2007; Chipera et al., 2007; Chou and Seal, 2007; Fairen et al., 2009; Fialips et al., 2005; Hogenboom et al., 1995; King and McSween, 2005; Peterson and Grant, 2005; Peterson et al., 2008; Peterson and Wang, 2006; Tosca et al., 2005; Vaniman et al., 2004; Vaniman and Chipera, 2006; Wang et al., 2006a; Wang et al., 2009; Wang et al., 2006b; Wang et al., 2007). Because sulfates have such sensitive phase relations, they may be used to place constraints on environmental variables. In summary, sulfates play a key role in the formation of geomorphic and textural features on Mars, including some catastrophic outflow features and gullies (Chevrier et al., 2009), secondary pores/veins in sedimentary rocks, physical properties in the soils (e.g., clods), and formation of small-scale fracture/vein systems.

2.6.2. Age of the sulfates on Mars

The absolute age of sulfate deposition is a topic of debate, and it is probable that sulfate formed *both* (1) from the late Noachian to Early Amazonian (e.g., recent summary by Ehlmann

and Edwards, 2014) and (2) during episodic events that remobilized sulfur (King et al., 2004; McLennan and Grotzinger, 2008). Most studies of the age of sulfate deposition are based on remote sensing linked with geomorphological evidence and crater counting to determine the age of a surface. As indicated in section 2.5.C, sulfate minerals are closely associated with areas enriched in phyllosilicate minerals (Fig. 19c). Bibring et al. (2006) proposed that sulfates record a significant change in the past climate on Mars, specifically that the oldest Noachian terrains contained phyllosilicate minerals formed by pervasive aqueous alteration and that in the late Noachian to Hesperian, sulfates formed in an acidic environment. This environmental change is linked to the end of the heavy bombardment and the formation of major valley networks (Fig. 23) that transported saline solutions to basins where sulfates and chlorides precipitated (e.g., King et al., 2004; Bibring et al., 2006; Murchie et al., 2009b). This hypothesis agrees with subsequent work showing that sulfates occur most abundantly in areas of groundwater upwelling (Andrews-Hanna et al., 2007), including Terra Sirenum, Meridiani Planum, and Aram Chaos (Murchie et al. 2009a, Roach et al. 2010, Wray et al. 2011). After about 3 Ga, sulfates predominantly co-exist with silica, suggesting that they are most likely linked to volcanic and impact processes (Ehlmann and Edwards, 2014; Murchie et al., 2009b; Newsom et al., 1999). From the Amazonian onward, ferric oxides (hematite, magnetite, maghemite), oxyhydroxides (goethite) and hydroxides (ferrihydrite) dominate the surface of Mars, which is interpreted to indicate the occurrence of a drying process, co-incident with geomorphic evidence for only episodic water flow.

Despite remote sensing data indicating drying, a number of martian meteorites contain sulfate and/or sulfide with mass-independent ^{33}S anomalies (i.e., non-zero values of $\Delta^{33}\text{S}$, Section 1.2), indicating the presence of sulfur that has been processed in Mars' atmosphere (Farquhar et al., 2000, 2007; Franz et al., 2014; Section 2.6.1). The largest $\Delta^{33}\text{S}$ anomalies have been observed in the nakhlite meteorites (magmatic age ~ 1.3 Ga), which contain both sulfate and magmatic sulfide minerals with negative $\Delta^{33}\text{S}$ (Farquhar et al., 2007; Franz et al., 2014). Thus, 1.3 Ga provides a maximum age constraint for fluids that exchanged sulfur with the atmosphere and then deposited sulfur-bearing minerals onto the surface prior to their assimilation into nakhlite parent magmas to form isotopically anomalous sulfides (Franz et al., 2014). However, some secondary sulfates in the nakhlites may have formed during later alteration events, suggesting episodic periods of water activity in the vicinity of the nakhlite parent rock as recently as ~ 600 - 650 Ma (Misawa et al., 2003; Swindle et al., 2000). In addition, the Lafayette and Chassigny meteorites, which both have magmatic ages of ~ 1.3 Ga, as well as shergottites dating to as recently as ~ 175 Ma, contain sulfates and/or sulfides with positive $\Delta^{33}\text{S}$ anomalies (Farquhar et al., 2000; Franz et al., 2014). This observation extends the possible window for sulfur exchange between the martian atmosphere and surface fluids to at least ~ 175 Ma (Franz et al., 2014).

2.7. Atmospheric sulfur

2.7.1. Atmospheric abundance of sulfur

Telescopic surveys focused on atmospheric trace gases have found no evidence for currently active sources releasing sulfur into the atmosphere, with the most recent observations establishing upper limits of 0.3 ppb (Encrenaz et al., 2011; Krasnopolsky, 2012) to 1.1 ppb

(Khayat et al., 2015) SO₂, 0.7 ppb SO, and 1.3 ppb H₂S (Khayat et al., 2015). Of these gases, SO₂ represents the best candidate in the search for active volcanism on Mars, because in addition to its expected dominance during magmatic degassing under current surface conditions, it has a photochemical lifetime of 600 days (Wong et al., 2005), compared to 9 days for H₂S and 4.6 hours for SO (Wong and Atreya, 2003; Wong et al., 2005). Given the global mixing timescale for the martian atmosphere of 0.5 year (Krasnopolsky et al., 2004), detection of H₂S or SO would probably require contemporaneous emission from multiple sources on Mars (Khayat et al., 2015) or one very large source.

2.7.2. Photochemical processing and isotopic fractionation of sulfur

Evidence for atmospheric processing of sulfur during Mars' past is found in the form of MIF isotopic signatures in sulfur-bearing phases of some martian meteorites (Farquhar et al., 2007b; Farquhar et al., 2000b; Franz et al., 2014a). These meteorites reveal the fingerprint of a S-MIF signature unique among solar system bodies and indicate that the photochemical mechanism for fractionation of sulfur isotopes on Mars was different from that of Earth (Franz et al., 2014a). Specifically, S-MIF signatures on Earth show a distinctive covariation between $\Delta^{33}\text{S}$ and $\Delta^{36}\text{S}$ (Farquhar et al., 2000a), while S-MIF signatures on Mars are characterized by variations in $\Delta^{33}\text{S}$ with near-zero values of $\Delta^{36}\text{S}$ (Farquhar et al., 2007b; Franz et al., 2014a). It is not yet clear whether this is due to differences in chemical composition or optical depth of the planets' atmospheres that affected UV shielding conditions for sulfur-bearing gases such as SO₂ and thus the wavelengths at which reactions occurred or to a difference in dominant sulfur-bearing species in the martian atmosphere compared to Earth (Franz et al., 2014a). If martian outgassed sulfur comprised a mixture of oxidized and reduced species, variations in the SO₂:H₂S ratio, for example, would be expected to produce variability in the S-MIF signature over time, as observed in Archean terrestrial rocks (Halevy et al., 2010). Due to differences in the isotopic fractionation produced during H₂S and SO₂ photochemistry (Farquhar et al., 2000b), the net S-MIF signature would reflect a combination of these processes (Halevy et al., 2010). The continuity in S-MIF signature observed in meteorites of ages ranging from ~4.1 Ga to ~175 Ma suggests that the dominant photochemical mechanism operating in the martian atmosphere remained constant throughout this time period, supporting continuity in the sulfur speciation of atmospheric gases over time (Franz et al., 2014a). Although sulfur in Mars' protoatmosphere may have been dominated by H₂S or S₂, modeling by Gaillard et al. (2013) indicated that volcanic emissions over the last 4 to 4.5 Ga should have contained mostly SO₂ due to the relatively low atmospheric pressure compared to Earth, suggesting SO₂ as the most likely reactant for S-MIF production (Franz et al., 2014a). Laboratory experiments to simulate potential processes on Mars that may have produced the S-MIF signature observed in martian meteorites have proven difficult due to low product yields that compromise measurements of $\Delta^{36}\text{S}$ in experiments investigating optically thin conditions (Franz et al., 2013). However, *ab initio* modeling of SO₂ photolysis suggests that primary absorption effects in an optically thin SO₂ atmospheric column may offer a feasible scenario for explaining the martian signature (Franz et al., 2013). Additional laboratory experiments with SO₂ and other sulfur-bearing species are needed to understand martian sulfur photochemistry more fully.

Fig. 24 depicts $\Delta^{33}\text{S}$ and $\delta^{34}\text{S}$ for martian meteorites found to date to carry S-MIF signatures (Farquhar et al., 2007b; Farquhar et al., 2000b; Franz et al., 2014a). If these signatures were generated by a single common mechanism in the atmosphere, the presence of both positive

and negative $\Delta^{33}\text{S}$ signals among the meteorites indicates that different photochemical products must have followed different preservation pathways leading to surface deposition. Otherwise, recycling reactions in an oxidizing atmosphere would have favored ultimate homogenization of all products as sulfate and removal of the S-MIF signal (Pavlov and Kasting, 2002). S-MIF signatures are present in both oxidized and reduced phases of the meteorites, including igneous sulfides that provide evidence for assimilation of atmospherically-processed sulfur into magmas (Farquhar et al., 2007a; Farquhar et al., 2000b; Franz et al., 2014a).

Interestingly, regardless of oxidation state, the $\Delta^{33}\text{S}$ in sulfur phases of ALH 84001 and most nakhlites is negative, while all shergottites carrying S-MIF so far have shown positive $\Delta^{33}\text{S}$. The reason for this difference is uncertain, but the presence of sulfate with positive $\Delta^{33}\text{S}$ in Lafayette, in contrast to the other nakhlites analyzed to date, as well as Chassigny, with similar crystallization age to the nakhlites, may argue against a simple temporal explanation for the shift (Franz et al., 2014a). It is possible that the distinct signs observed in $\Delta^{33}\text{S}$ provide evidence tracing preservation of separate photochemical products in the meteorites in different proportions. The schematic diagram in Fig. 5, following that of Johnson et al. (2009), shows atmospheric reactions relevant to sulfur cycling and deposition. Based on their modeling results, Johnson et al. (2009) concluded that under weakly reducing conditions that may have existed on ancient Mars, sulfur could have been deposited in a variety of oxidation states, from elemental sulfur or sulfate aerosols or through rainout of SO_2 . The specific chemical pathways and dominant species deposited at the surface were found to be highly sensitive to other model parameters, especially atmospheric water abundance. Modeling of the Archean terrestrial sulfur cycle by Halevy et al. (2010) indicated sensitivity of the S-MIF signature to the partial pressure of CO_2 , primarily through its effect on surface temperature and the acidity of water reservoirs involved in S-MIF preservation. Although there were significant differences between the ancient terrestrial and martian atmospheres that prohibit application of terrestrial models directly to Mars, it is possible that episodic variations in local or global CO_2 abundance as a result of volcanic activity may have affected martian S-MIF preservation.

Ueno et al. (2009) proposed another potential mechanism for affecting the sign of $\Delta^{33}\text{S}$ preserved in Archean sulfate, which may also be relevant to Mars. Through *ab initio* modeling of SO_2 photolysis in the presence of various overlying UV absorbers, they determined that OCS could build up in a reducing atmosphere and produce a UV shielding effect that influenced the nature of S-MIF signal preserved in sulfates (Ueno et al., 2009). This topic deserves further attention of modeling and experimental efforts.

3. Sulfur and the martian climate

The process for depositing atmospheric sulfur onto the surface is intimately tied to the martian climate through the greenhouse effect exerted by sulfurous gases. The existence of geomorphological features (Carr and Head, 2010) and hydrated minerals (Bibring et al., 2005; Bibring et al., 2006; Ehlmann et al., 2011; Murchie et al., 2009b; Poulet et al., 2005) indicating past activity of liquid water has led to extensive debate about the nature of Mars' early climate and whether these features necessarily imply warm, wet conditions in the past or if they were carved by episodic outflows of groundwater on a cold planet (Baker, 1978; Carr, 1983; Gulick and Baker, 1989; Peale et al., 1975; Squyres, 1984; Wallace and Sagan, 1979). Questions pertinent to warm, wet scenarios include whether such conditions prevailed persistently (Pollack et al., 1987; Postawko and Kuhn, 1986; Ramirez et al., 2013; Sagan and Mullen, 1972; Toon et

al., 1980) or for discrete intervals of time (Halevy and Head, 2014; Johnson et al., 2008; Johnson et al., 2009; King et al., 2004; Squyres and Kasting, 1994), and whether they were achieved globally or in isolated geographical regions (Mischna et al., 2013). Attempts to explain warm, wet conditions through a CO₂ atmosphere alone (Kasting, 1991) have proven difficult, especially given a “faint young sun” with reduced luminosity early in solar system history (Gough, 1981; Sagan and Chyba, 1997). Therefore, various trace gases have been proposed as contributors to a greenhouse effect that warmed surface temperatures above the freezing point of water or brines (Halevy et al., 2007; Hirschmann and Withers, 2008; Johnson et al., 2008; Johnson et al., 2009; Mischna et al., 2013; Postawko and Kuhn, 1986; Ramirez et al., 2013; von Paris et al., 2013).

Both SO₂ and H₂S figure prominently in the list of candidate martian greenhouse gases, due to their absorption in the infrared (Haberle, 1998) as well as their potential presence in volcanic gases, as discussed above. Attempts to model the effects of these gases on the martian climate have produced a range of conflicting conclusions regarding their warming capacity. Early efforts using a 1-D annually averaged model suggested that 1000 ppmv of SO₂ could generate up to 8 – 10 K of warming in a dry 500 mb CO₂ atmosphere, insufficient to reach a global average temperature above the 273 K needed for stability of liquid water, but possibly high enough to enable the existence of brines (Postawko and Kuhn, 1986). Yung et al. (1997), applying a similar model, suggested that SO₂ could have significantly warmed the middle atmosphere of early Mars, inhibiting CO₂ condensation that would produce a cooling effect (Kasting, 1991). Their calculations showed that the addition of 0.1 ppmv of SO₂ to a 2 bar CO₂ atmosphere would produce ~10 K of warming in the middle atmosphere, raising surface temperatures to ~276 K and ensuring that the upper atmosphere remained above the condensation temperature of CO₂. In addition, they suggested that such abundance of SO₂ in the atmosphere could have served as an effective UV shield for an early martian biosphere (Yung et al., 1997).

Halevy et al. (2007) proposed that in an oxidant-limited system, outgassing of H₂S and SO₂ in approximately equal proportions during emplacement of the Tharsis province would have warmed the surface sufficiently to allow liquid water to exist. They implemented a model of early martian carbon and sulfur cycles featuring an ocean covering ~30% of the planet. Volcanic emissions of CO₂, SO₂, and H₂S were countered by formation of carbon and sulfur-bearing minerals. Dissolution of SO₂ (S⁴⁺) into surface waters would have promoted acidic surface conditions, favoring precipitation of Ca-sulfite and inhibiting formation of Ca-carbonate. Exhaustion of the oxidant supply would have allowed buildup of SO₂ to levels of a few ppm to several hundred ppm near the surface. A climate feedback involving SO₂ would result, in which an increase in supply of volcanic SO₂ caused atmospheric *p*SO₂ and thus temperature to rise, raising rates of weathering reactions and SO₂ removal by sulfite precipitation. The large reservoir of dissolved S⁴⁺ would buffer atmospheric SO₂ and stabilize surface temperatures. The partial pressure of CO₂ would have increased gradually up to a critical point at which the combined radiative effect of CO₂ and SO₂ allowed liquid water at the surface. Later alteration processes may have oxidized sulfite to sulfate after cessation of volcanic activity and a return to cold, more oxidized conditions (Halevy et al., 2007).

More recent modeling work has focused on SO₂ based on its longer photochemical lifetime (Wong and Atreya, 2003; Wong et al., 2005), pathways favoring atmospheric oxidation of H₂S to SO₂, and estimates that SO₂ was actually the dominant sulfur species outgassed under conditions prevalent during most of Mars’ history (Gaillard et al., 2013; Gaillard and Scaillet, 2009). Johnson et al. (2008) explored scenarios for pulsed degassing of sulfur volatiles into atmospheres with background of 50 and 500 mb CO₂ and H₂S and SO₂ mixing ratios from 10⁻³ to 10⁻⁶. Using

the Mars Weather Research and Forecasting (MarsWRF) general circulation model, they investigated the greenhouse effect produced by this range of sulfur abundances with variable water mixing ratios. Their results suggested that the pulses of sulfur gases alone could have generated surface warming of up to 25 K above a CO₂ atmosphere. With the addition of a water vapor feedback, the surface temperature could have reached a point where brines and possibly transient liquid water could exist (Johnson et al., 2008).

Johnson et al. (2009) further explored scenarios for an ancient martian atmosphere with pressures of 500 mb CO₂ and 100 mb or 6 mb N₂ through adaptation of a 1-D photochemical model previously developed for sulfur cycling on the Archean Earth (Pavlov and Kasting, 2002). Water vapor was controlled by temperature within the troposphere such that it remained beneath saturation pressure, and precipitation constraints were based on extremely arid conditions of the Atacama Desert in Chile, which was taken as a suitable analogue for Mars. The lifetime of SO₂ in the atmosphere was controlled by the relative efficiencies of removal as S₈ or sulfate aerosols or through SO₂ rainout. Results of their simulations showed that SO₂ could persist for much longer time periods than previously assumed under weakly reducing conditions, reaching *e*-folding times on the order of hundreds of years for SO₂ mixing ratios of 1 to 100 ppmv, with rainout as the dominant removal mechanism (Johnson et al., 2009).

Tian et al. (2010) questioned the results of Halevy et al. (2007) and Johnson et al. (2008, 2009), suggesting that the greenhouse warming produced by 1 to 100 ppmv SO₂ in atmospheres with 0.5 to 3 bar CO₂ and baseline surface temperatures of 235 K would have been more than offset by a cooling effect due to Rayleigh scattering by elemental sulfur and sulfate aerosols. In contrast to the work of Johnson et al. (2009), Tian et al. (2010) assumed zero dry deposition or rainout for SO₂, and terrestrial rates of rainout for other gases and aerosols. The lack of rainout as a removal mechanism for SO₂ in their model would increase its lifetime in the atmosphere and allow more buildup of aerosols, enhancing the radiative cooling effect (Tian et al., 2010). Tian et al. (2010) concluded that any transient warming effects would prevail only for months, not years.

Mischna et al. (2013) followed up on the work of Johnson et al. (2008) using the same MarsWRF GCM with improvements in the radiation code. They point out that while the current martian climate is controlled primarily by changes in obliquity, with minimal effect from volcanically-generated greenhouse gases, the reverse was likely true during the Noachian when the Tharsis province developed. During an extensive transitional period between these two extremes, obliquity may have served as a switch that initiated transitions between cold/dry and warm/wet periods (Mischna et al., 2013). Mischna et al. (2013) applied their modified GCM model to a range of obliquity conditions, but with the same atmospheric conditions assumed by Johnson et al. (2008). Their results showed that the presence of water vapor and SO₂ in the atmosphere did not produce warm periods globally, but rather that localized environments experienced warm conditions for brief time periods. Notably, the water cycle was influenced by obliquity cycles such that when obliquity decreased, atmospheric water vapor abundance dropped sharply and the atmosphere became incapable of sustaining warm temperatures anywhere but in limited equatorial regions and only for very short time periods. Similar to the finding of Johnson et al. (2008), however, a trace gas was necessary to trigger sufficient warmth initially to allow widespread sublimation from surface water reservoirs. The greenhouse effect of water alone was moderate and generally insufficient to maintain warm temperatures through the diurnal cycle. Mischna et al. (2013) also note that they had to reduce planetary albedo in their model to obtain perpetually warm temperatures, which could be reached by the presence of a dark liquid water ocean or widespread occurrence of low-albedo rock at the surface in earlier

periods. Since they neglected the formation of water clouds and sulfur aerosols in their model, which would have had a cooling effect, Mischna et al. (2013) acknowledged that their results represent an optimistic estimate for the plausibility of liquid water on Mars.

Halevy and Head (2014) investigated the climatic effects of brief, intense volcanic eruptions on Mars using a microphysical aerosol model. Their study focused on post-Tharsis volcanism that produced extensive basaltic plains covering over 30% of the planet's surface. Evidence suggests that the basalts were formed through a series of brief eruptions with extremely high effusion rates that were separated by quiescent periods lasting thousands of years, analogous to those responsible for generating continental flood basalts on Earth (Head et al., 2002; Head et al., 2006; Self et al., 2006; Tanaka et al., 2014). Effusion rates during these eruptive episodes are estimated to be more than 1000 times higher than those associated with the earlier formation of the Tharsis province (Wilson et al., 2001). Based on the higher sulfur content of martian magmas compared to terrestrial magmas and the much greater areal extent of the basaltic plains on Mars compared to continental flood basalts, Halevy and Head (2014) estimate that transient sulfur outgassing rates up to a few thousand times the global terrestrial average were likely during emplacement of the martian plains. The microphysical model employed for their study tracked populations of both homogeneous H₂O-H₂SO₄ aerosols and H₂SO₄-coated dust. They found that higher SO₂ abundances produced during volcanic episodes generated net positive radiative forcing up to 27 W/m², despite formation of H₂SO₄-bearing aerosols (Halevy and Head, 2014). Halevy and Head (2014) attributed this to the physical properties of some aerosols comprising moderately absorptive dust cores with reflective H₂SO₄ coating of variable thickness, as well as the background load of atmospheric dust, which offset the cooling effect due to scattering. Punctuated episodes characterized by high SO₂ emissions allowed higher transient concentrations of SO₂ than would be possible with lower, long-term outgassing rates and generated peak daily temperatures at low latitudes exceeding 273 K for several months of the year (Halevy and Head, 2014). The duration of warm episodes was limited to tens or hundreds of years following volcanic events, with cold, dry conditions prevailing during intervening quiescent periods (Halevy and Head, 2014). Melted ice and snow at low latitudes during warm periods may have mobilized soluble sulfate and transported it to low-lying regions (Halevy and Head, 2014).

Kerber et al. (2015) revisited the question of SO₂ greenhouse with the Laboratoire de Météorologie Dynamique Generic GCM and investigated sensitivity of results to SO₂ and H₂O mixing ratios, background atmospheric pressure, and the abundance, size and composition of aerosols. They concluded that the presence of aerosols of realistic physical dimensions even in minute quantities has a pronounced cooling effect, rendering SO₂ incapable of producing sustained greenhouse conditions on early Mars (Kerber et al., 2015). Their model predicted local temperatures above 273 K only for transient periods with CO₂ pressures above 500 mb, extremely high SO₂ mixing ratios above ~100 ppmv, and an absence of aerosols. Less SO₂ may have been required at higher pressures, which may have produced an increase in temperature, but would have also decreased the total abundance of sulfur gases and raised the ratio of H₂S, a less efficient greenhouse gas, to SO₂ (Gaillard and Scaillet, 2009; Kerber et al., 2015).

Kerber et al. (2015) highlighted several areas of uncertainty that plague modeling efforts. Results of climate models are very sensitive to pressure, but the pressure of the early martian atmosphere is poorly constrained, with values from 100 mb (Postawko and Kuhn, 1986) to 4 bars (Tian et al., 2010) appearing in the literature. Both pressure and the redox state of the atmosphere affect the species of sulfur-bearing species outgassed by volcanoes (Gaillard and Scaillet, 2009),

and the redox state further affects reaction networks in the atmosphere (Kerber et al., 2015). The outgassing rate of sulfur is also critical in determining the strength of any SO₂ greenhouse effect and the rate of aerosol formation (Kerber et al., 2015), which also depends on the partial pressures of other gases such as CO₂ and H₂O. As we have already discussed, the effusion and outgassing rates may have differed between volcanic events associated with the formation of the Tharsis province and the basaltic plains that were emplaced later (Halevy and Head, 2014). Details of Mars' past hydrologic cycle, including effects of high weathering rates of the mid-Noachian, the valley networks that arose in the late Noachian and early Hesperian, and the existence of pure water as opposed to brines, should also be considered in the evaluation of SO₂ greenhouse potential (Kerber et al., 2015).

4. Future directions

Current research seeks to synthesize information about martian sulfur from all available sources to enable better understanding of the processes that have mobilized sulfur between different reservoirs and chemical phases throughout Mars' history. In particular, future work is needed to account for multiple brine compositions possible on Mars and the processes by which sulfate has been remobilized and redeposited (e.g., King and McSween, 2005; Tosca et al., 2005).

Sulfates have high potential to preserve biomarkers and paleoenvironmental conditions since they may be rapidly precipitated from a brine (e.g., Foster et al., 2010; Rouchy and Monty, 1981) and impurities in sulfate crystals can form a barrier to radiation (Aubrey et al., 2006; Hughes and Lawley, 2003). Furthermore, laboratory experiments at near-equatorial martian surface temperature and relative humidity suggest that co-existence with smectites may extend the stability field of hydrated Mg-sulfate minerals and improve the prospects of biomarker preservation within sulfate crystals (Wilson and Bish, 2012). Analog studies on Earth show that biological material is commonly trapped in fluid inclusions or along grain boundaries (Foster et al., 2010). Future work is needed on examining how halophilic bacteria, Archaea and their genetic lineages respond to conditions like those on Mars.

In addition to the potential for preservation of organic compounds as biomarkers within sulfate minerals, sulfur isotope ratios may function directly as biomarkers (e.g., Canfield, 2001a; Thode et al., 1953) and thus are of prime interest from an astrobiological perspective. Sulfur is one of the six elements essential to all known life forms on Earth and is incorporated into a variety of biochemically relevant compounds, including amino acids, enzymes, and proteins (Clark, 1981). Its role in biomarker generation is most closely associated with energy production, in which sulfur is cycled through redox reactions that typically produce sulfide isotopically depleted compared to sulfur of higher valence states (Canfield, 2001a). For example, dissimilatory sulfate reduction introduces fractionations of 30 to 50‰ between sulfide and sulfate (Canfield, 2001b; Kemp and Thode, 1968). The difference in $\delta^{34}\text{S}$ of sulfide and sulfate may grow to even larger values through successive redox reactions by consortia of sulfur-metabolizing microbes (Canfield, 2001a).

Sulfur isotope ratios provide biomarkers for some of the earliest life to emerge on Earth, with evidence for sulfate reduction dating back to ~3.47 Ga (Shen et al., 2001) and sulfide oxidation to ~3.4 Ga (Wacey et al., 2011). In extant life on Earth, we observe the versatility of sulfur metabolisms and their pervasiveness in a range of extreme environments, such as deep seafloor basalt (e.g., Lever et al., 2013; Orsi et al., 2016; Turchyn et al., 2016), geothermal

springs and hydrothermal vents (e.g., Elsgaard et al., 1994; Frank et al., 2015; Kamyshny et al., 2014; Lin et al., 2016; Topcuoglu et al., 2016), perennially cold habitats (e.g., Knoblauch and Jorgensen, 1999; Konneke et al., 2013; Lamarche-Gagnon et al., 2015; Sagemann et al., 1998; Sattley and Madigan, 2010), and highly saline environments (e.g., Benison and Bowen, 2013; Blum et al., 2012; Johnson et al., 2015; Lamarche-Gagnon et al., 2015; Stam et al., 2010).

For all of these reasons, the possibility that sulfur-metabolizing microbes may have emerged on Mars at some point in history is of great interest to astrobiology. Assuming similarities between terrestrial and martian biota, sulfur isotopic biomarkers would be the most likely evidence of these life forms. The sulfur isotopic composition of sediments at Gale crater is a key target of investigations by the Curiosity rover's SAM instrument for this reason (Franz et al., 2014b). Identification of sulfur isotope biosignatures from *in situ* measurements such as these is complicated by other fractionation mechanisms, such as atmospheric photochemistry (see Section 2.7), that could produce similar values of $\delta^{34}\text{S}$. Analyses of martian sedimentary materials returned to Earth could provide additional means to distinguish between different sources of fractionation, such as the presence or absence of S-MIF signatures accompanying variations in $\delta^{34}\text{S}$.

For Mars sample return, improved methods are needed to prepare samples while avoiding contamination and modification of the mineralogy. Dependent on environmental conditions, sulfates may dissolve or react with water, exchange with clays, decompose in the presence of heat, react with organic material in epoxy (e.g., some sulfates), or decompose under vacuum. Delicate sulfates require preparation in specific conditions (e.g., under kerosene, H-free ethanol, etc.) and may require specific analysis steps (e.g., Fe-sulfates; Hyde et al., 2011). Understanding sulfate phase changes is critical for preparing transport devices for Mars sample return (King et al., 2008; MacPherson and II, 2005; McLennan et al., 2012; Vaniman et al., 2008).

By facilitating isotopic (S-MIF) analyses of sedimentary materials at a high level of precision currently achievable only in terrestrial laboratories, Mars sample return also promises an opportunity for significant growth in understanding martian sulfur photochemistry and interactions between the atmosphere and surface. Continued progress in improving technology for *in situ* measurements of sulfur isotope ratios, such as tunable laser spectrometry, may also allow future surface missions to contribute to this effort. These results in turn will help to tighten constraints on past martian atmospheric composition and climate.

Figure Captions

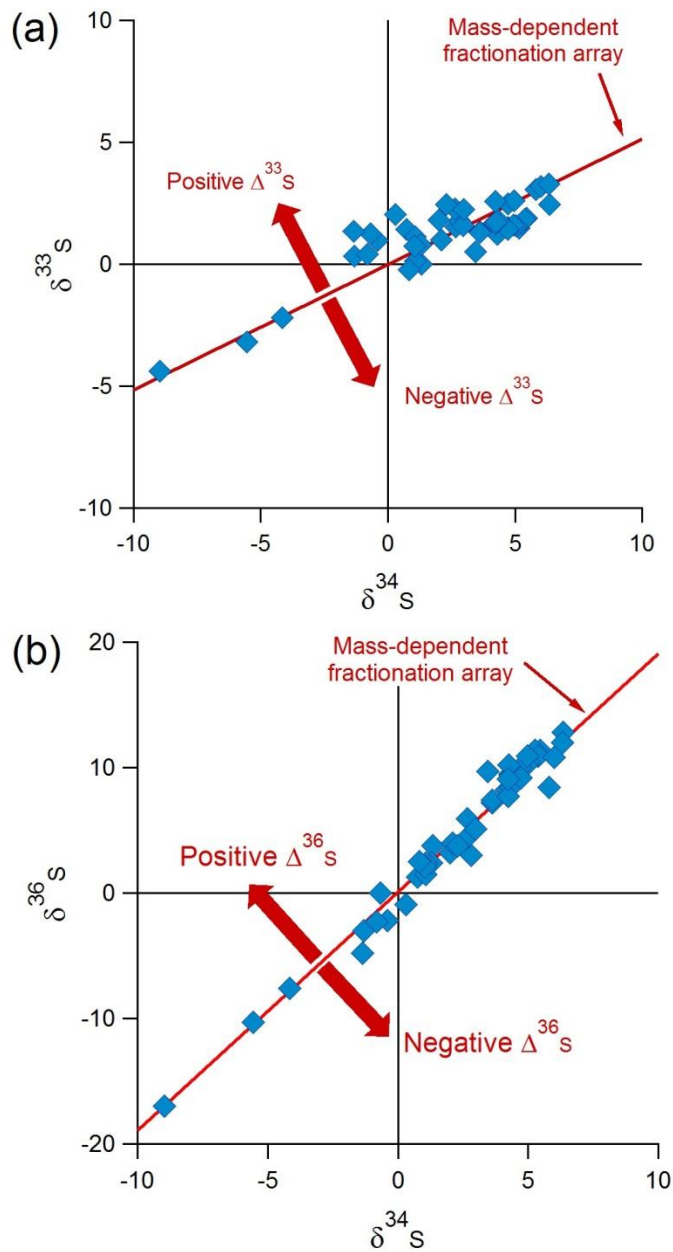


Fig. 1. Illustration of mass-independent fractionation (MIF) of sulfur isotopes, (a) $\Delta^{33}\text{S}$ and (b) $\Delta^{36}\text{S}$. Points on the red line display mass-dependent fractionation, while points above or below the red line (i.e., possessing non-zero values of $\Delta^{33}\text{S}$ or $\Delta^{36}\text{S}$) display MIF. Data shown are from Archean samples (Farquhar et al., 2000a).

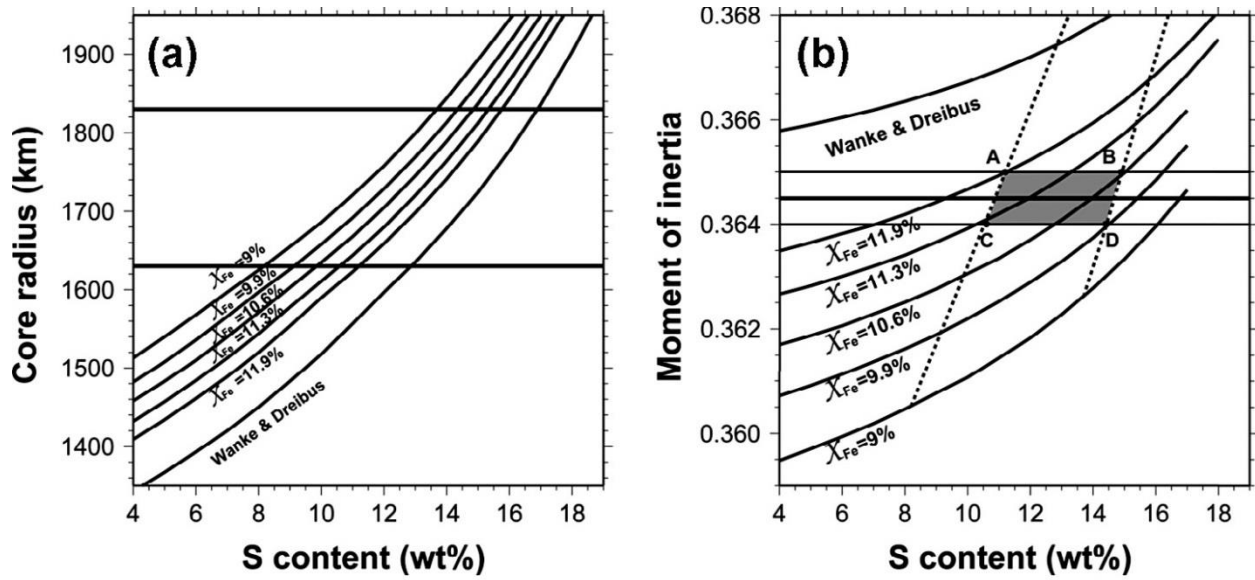


Fig. 2. Calculated (a) core radius and (b) MOI factor as a function of sulfur content in the core for various Fe contents (X_{Fe}) in the mantle, assuming a martian crust with thickness of 50 km and density of 3.0 g/cm^3 . Solid lines in (a) and dashed lines in (b) denote the range of possible core radius, 1630 km and 1830 km, inferred by (Konopliv et al., 2011); solid lines in (b) are the observed value and error bars of the mean MOI factor. Figure reproduced from (Wang et al., 2013b) with permission.

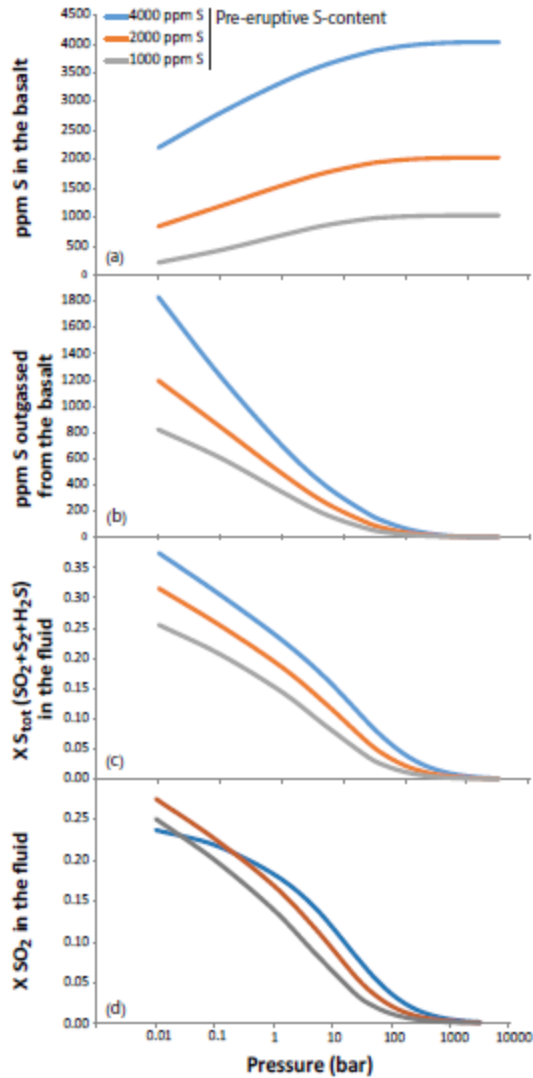


Fig. 3. Degassing of sulfur from martian basalts containing variable amounts of sulfur. In each plot, the pre-eruptive concentrations of water (500 ppm) and CO₂ (1600 ppm) are constant and taken from (Usui et al., 2012), while fO_2 is taken as QFM-0.8, i.e., the uppermost range of martian fO_2 upon melting, which represents the most favorable case for sulfur degassing. (a) the equilibrium S content in basalt during degassing vs. pressure; (b) the mass of S degassed as g/Mg basalt; (c) the mole fraction of total sulfur in the gas (H₂S+S₂+SO₂); (d) the mole fraction of SO₂; comparison with (a) demonstrates that the fraction of SO₂ at equilibrium is independent of the initial, pre-eruptive, sulfur content in the undegassed melt.

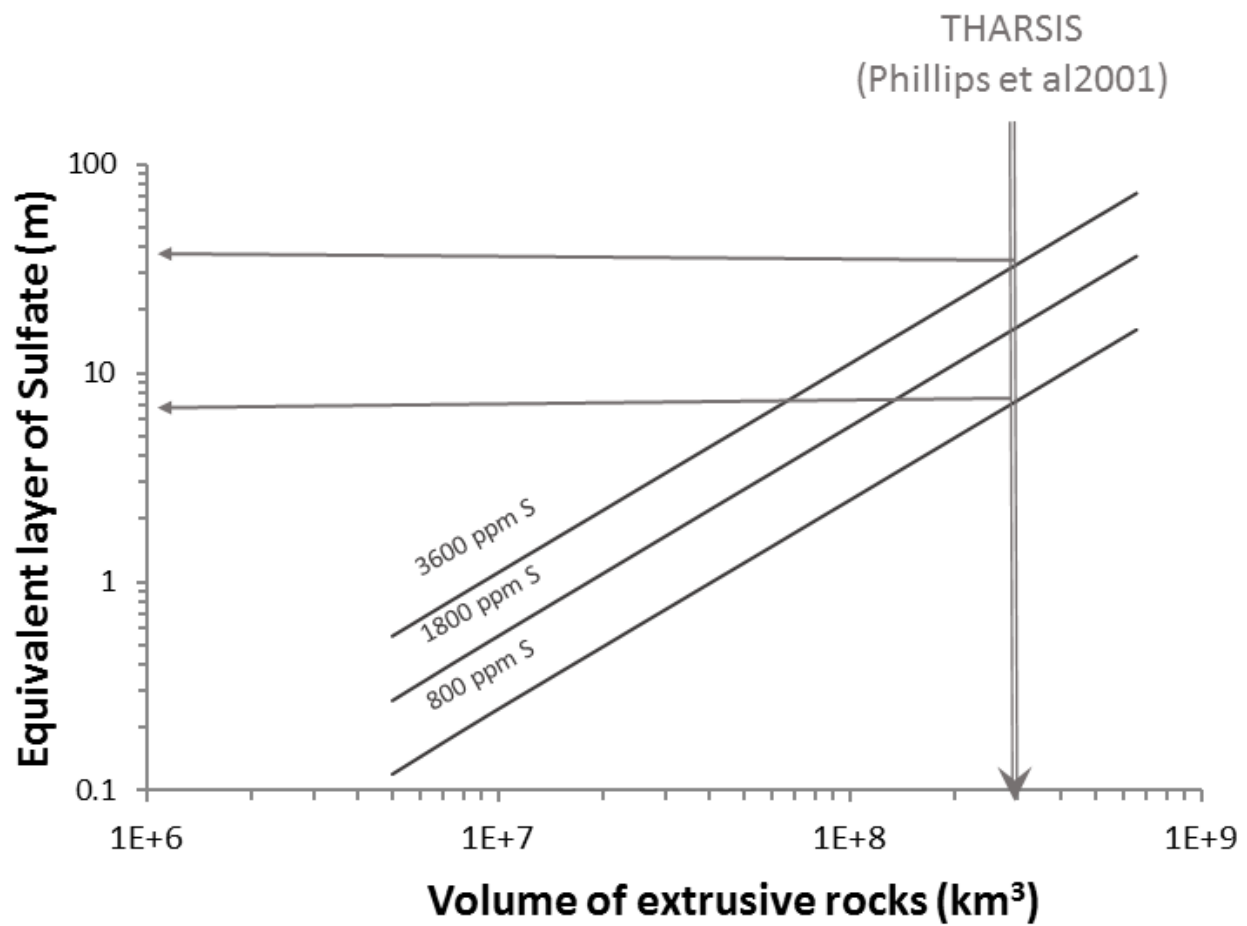


Fig. 4. Model predictions for sulfate precipitated due to volcanic degassing, expressed as equivalent to a uniform layer around the planet. Arrow indicates the volume of extrusive rocks produced by the Tharsis province as estimated by (Phillips et al., 2001). The Tharsis province is expected to have produced a uniform layer of sulfate covering the surface of Mars with depth from a few meters to a few tens of meters.

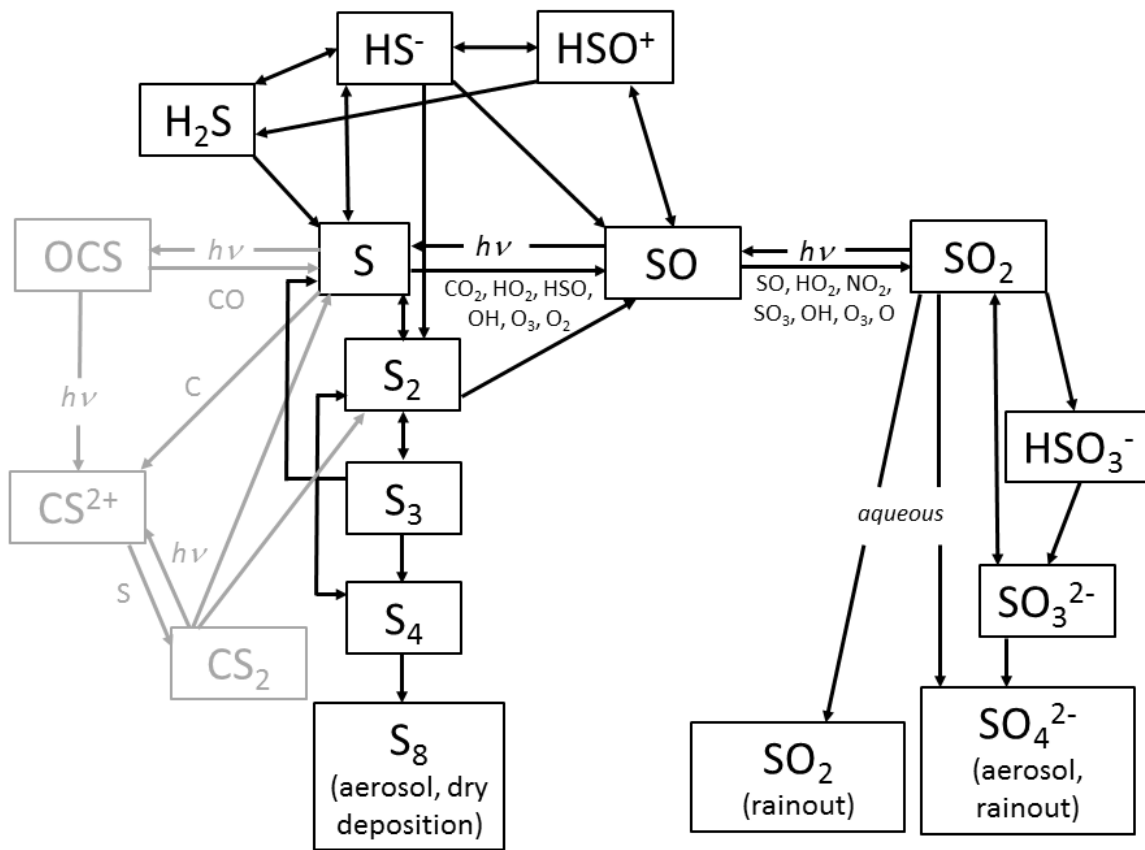


Fig. 5. Schematic diagram of the primary atmospheric reactions involving sulfur species (after Johnson et al., 2009). Species are assumed to occur in gas phase with the exceptions of SO_2 and SO_4^{2-} rainout (aqueous phase) and S_8 and SO_4^{2-} aerosol deposition (solid phase). Black lines and text indicate species included in the model of Johnson et al. (2009), and grey lines and text indicate notional representation of reactions between S- and C-bearing species that were not considered in that model but may have played a significant role in the martian atmosphere during periods of active volcanism. Notation “ $h\nu$ ” generally refers to wavelengths in the ultraviolet (UV) range; discussion of specific wavelengths responsible for these reactions is beyond the scope of this chapter.

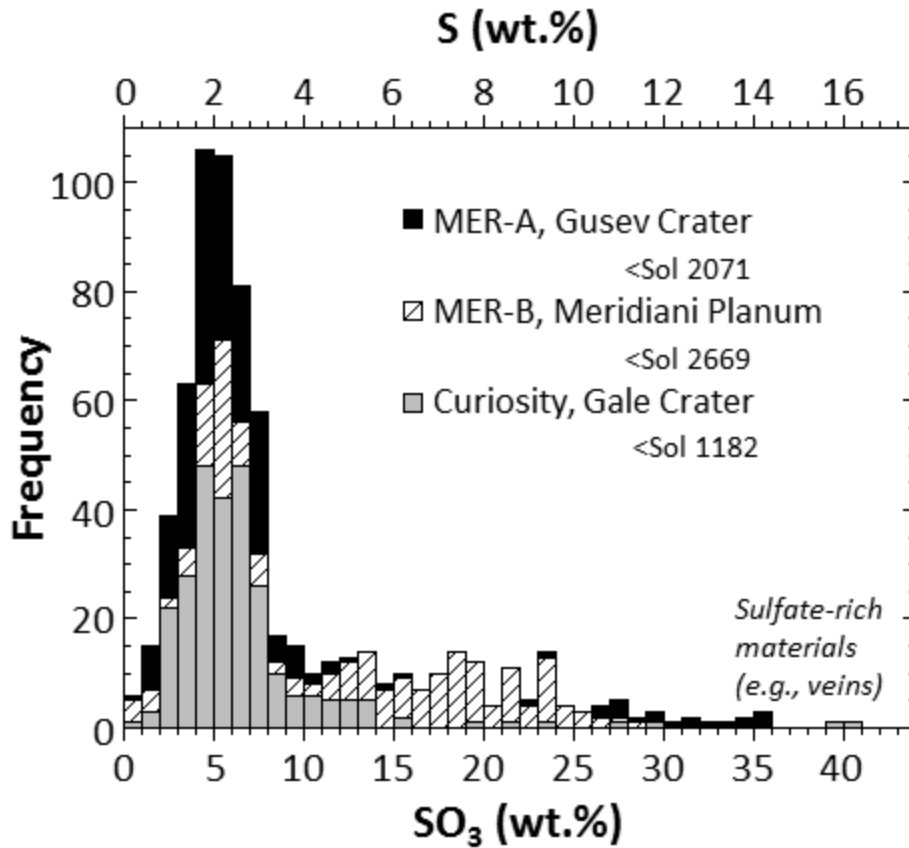


Fig. 6. Histograms showing sulfur contents (as both S and SO₃ wt.%) from APXS measurements of bulk rock samples using bins of 1 wt.% (larger than the error for most measurements). Data are available in the Planetary Data System: MER-A, Gusev Crater (<Sol 2071), MER-B, Meridiani Planum (<Sol 2669) & Curiosity, Gale Crater (<Sol 1182), where “<” refers to sols prior to the given sol number.

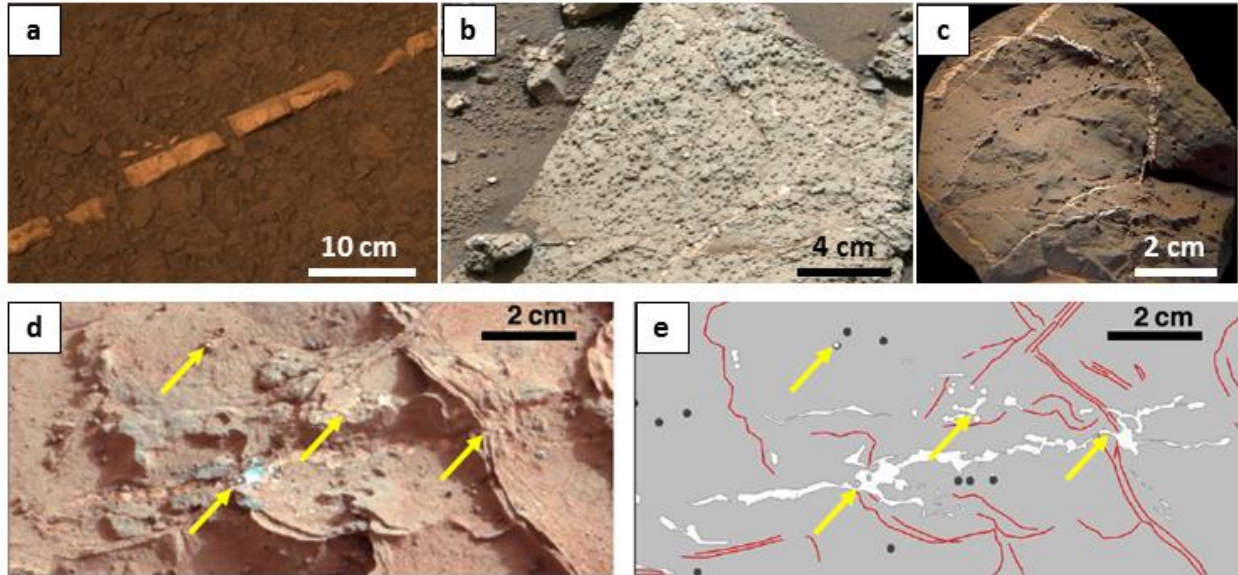


Fig. 7. Compilation of images from the martian surface showing sulfate-rich veins. (a) “Homestake” Vein from the western rim of Endeavour Crater. This image was collected from the panoramic camera (Pancam) on NASA's Mars Exploration Rover Opportunity using light with wavelengths centered at 601 nm (red), 535 nm (green) and 482 nm (blue). Modified after Squyres et al. (2012), image credit NASA/JPL-Caltech/Cornell/ASU. (b) Sheepbed target showing millimeter-sized nodules (dark) and also crosscutting white sulfate-bearing fractures. This image was collected as a Mastcam324 mosaic on NASA's Mars Science Laboratory mission. Modified after Grotzinger et al. (2014), image credit NASA/JPL-Caltech/MSSS. (c) Sheepbed target with sulfate veins (white) through nodule-rich mudstone. This image was collected as a ChemCam RMI image on NASA's Mars Science Laboratory mission. Modified after Grotzinger et al. (2014), image credit NASA/JPL-Caltech/MSSS. (d, e) Raised ridges (red lines in E are cements likely composed of akaganeite, magnetite and/or smectite; Siebach et al. (2014), nodules (black in e) and Ca-sulfate veins in the Sheepbed target (white in e). Images are mosaics from MastCam, image credit NASA/JPL-Caltech/MSSS, interpretation from Siebach et al. (2014).

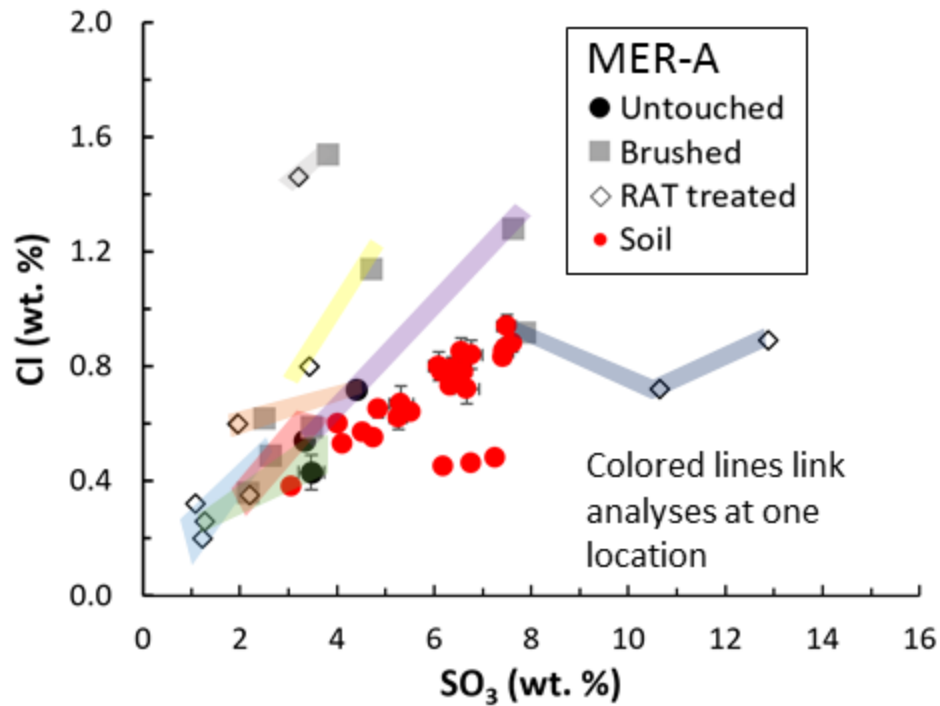


Fig. 8. Cl versus SO₃ (wt. %) for outcrop and float targets analysed by MER-A, Gusev Crater. Analyses at a single location are linked by coloured lines. The pre-treatment prior to analysis is indicated as untouched, brushed and RAT treated (i.e., cleaned with a rock abrasion tool). The precision error bars are within the size of the larger symbols and are small when present. We do not report the precision errors in subsequent figures because they are small and likely lower than the accuracy errors, which depend on detector performance, consolidation of the material being analyzed, distance, and angle from the target, which in combination are poorly constrained by robotic analyses on another planet.

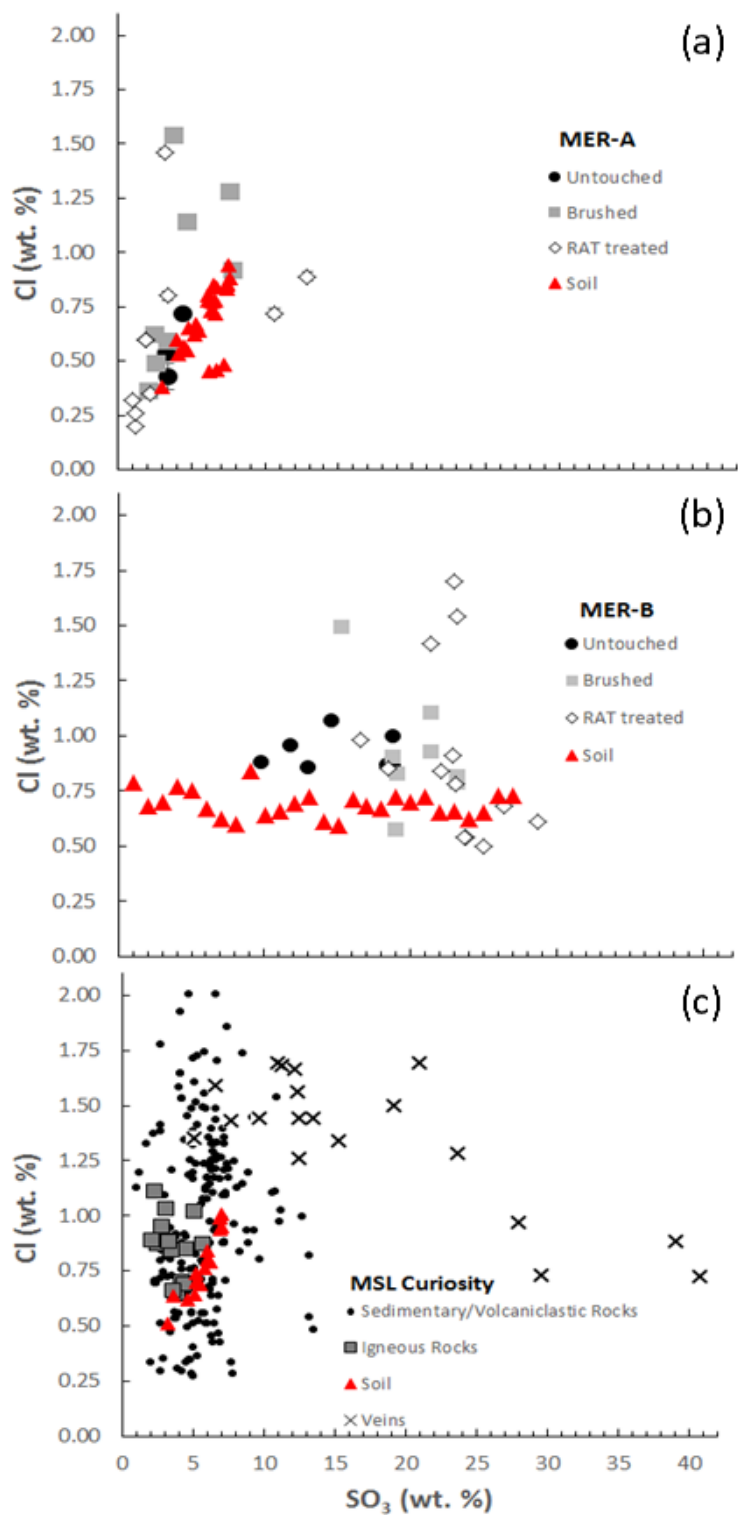


Fig. 9. Cl versus SO₃ (wt. %) for targets analysed by (a) MER-A (Gusev Crater), (b) MER-B (Meridiani Planum) and (c) Curiosity (Gale Crater).

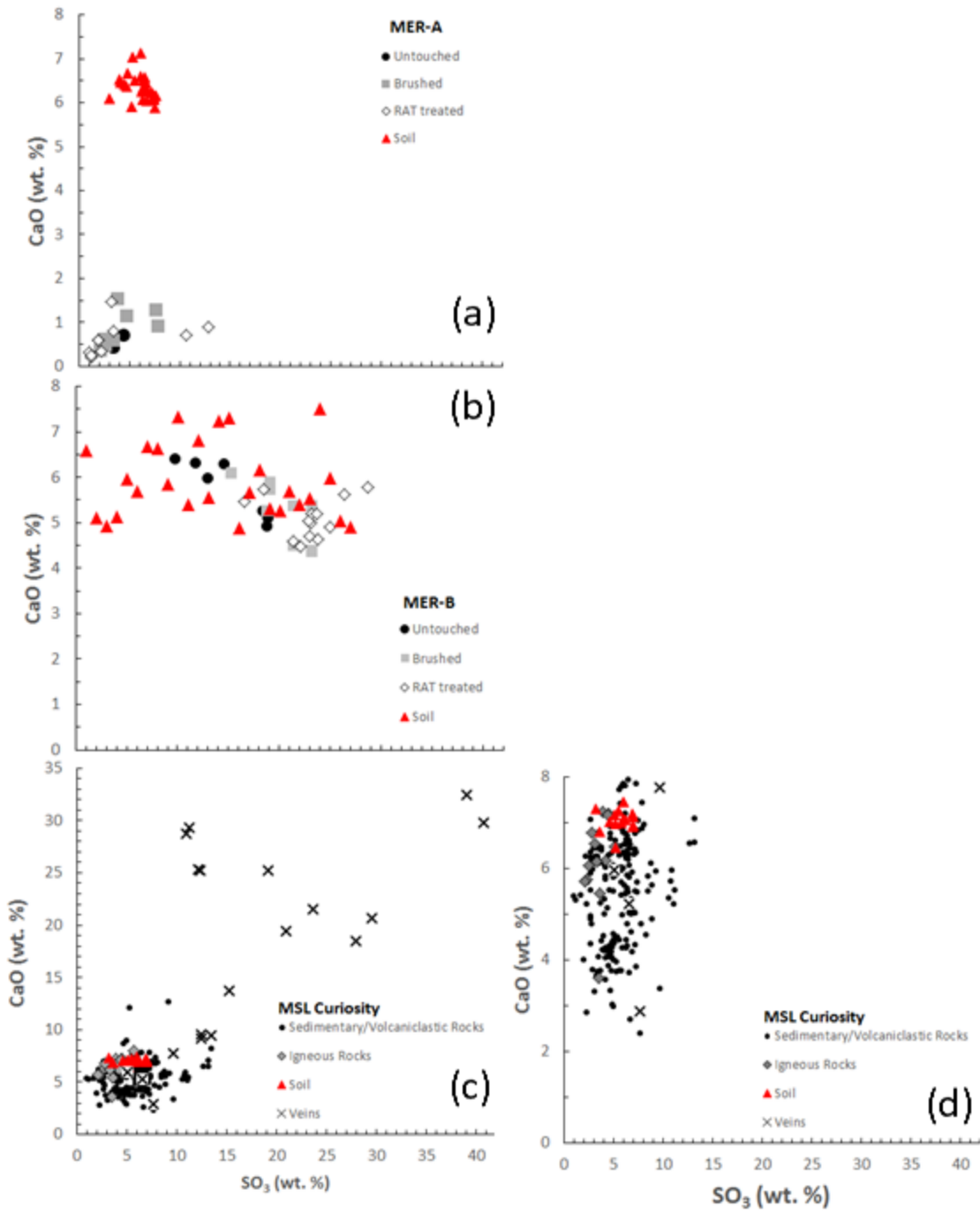


Fig. 10. CaO versus SO₃ (wt. %) for targets analysed by (a) MER-A (Gusev Crater), (b) MER-B (Meridiani Planum) and (c,d) Curiosity (Gale Crater); (d) presents an expanded view of the graph in (c) to show data only for CaO mass fractions up to 8 wt. %.

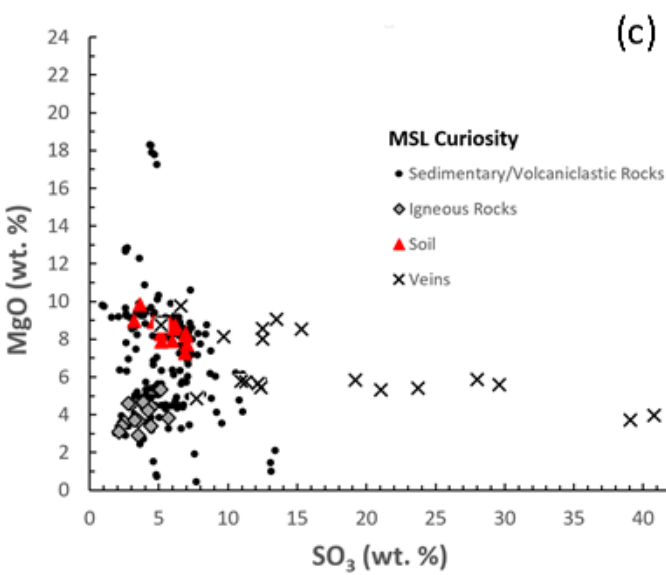
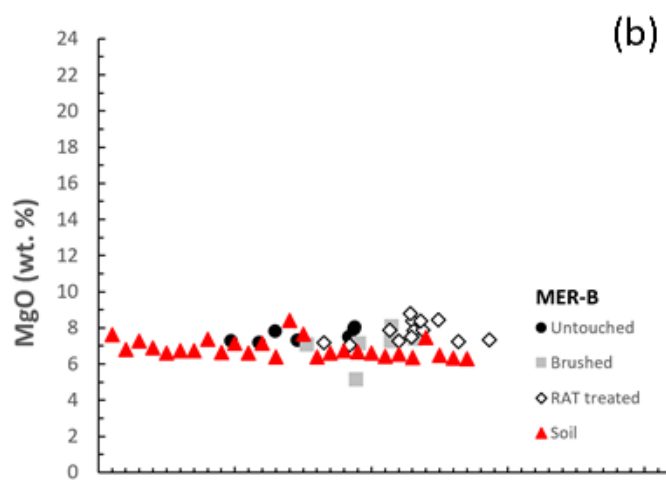
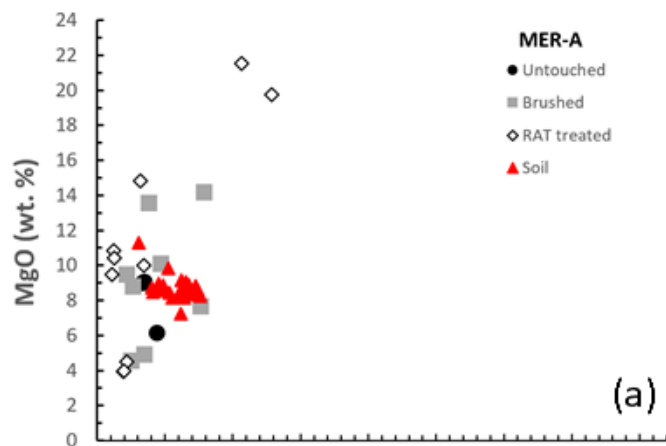


Fig. 11. MgO versus SO₃ (wt. %) for targets analysed by (a) MER-A (Gusev Crater), (b) MER-B (Meridiani Planum) and (c) Curiosity (Gale Crater).

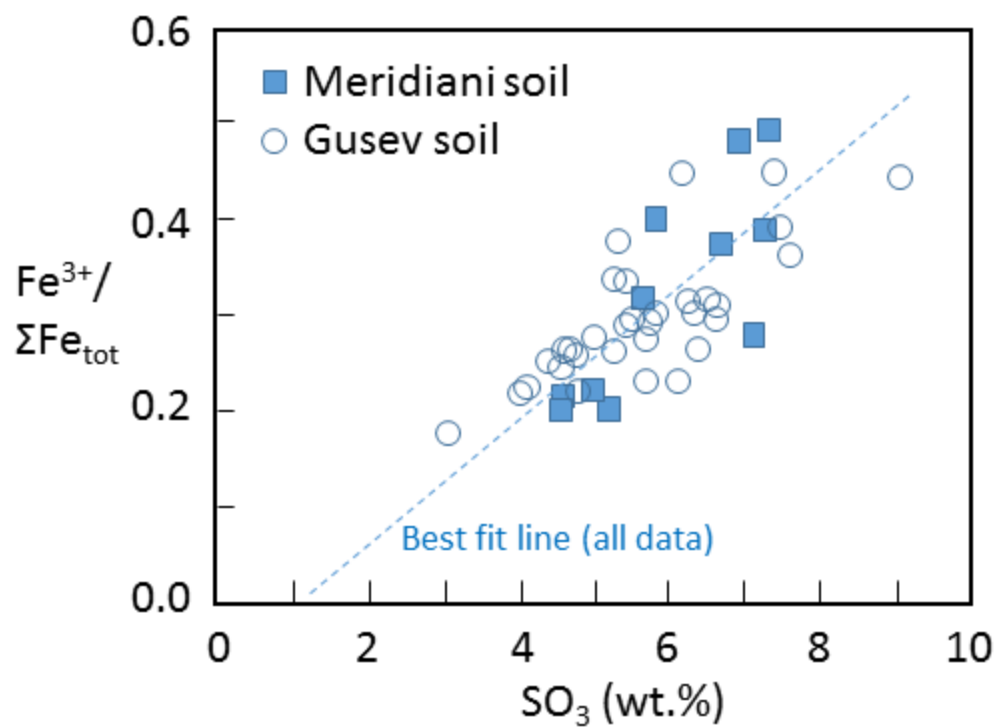


Fig. 12. Fe³⁺/Fe_{total} vs SO₃ (wt. %) for Meridiani and Gusev soils based on Mössbauer and APXS analyses, respectively, with a best fit line through all data (modified after Morris et al., 2013).

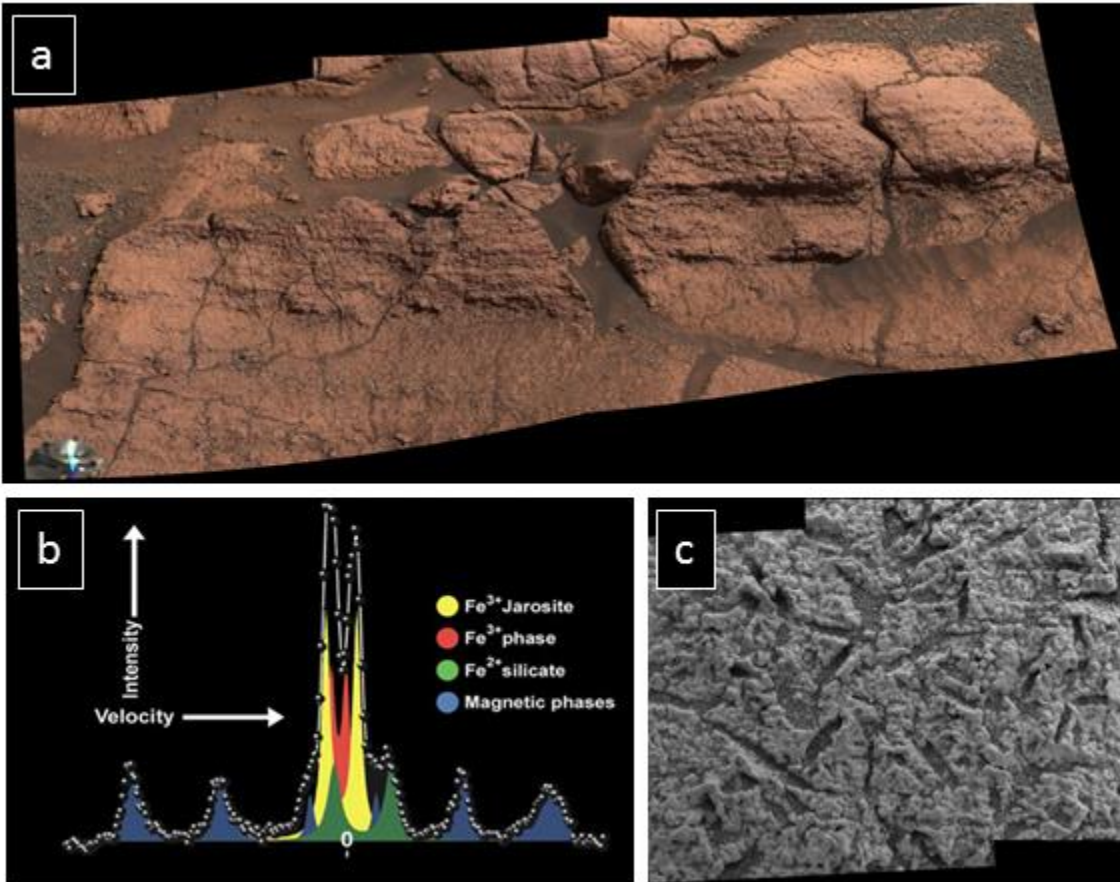


Fig. 13. (a) Sulfate-rich sedimentary beds at El Capitan, Endurance Crater, Meridiani Planum (NASA/JPL/Cornell/ASU). (b) Mössbauer spectrum of El Capitan (NASA/JPL/University of Mainz) reported in full in Klingelhöfer et al. (2004). Note that Mössbauer spectra are generally sensitive only to Fe-bearing phases. (c) Microscopic Imager mosaic of El Capitan outcrop with elongate holes inferred to result from the removal of salt minerals that formed in the sediment near deposition (McLennan et al., 2005).

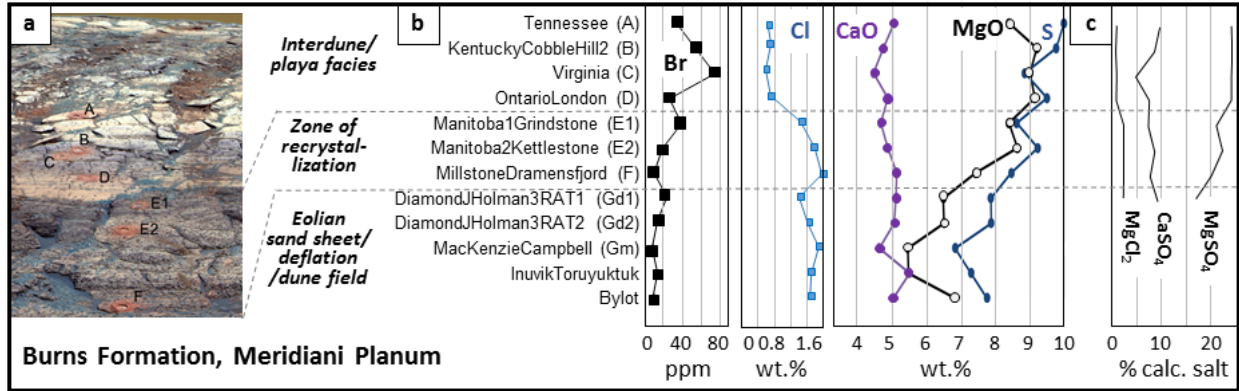


Fig. 14. Burns formation, Meridiani Planum. (a) Outcrop showing the RAT-abraded analysis location (Grotzinger et al., 2005). (b) Variations in chemical elements as a function of the stratigraphy (data plotted from the Planetary Data System). (c) Calculated salt mineralogy of units A through Gd1 (McLennan et al., 2005).

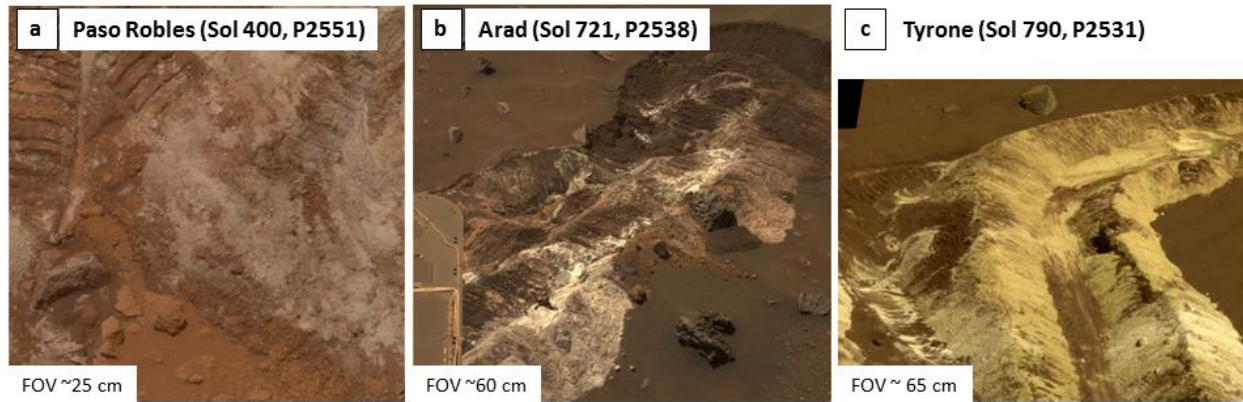


Fig. 15. Approximately true-color images from Gusev Crater with white Fe^{3+} -sulfate (blue=432 nm, green=535 nm, red=754 nm) from NASA/JPL/Cornell University: (a) Paso Robles soil. (b) Arad soil. (c) Tyrone soil. These images were generated from a combination of filters ranging from 430 to 750 nm wavelength.

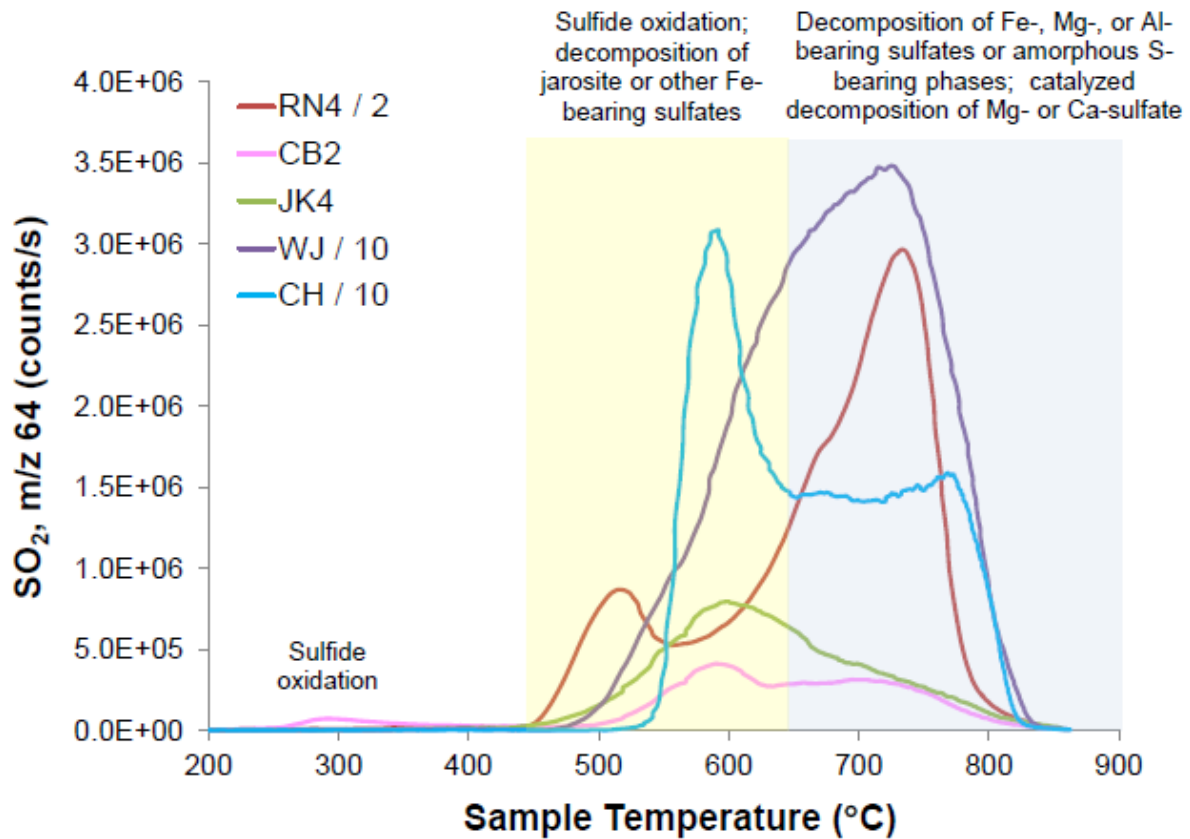


Fig. 16. SO₂ released from thermal processing of Gale Crater rocks and soils by SAM, shown as the signal for the major SO₂ isotopologue at m/z 64 as a function of sample temperature (modified after McAdam et al., 2016). The legend identifies samples of the Rocknest (RN) eolian deposit, Cumberland (CB) mudstone, John Klein (JK) mudstone, Windjana (WJ) sandstone, and Confidence Hills (CH) mudstone. A number after the sample identifier indicates a specific aliquot in repeated analyses of a given sample – e.g., “RN4” refers to the fourth analysis of the Rocknest sample by SAM.

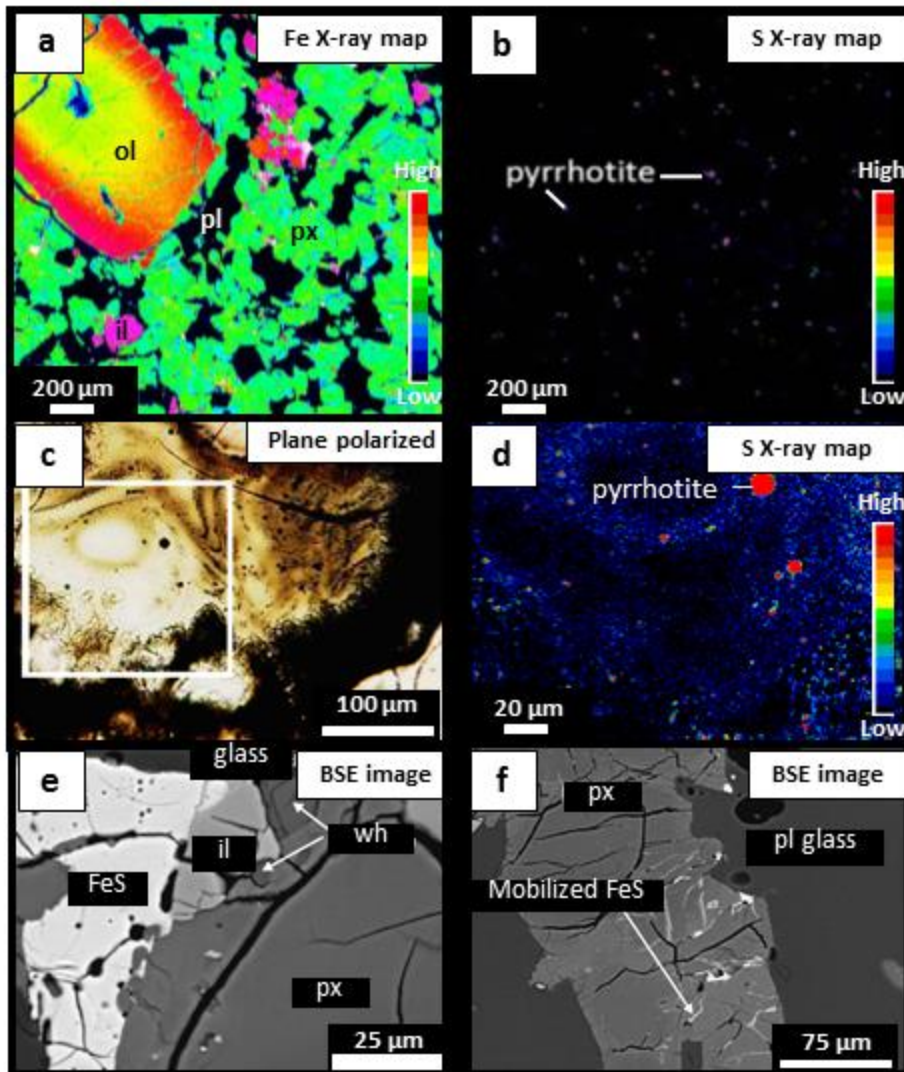


Fig. 17. Iron sulfides in martian meteorites. (a) Iron and (b) sulfur distribution from X-ray maps of the martian meteorite NWA1110, where ol = olivine, pl = plagioclase, px = pyroxene, & il = ilmenite (King & McLennan, 2010; courtesy of Paul Burger & Jim Papike, University of New Mexico). (c) Plane polarized light map of a large impact melt pocket in Tissint, showing schlierens and black sulfide globules (polished section #NHM-Vienna N 9404, glass “C”). (d) Sulfur X-ray map of the white area outlined in (c), showing the red sulfides. (e) Vesicular pyrrhotite in EETA79001, shown in a BSE image from Walton et al. (2010). (f) Mobilized pyrrhotite infills cracks and fractures in pyroxene adjacent to plagioclase glass in EETA79001, as shown in a BSE image from Walton et al. (2010).

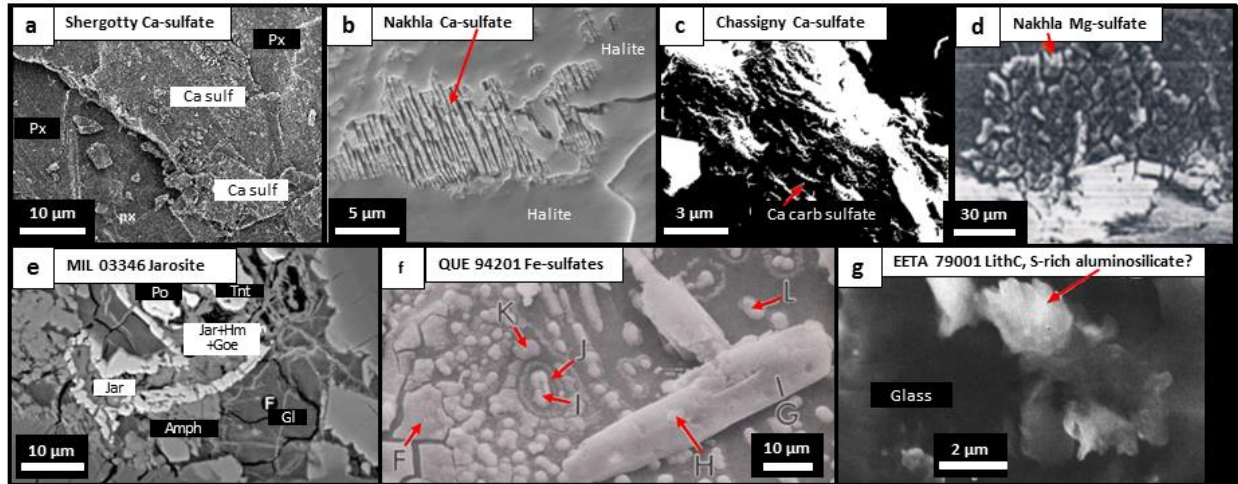


Fig. 18. Sulfate minerals in the martian meteorites. (a) Ca-sulfates in the Shergotty meteorite (Wentworth et al., 2000). (b) Ca-sulfate in the Nakhla meteorite covered in a thin layer of halite (Wentworth and McKay, 1999). (c) Ca-sulfate in Chassigny meteorite, associated with carbonate in some cases (Wentworth and Gooding, 1994). (d) Mg-sulfate in the Nakhla meteorite (Gooding et al., 1991). (e) Jarosite hosted in a melt inclusion inside clinopyroxene from MIL 03346 (McCubbin et al., 2009). (f) Fe-sulfates (red arrows) in QUE 94201 (Wentworth and Gooding, 1996). (g) A S-rich aluminosilicate or S-mineral on glass (Gooding and Muenow, 1986).

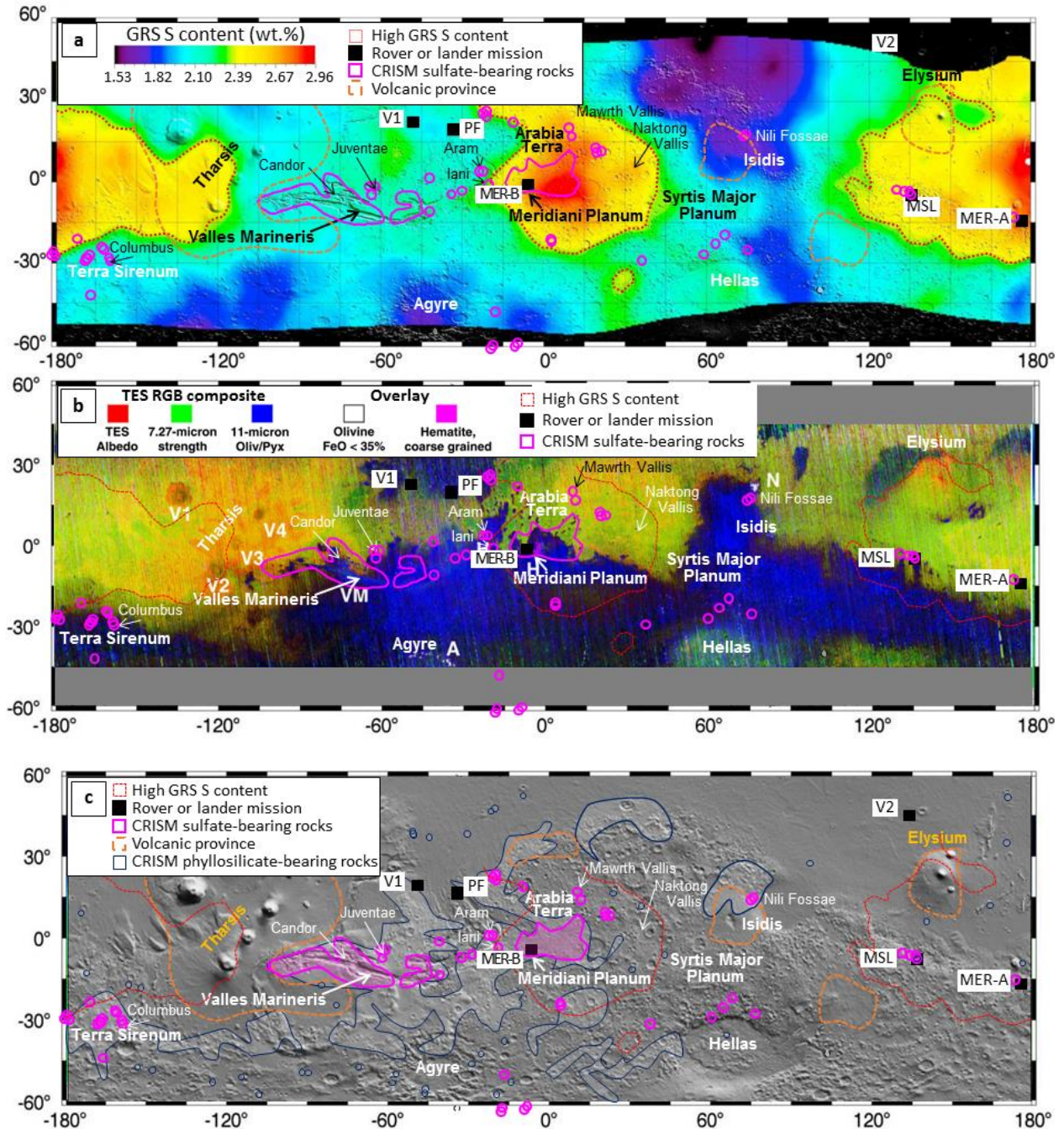


Fig. 19. Sulfur or sulfate concentrations and locations on the surface of Mars. Viking (V-1, V-2), Pathfinder (PF), Spirit (MER-A), Opportunity (MER-B), Phoenix (PH) & Curiosity (MSL) landing sites are plotted. Localities discussed in the text are labelled. (a) S content (in stoichiometrically equivalent mass fractions) in the upper few decimeters of the Martian surface, as mapped by the Mars Odyssey Gamma Ray Spectrometer (GRS). The GRS map, from (Karunatillake et al., 2014), is based on $10^\circ \times 10^\circ$ bins using a boxcar filter with a smoothing radius of 25° and is draped onto a Mars Orbiter Laser Altimeter shaded-relief map. Regions of very high hydrogen content are not shown (grey) due to the presence of abundant subsurface ice.

(b) Thermal Emission Spectrometer (TES) red-green-blue (RGB) composite showing areas expected to be sulfate rich (7.27 micron) in green. This diagram is modified from Hoefen and Clark presented at <http://speclab.cr.usgs.gov/mars.press.release.10.2000.html>. (c) Diagram showing sulfate-bearing rocks and phyllosilicate-bearing rocks based on data from CRISM (Ehlmann and Edwards, 2014). Volcanic provinces are from Michalski & Bleacher (2013).

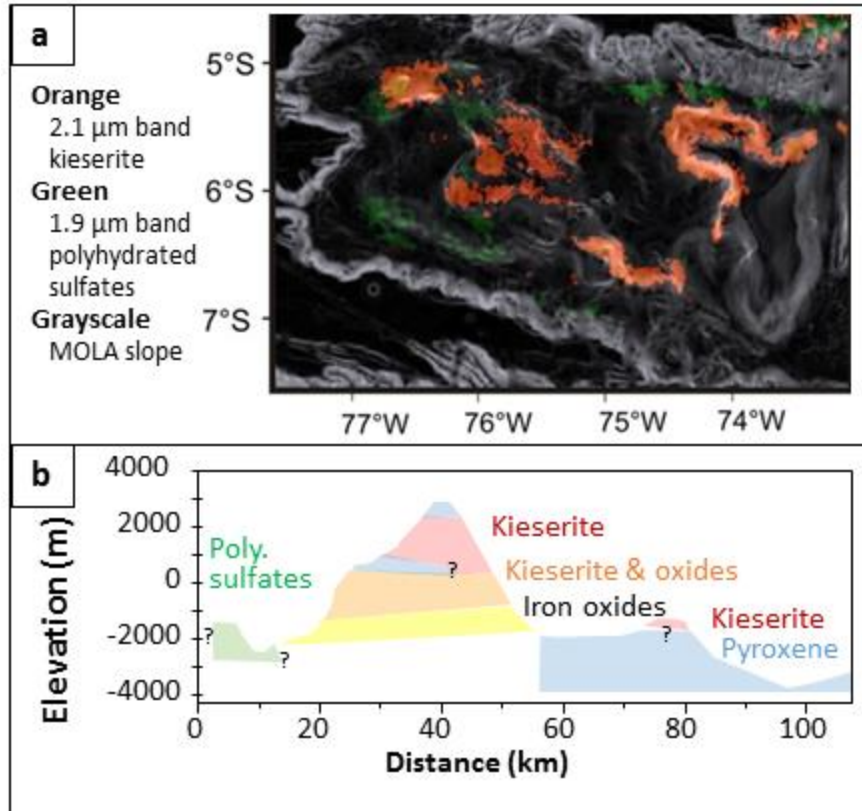


Fig. 20. Interpretation of an area in Candor Mensa with figures modified from Mangold et al. (2008). (a) CRISM data with the 2.1 μm band diagnostic of kieserite (red to yellow) and 1.9 μm band related to polyhydrated sulfates (green to light green) plotted over MOLA slope map in grayscale. (b) Modification of a N-S cross section of Candor Mensa with layering postulated as subhorizontal and “?” indicating uncertain boundaries.

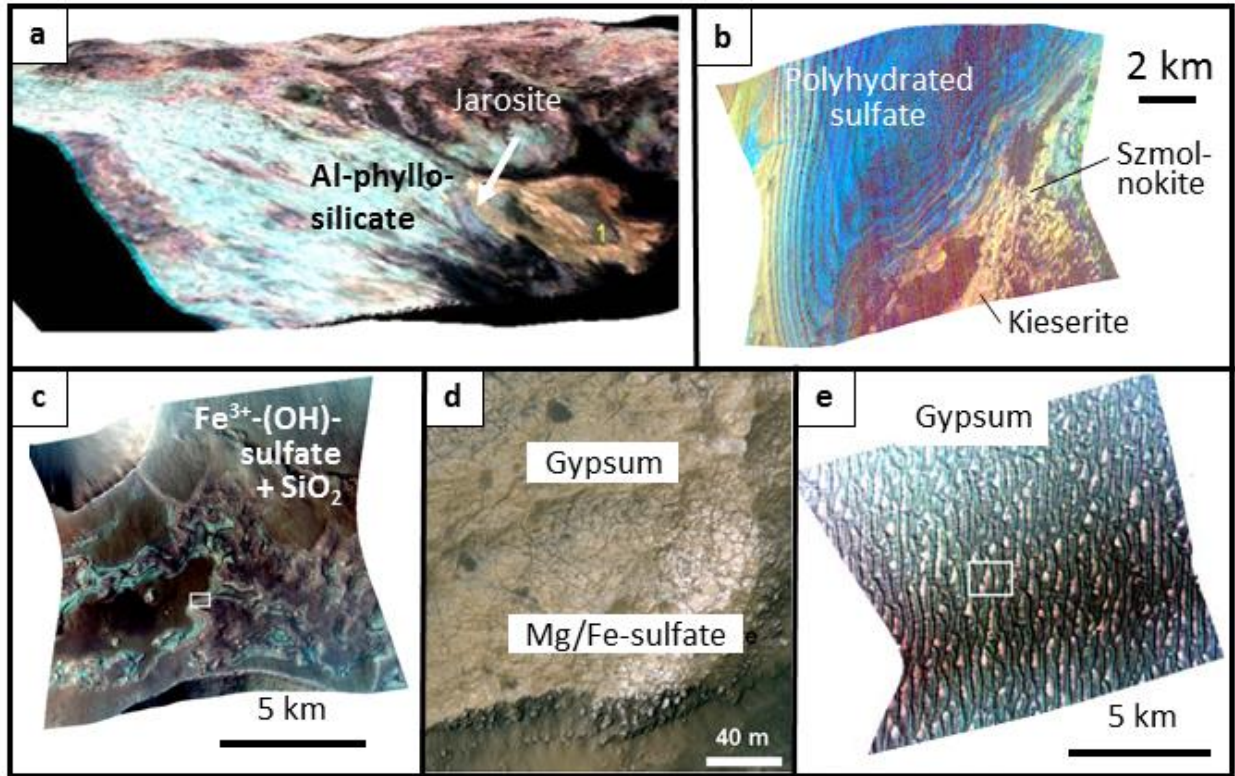


Fig. 21. Sulfates in different settings on the martian surface inferred from CRISM-derived spectra. (a) Jarosite in Mawrth Vallis from a CRISM composite draped over topography with 20x vertical exaggeration from HighRise showing jarosite-bearing unit (yellow) and Al-phyll-silicate unit (light blue) from Farrand et al. (2009). (b) Fe-sulfates at Juventae Chasma showing szmolnokite (yellow) and kieserite (orange) with polyhydrated sulfates in blue (Bishop et al., 2009). (c) Fe^{3+} -OH-sulfate (e.g., jarosite) in pink in the plains W of Juventae Chasma with sulfate beds in pink and silica beds – light blue. $R=2.53$, $G=1.51$, $B=1.08$ from Murchie et al. (2009b). (d) Gypsum and Mg/Fe-sulfate rich units in the Columbus Crater near the crater wall showing albedo and textural contrast between the different spectral (mineralogic) units in the ring based on HiRISE image (ESP_013960_1510) (Wray et al., 2011). (e) Gypsum (dark color) in dunes from the northern plains (Murchie et al., 2009). $R=2.53\mu\text{m}$, $G=1.51\mu\text{m}$, $B=1.08\mu\text{m}$.

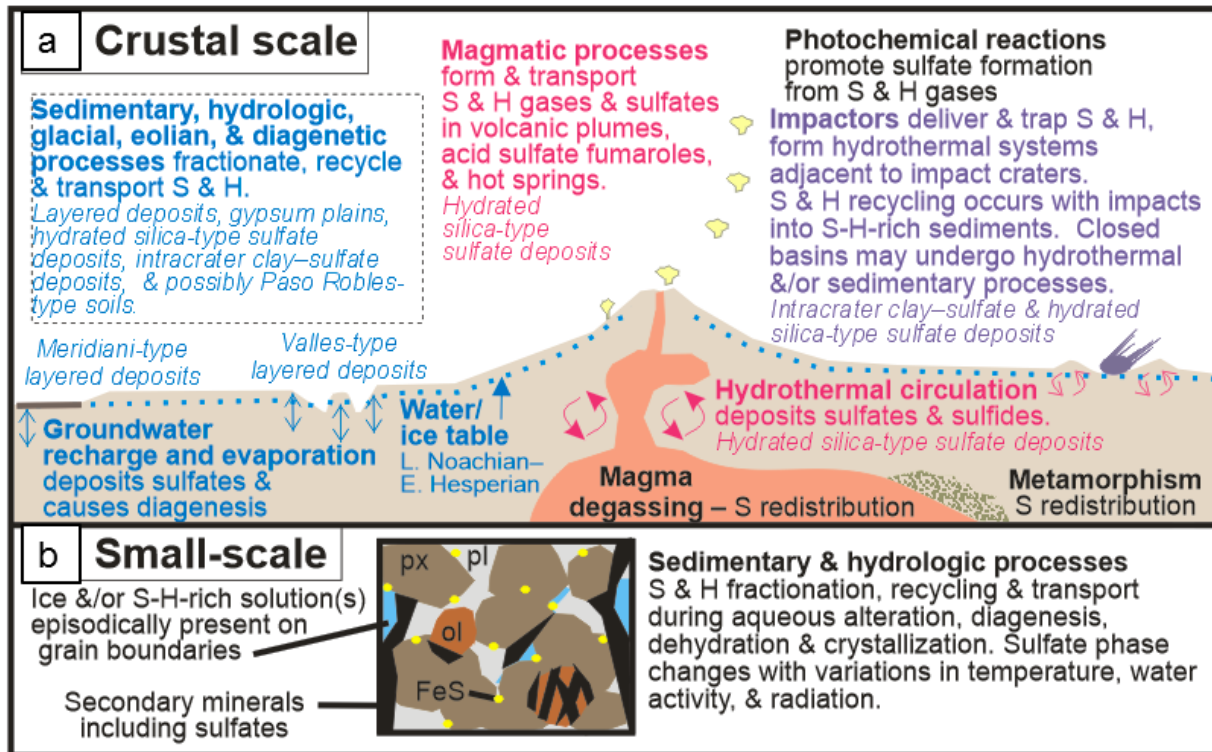


Fig. 22. Mechanisms for distributing sulfur (and also H) on Mars's near surface on both (a) the crustal scale; and (b) the small scale. After King and McLennan (2010).

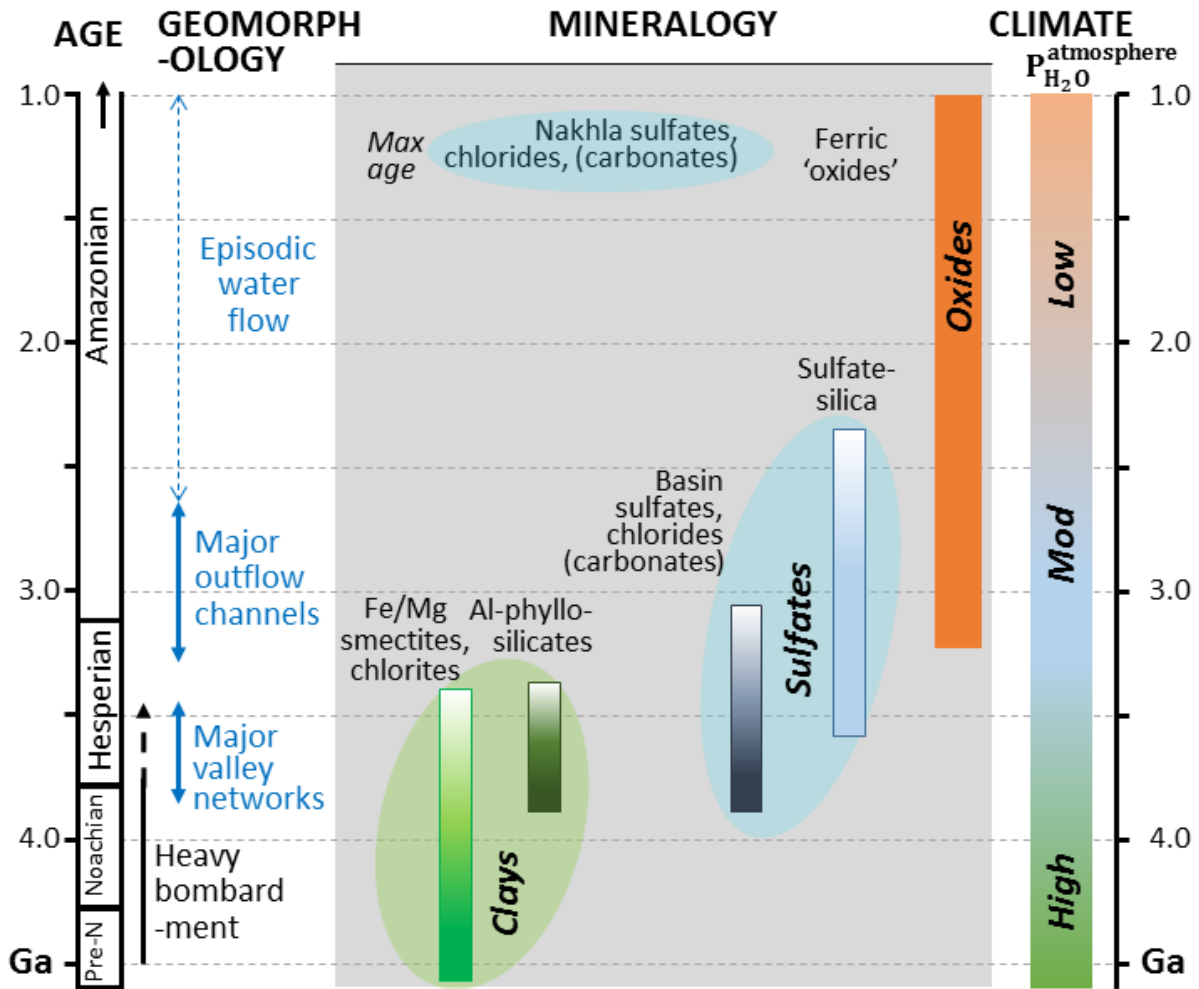


Fig. 23. Generalized stratigraphy on Mars based on CRISM data (Bibring et al., 2006; Ehlmann and Edwards, 2014). Major events modifying the surface are shown also. Note that “oxides” include anhydrous oxides (e.g., magnetite, hematite, maghemite), oxyhydroxides (goethite), hydroxides (ferrihydrite) and hydrated iron oxide minerals.

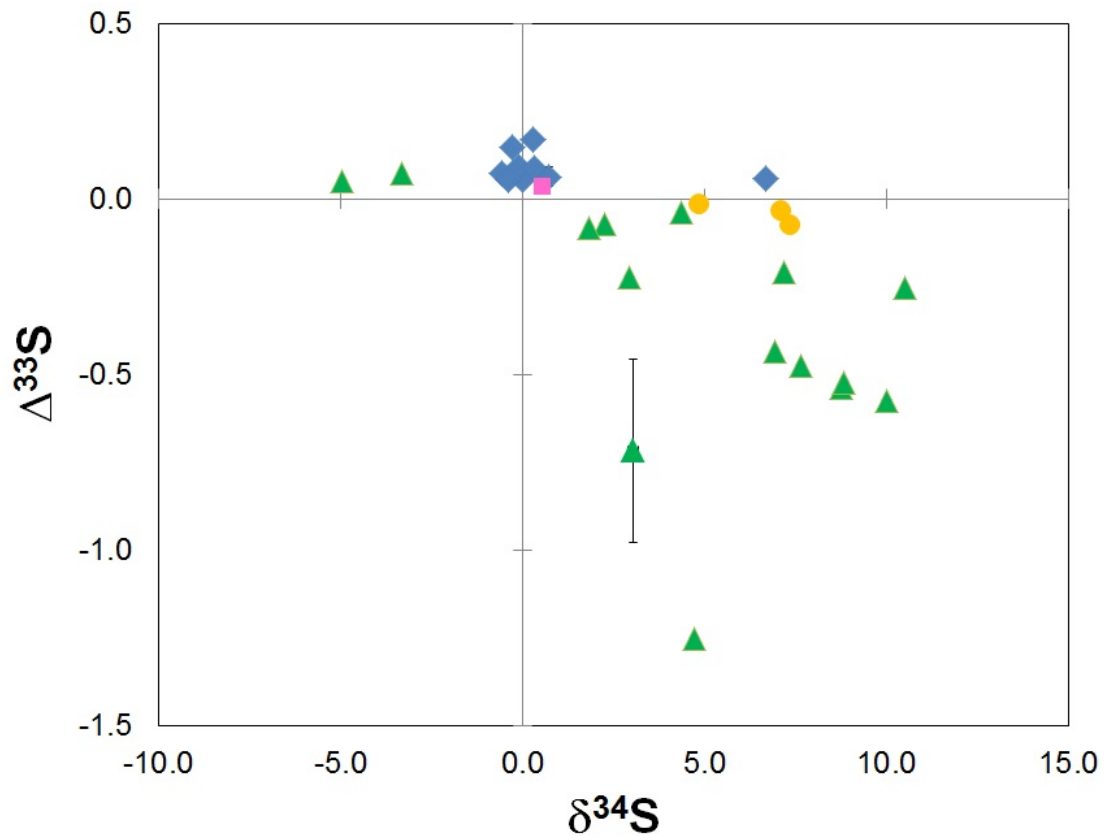


Fig. 24. Plot of $\Delta^{33}\text{S}$ and $\delta^{34}\text{S}$ for isotopically anomalous sulfur extracted from martian meteorites (Farquhar et al., 2000b; Farquhar et al. 2007; Franz et al., 2014). ALH 84001 - gold circles; nakhlites – green triangles; Chassigny – pink square; shergottites – blue diamonds. The single point with the large error bar represents average results of ion microprobe analyses of MIL 03346 pyrrhotite (Franz et al., 2014). All other points were obtained through bulk extraction protocols and have error bars smaller than the symbols.

Table 1: S contents of different reservoirs on Mars

<u>Reservoir</u>	<u>Sulfur</u>	<u>Reference</u>
Bulk Mars	2.2 wt %	(Lodders and Fegley, 1997)
Core	14.24 wt %	(Dreibus and Wanke, 1985)
	10.6 wt %	(Lodders and Fegley, 1997)
	16.2 wt %	(Sanloup et al., 1999)
	16 ± 2 wt %	(Rivoldini et al., 2011)
	10.6 – 14.9 wt %	(Wang et al., 2013b)
	> 20 wt%	(Khan and Connolly, 2008)
	< 8 wt%	(Shahar et al., 2015)
	5-10 wt%	(Wang and Becker, 2017)
Primitive mantle	700 – 1000 ppm	(Ding et al., 2015; Gaillard and Scaillet, 2009)
	700 – 2000 ppm	(Gaillard et al., 2013) & references therein
	3000 – 7000 ppm	(Gaillard and Scaillet, 2009; Righter et al., 2009)
	900 ppm	(Lodders and Fegley, 1997)
	360 ppm	(Wang and Becker, 2017)
Meteorites		
Olivine-phyric shergottites	408 – 2700 ppm	(Aoudjehane et al., 2012; Basu Sarbadhikari et al., 2009; Ding et al., 2015; Franz et al., 2014a; Gibson et al., 1985; Lodders, 1998; Shirai and Ebihara, 2004; Zipfel et al., 2000)
Basaltic shergottites	65 – 2865 ppm	(Ding et al., 2015; Franz et al., 2014a; Gibson et al., 1985; Lodders, 1998)
Nakhlites	34-1287	(Ding et al., 2015; Farquhar et al., 2007b; Franz et al., 2014a; Gibson et al., 1985; Lodders, 1998)
Chassignites	67-440	(Franz et al., 2014a; Gibson et al., 1985; Lodders, 1998)
Orthopyroxenite	103-110	(Dreibus et al., 1994; Franz et al., 2014a)
Surface rocks measured in situ		
<i>Viking 1 & 2</i>	2.4 – 3.8 wt %	(Clark, 1993)
<i>Mars Pathfinder</i>	1.6 – 2.6 wt %	(Bell et al., 2000)
<i>MER-A Spirit</i>	Soil	0.99-35.8
	Brushed Rocks	1.52-9.28
	Abraded Rocks	1.23-7.96
		(12.88)
		NASA Planetary Data System
<i>MER-B</i>	Soil	4.56-7.36
		(16.46)
<i>Opportunity</i>	Brushed Rocks	2.33-25.2
	Abraded Rocks	(0.56) 17-28.62
<i>MSL</i>	Soil	1.85 – 2.81
<i>Curiosity</i> (<i><Sol 1182</i>)	Igneous rocks	0.85 – 2.37
<i>APXS</i>	Sed. rocks	0.36 – 5.36

<i>Phoenix Wet Chemistry Lab</i>	Rosy Red Sorceress-2	0.40 ± 0.12 0.48 ± 0.12	(Kounaves et al., 2010)
GRS Global average		1.76 wt %	(McLennan et al., 2010)
Layered sulfate deposits		8 – 12 wt %	(Gaillard et al., 2013)

Table 2: Sulfur minerals detected by the Mars Science Laboratory CheMin in Gale Crater, Mars*

Rock type		Sample	Sulfates			Sulfides		Reference
			Anhy-drite	Bass-anite	Jaro-site	Pyrrho-tite	Py-rite	
Modern sand deposit		Rocknest	1.1					(Bish et al., 2013; Blake et al., 2013)
Sheepbed mudstone		John Klein	2.6	1.0		1.0	(0.3)	(Vaniman et al., 2014)
		Cumber-land	0.8	0.7		1.0		(Vaniman et al., 2014)
Dillinger sandstone		Windjana	1.0			0.7		(Treiman et al., 2016)
Pahrump Hills mudstone	Concre-tions	Confidence Hills			(0.2)			(Rampe et al., 2016)
	mineral pseudo-morphs	Mojave2			~1			(Rampe et al., 2016)
	lamina-tions	Telegraph Pass			(~0.4)			(Rampe et al., 2016)
Mudstone		Buckskin	1.8 ± 0.6					(Morris et al., 2016)
Stimson unit (cross-bedded sandstone)		Big Sky	Yes					(Yen et al., 2016)
Stimson unit in a fracture		Greenhorn	~7	~2				(Yen et al., 2016)

*Quoted uncertainties are as reported in original publications. Parentheses around numbers in the table indicate tentative values near the CheMin detection limit.

References

- Acuna, M.H., et al., 1999. Global distribution of crustal magnetization discovered by the Mars Global Surveyor MAG/ER experiment. *Science* 284, 790-793.
- Agee, C.B., et al., 2013. Unique meteorite from early Amazonian Mars: Water-rich basaltic breccia Northwest Africa 7034. *Science* 339, 780-785.
- Allègre, C., et al., 2001. Chemical composition of the Earth and the volatility control on planetary genetics. *Earth Planet. Sci. Lett.* 185, 49-69.
- Altheide, T.S., et al., 2009. Experimental investigation of the stability and evaporation of sulfate and chloride brines on Mars. *Earth Planet. Sci. Lett.* 282, 69-78.
- Anderson, R., et al., 2015. ChemCam results from the Shaler outcrop in Gale crater, Mars. *Icarus* 249, 2-21.
- Andrews-Hanna, J.C., et al., 2007. Meridiani Planum and the global hydrology of Mars. *Nature* 446, 163-166.
- Aoudjehane, H.C., et al., 2012. Tissint martian meteorite: a fresh look at the interior, surface, and atmosphere of Mars. *Science* 338, 785-788.
- Arvidson, R.E., et al., 2010. Spirit Mars rover mission: Overview and selected results from the northern Home Plate Winter Haven to the side of Scamander crater. *J. Geophys. Res.* 115, CiteID E00F03.
- Arvidson, R.E., et al., 2005. Spectral reflectance and morphologic correlations in eastern Terra Meridiani, Mars. *Icarus* 307, 1591-1594.
- Arvidson, R.E., et al., 2006. Nature and origin of the hematite-bearing plains of Terra Meridiani based on analyses of orbital and Mars Exploration rover data sets. *J. Geophys. Res.* 111.
- Aubrey, A., et al., 2006. Sulfate minerals and organic compounds on Mars. *Geology* 34, 357.
- Baird, A.K., et al., 1976. Mineralogic and petrologic implications of Viking geochemical results from Mars: Interim report. *Science* 194, 1288-1293.
- Baker, V.R., 1978. The Spokane flood controversy and the Martian outflow channels. *Science* 202, 1249-1256.
- Baldrige, A.M., et al., 2013. Searching at the right time of day: Evidence for aqueous minerals in Columbus crater with TES and THEMIS data. *J. Geophys. Res. Planets* 118, 179-189.
- Balta, J.B., et al., 2015. Petrology and geochemistry of new Antarctic shergottites: LAR 12011, LAR 12095, and LAR 12240, *Lunar Planet. Sci. XLVI*, The Woodlands, TX, p. 2294.
- Bandfield, J.L., et al., 2003. Spectroscopic identification of carbonate minerals in the Martian dust. *Science* 301, 1084-1087.
- Banin, A., et al., 1997. Acidic volatiles and the Mars soil. *J. Geophys. Res.* 102, 13341-13356.

Baratoux, D., et al., 2013. The petrological expression of early Mars volcanism. *J. Geophys. Res. Planets* 118, 59-64.

Barrat, J.A., et al., 2014. No Martian soil component in shergottite meteorites. *Geochim. Cosmochim. Acta* 125, 23-33.

Basilevsky, A.T., et al., 2006. Geologically recent tectonic, volcanic and fluvial activity on the eastern flank of the Olympus Mons volcano, Mars. *Geophys. Res. Lett.* 33, L13201.

Basu Sarbadhikari, A., et al., 2009. Petrogenesis of olivine-phyric shergottite Larkman Nunatak 06319: Implications for enriched components in martian basalts. *Geochim. Cosmochim. Acta* 73, 2190-2214.

Beaudoin, G., et al., 1994. Variations in the sulfur isotope composition of troilite from the Cañon Diablo iron meteorite. *Geochim. Cosmochim. Acta* 58, 4253-4255.

Bell, J.F., et al., 2000. Mineralogic and compositional properties of Martian soil and dust: Results from Mars Pathfinder. *J. Geophys. Res.* 105, 1721-1756.

Bell, J.F., et al., 1994. Spectroscopy of Mars from 2.04 to 2.44 μm during the 1993 opposition: Absolute calibration and atmospheric VS mineralogic origin of narrow absorption features. *Icarus* 111, 106-123.

Benison, K.C., Bowen, B.B., 2013. Extreme sulfur-cycling in acid brine lake environments of Western Australia. *Chem. Geol.* 351, 154-167.

Berger, J.A., et al., 2014. MSL-APXS titanium observation tray measurements: Laboratory experiments and results for the Rocknest fines at the Curiosity field site in Gale Crater, Mars. *J. Geophys. Res. Planets* 119, 1046-1060.

Berger, J.A., et al., 2015. Germanium enrichments in sedimentary rocks in Gale Crater, Mars: Constraining the timing of alteration and character of the protolith, *Lunar Planet. Sci. XLVI*, The Woodlands, TX, p. 1832.

Berger, J.A., et al., 2016. A global Mars dust composition refined by the Alpha-Particle X-ray Spectrometer in Gale Crater. *Geophys. Res. Lett.* 43, 67-75.

Bertka, C.M., Fei, Y., 1998. Implications of Mars Pathfinder data for the accretion history of the terrestrial planets. *Science* 281, 1838-1840.

Bibring, J.P., et al., 2007. Coupled ferric oxides and sulfates on the Martian surface. *Science* 317, 1206-1210.

Bibring, J.P., et al., 2005. Mars surface diversity as revealed by the OMEGA/Mars Express observations. *Science* 307, 1576-1581.

Bibring, J.P., et al., 2006. Global mineralogical and aqueous Mars history derived from OMEGA/Mars Express data. *Science* 312, 400-404.

Biemann, K., et al., 1976. Search for organic and volatile inorganic compounds in two surface samples from the Chryse Planitia region of Mars. *Science* 194, 72-76.

- Bish, D.L., et al., 2013. X-ray diffraction results from Mars Science Laboratory: Mineralogy of Rocknest at Gale Crater. *Science* 341.
- Bish, D.L., et al., 2003. Stability of hydrous minerals on the martian surface. *Icarus* 164, 96-103.
- Bishop, J.L., et al., 2009. Mineralogy of Juventae Chasma: Sulfates in the light-toned mounds, mafic minerals in the bedrock, and hydrated silica and hydroxylated ferric sulfate on the plateau. *J. Geophys. Res.* 114, E00D09.
- Blake, D., et al., 2012. Characterization and calibration of the CheMin mineralogical instrument on Mars Science Laboratory. *Space Sci. Rev.* 170, 341-399.
- Blake, D.F., et al., 2013. Curiosity at Gale Crater, Mars: Characterization and analysis of the Rocknest sand shadow. *Science* 341.
- Blaney, D.L., McCord, T.B., 1995. Indications of sulfate minerals in the Martian soil from Earth-based spectroscopy. *J. Geophys. Res.* 100, 14433-14442.
- Blum, J.S., et al., 2012. *Desulfohalophilus alkaliarsenatis* gen. nov., sp. nov., an extremely halophilic sulfate- and arsenate-respiring bacterium from Searles Lake, California. *Extremophiles* 16, 727-742.
- Boynton, W.V., et al., 2001. Thermal and Evolved Gas Analyzer: Part of the Mars Volatile and Climate Surveyor integrated payload. *J. Geophys. Res.* 106, 17683-17698.
- Boynton, W.V., et al., 2004. The Mars Odyssey Gamma-Ray Spectrometer instrument suite. *Space Sci. Rev.* 110, 37-83.
- Brass, G.W., 1980. Stability of brines on Mars. *Icarus* 42, 20-28.
- Bridges, J.C., et al., 2001. Alteration assemblages in martian meteorites: Implications for near-surface processes. *Space Sci. Rev.* 96, 365-392.
- Bridges, J.C., Grady, M.M., 2000. Evaporite mineral assemblages in the nakhlite (martian) meteorites. *Earth Planet. Sci. Lett.* 176, 267-279.
- Bruckner, J., et al., 2008. Mars Exploration Rovers: Chemical composition by the APXS, In: Bell III, J.F. (Ed.), *The Martian Surface: Composition, Mineralogy, and Physical Properties*. Cambridge Univ. Press, Cambridge, pp. 58-102.
- Bruckner, J., et al., 2001. Revised data of the Mars Pathfinder Alpha Proton X-Ray Spectrometer: Geochemical behavior of major and minor elements, *Lunar Planet. Sci.* XXXII, Houston, TX, p. 1293.
- Burgess, R., et al., 1989. Distribution of sulphides and oxidised sulphur components in SNC meteorites. *Earth Planet. Sci. Lett.* 93, 314-320.
- Burns, R.G., 1987. Ferric sulfates in Mars. *J. Geophys. Res.* 92, 570-674.
- Burns, R.G., 1988. Gossans on Mars, *Lunar Planet Sci.* XVIII, pp. 713-721.

- Burns, R.G., 1993. Rates and mechanisms of chemical weathering of ferromagnesium silicate minerals on Mars. *Geochim. Cosmochim. Acta* 57, 4555-4574.
- Burns, R.G., Fisher, D.S., 1990. Chemical evolution and oxidative weathering of magmatic iron sulfides on Mars, *Lunar Planet Sci.*, XXI, p. 145.
- Campbell, J.L., et al., 2012. Calibration of the Mars Science Laboratory Alpha Particle X-Ray Spectrometer. *Space Sci. Rev.* 170, 319-340.
- Canfield, D.E., 2001a. Biogeochemistry of Sulfur Isotopes. *Reviews in Mineralogy* 43, 607-636.
- Canfield, D.E., 2001b. Isotope fractionation by natural populations of sulfate-reducing bacteria. *Geochim. Cosmochim. Acta* 65, 1117-1124.
- Carr, M.H., 1983. Stability of streams and lakes on Mars. *Icarus* 56, 476-495.
- Carr, M.H., Head, J.W., 2010. Geologic history of Mars. *Earth Planet. Sci. Lett.* 294, 185-203.
- Carroll, M.R., Rutherford, M.J., 1985. Sulfide and sulfate saturation in hydrous silicate melts, 15th Lunar and Planetary Science Conference, Part 2, Houston, TX, pp. C601-C612.
- Catling, D.C., 1999. A chemical model for evaporites on early Mars: Possible sedimentary tracers of early climate and implications for exploration. *J. Geophys. Res.* 104, 16453-16469.
- Chevrier, V., et al., 2011. Sulfide petrology of four nakhlites: Northwest Africa 817, Northwest Africa 998, Nakhla, and Governador Valadares. *Met. Planet. Sci.* 46, 769-784.
- Chevrier, V., Mathé, P.E., 2007. Mineralogy and evolution of the surface of Mars: A review. *Planet. Space Sci.* 55, 289-314.
- Chevrier, V.F., Altheide, T.S., 2008. Low temperature aqueous ferric sulfate solutions on the surface of Mars. *Geophys. Res. Lett.* 35, CiteID L22101.
- Chevrier, V.F., et al., 2009. Viscosity of liquid ferric sulfate solutions and application to the formation of gullies on Mars. *J. Geophys. Res.* 114, CiteID E06001.
- Chipera, S.J., Vaniman, D.T., 2007. Experimental stability of magnesium sulfate hydrates that may be present on Mars. *Geochim. Cosmochim. Acta* 71, 241-250.
- Chipera, S.J., et al., 2007. The effect of temperature and water on ferric-sulfates, Lunar planet. *Sci.* XXXVIII, p. 1409.
- Chou, I.M., Seal, R.R., 2007. Magnesium and calcium sulfate stabilities and the water budget of Mars. *J. Geophys. Res.* 112.
- Christensen, P.R., et al., 2001. Mars Global Surveyor Thermal Emission Spectrometer experiment: Investigation description and surface science results. *J. Geophys. Res.* 106, 23823-23871.
- Christensen, P.R., et al., 2004a. The Thermal Emission Imaging System (THEMIS) for the Mars 2001 Odyssey Mission. *Space Sci. Rev.* 110, 85-130.

- Christensen, P.R., et al., 2004b. Initial results from the Mini-TES experiment in Gusev Crater from the Spirit Rover. *Science* 305, 837-842.
- Christensen, P.R., et al., 2004c. Mineralogy at Meridiani Planum from the Mini-TES experiment on the Opportunity rover. *Science* 306, 1733-1739.
- Clark, B.C., 1981. Sulfur: Fountainhead of life in the universe?, In: Billingham, J. (Ed.), *Conference on Life in the Universe*. MIT Press.
- Clark, B.C., 1993. Geochemical components in Martian soil. *Geochim. Cosmochim. Acta* 57, 4575-4581.
- Clark, B.C., et al., 1976. Inorganic analyses of martian surface samples at the Viking landing sites. *Science* 194, 1283-1288.
- Clark, B.C., et al., 1977. The Viking X-ray fluorescence experiment: Analytical methods and early results. *J. Geophys. Res.* 82, 4577-4594.
- Clark, B.C., et al., 1982. Chemical composition of Martian fines. *J. Geophys. Res.* 87, 10059.
- Clark, B.C., et al., 2005. Chemistry and mineralogy of outcrops at Meridiani Planum. *Earth Planet. Sci. Lett.* 240, 73-94.
- Clark, B.C., Van Hart, D.C., 1981. The salt on Mars. *Icarus* 45, 370-378.
- Clayton, R.N., 1993. Oxygen isotopes in meteorites. *Ann. Rev. Earth Planet. Sci.* 21, 15-149.
- Clayton, R.N., 2002. Self-shielding in the solar nebula. *Nature* 415, 860-861.
- Clayton, R.N., 2003. Oxygen isotopes in the solar system. *Space Sci. Rev.* 106, 19-32.
- Clayton, R.N., Mayeda, T.K., 1983. Oxygen isotopes in eucrites, shergottites, nakhlites, and chassignites. *Earth Planet. Sci. Lett.* 62, 1-6.
- Clayton, R.N., Mayeda, T.K., 1984. The oxygen isotope record in Murchison and other carbonaceous chondrites. *Earth Planet. Sci. Lett.* 67, 151-161.
- Clayton, R.N., Mayeda, T.K., 1996. Oxygen isotope studies of achondrites. *Geochim. Cosmochim. Acta* 60, 1999-2017.
- Clayton, R.N., et al., 1991. Oxygen isotope studies of ordinary chondrites. *Geochim. Cosmochim. Acta* 55, 2317-2337.
- Clayton, R.N., et al., 1976. A classification of meteorites based on oxygen isotopes. *Earth Planet. Sci. Lett.* 30, 10-18.
- Cloutis, E.A., et al., 2007. Stability of hydrated minerals on Mars. *Geophys. Res. Lett.* 34, L20202.
- Connerney, J.E.P., et al., 1999. Magnetic lineations in the ancient crust of Mars. *Science* 284.

- Dehouck, E., et al., 2012. Evaluating the role of sulfide-weathering in the formation of sulfates or carbonates on Mars. *Geochim. Cosmochim. Acta* 90, 47-63.
- Ding, S., et al., 2015. New bulk sulfur measurements of Martian meteorites and modeling the fate of sulfur during melting and crystallization - Implications for sulfur transfer from Martian mantle to crust-atmosphere system. *Earth Planet. Sci. Lett.* 409, 157-167.
- Ding, S., et al., 2014. Sulfur concentration of martian basalts at sulfide saturation at high pressures and temperatures - Implications for deep sulfur cycle on Mars. *Geochim. Cosmochim. Acta* 131, 227-246.
- Ding, T., et al., 2001. Calibrated sulfur isotope abundance ratios of three IAEA sulfur isotope reference materials and V-CDT with a reassessment of the atomic weight of sulfur. *Geochim. Cosmochim. Acta* 65, 2433-2437.
- Dreibus, G., et al., 1994. Chemical and mineral composition of ALH 84001: A martian orthopyroxenite. *Meteoritics* 29, 461.
- Dreibus, G., Palme, H., 1996. Cosmochemical constraints on the sulfur content in the Earth's core. *Geochim. Cosmochim. Acta* 60, 1125-1130.
- Dreibus, G., Wanke, H., 1985. Mars, a volatile-rich planet. *Meteoritics* 20, 367-381.
- Dyar, M.D., 2005. MIL03346, the most oxidized Martian meteorite: A first look at spectroscopy, petrography, and mineral chemistry. *J. Geophys. Res.* 110.
- Dyar, M.D., et al., 2011. Strategies for Mars remote Laser-Induced Breakdown Spectroscopy analysis of sulfur in geological samples. *Spectrochimica Acta Part B: Atomic Spectroscopy* 66, 39-56.
- Ebel, D.S., 2011. Sulfur in Extraterrestrial Bodies and the Deep Earth, In: Behrens, H., Webster, J.D. (Eds.), *Reviews in Mineralogy and Geochemistry*. Min. Soc. Amer., pp. 315-336.
- Edmonds, C.G., et al., 1991. Posttranscriptional modification of transfer-RNA in thermophilic archaea (archaeobacteria). *J. Bacteriol.* 173, 3138-3148.
- Ehlmann, B.L., Edwards, C.S., 2014. Mineralogy of the martian surface. *Ann. Rev. Earth Planet. Sci.* 42, 291-315.
- Ehlmann, B.L., et al., 2011. Subsurface water and clay mineral formation during the early history of Mars. *Nature* 479, 53-60.
- Ehlmann, B.L., et al., 2009. Identification of hydrated silicate minerals on Mars using MRO-CRISM: Geologic context near Nili Fossae and implications for aqueous alteration. *J. Geophys. Res.* 114.
- Elkins-Tanton, L., 2008. Linked magma ocean silidification and atmospheric growth for Earth and Mars. *Earth Planet. Sci. Lett.* 271, 181-191.
- Elkins-Tanton, L.T., et al., 2005. Possible formation of ancient crust on Mars through magma ocean processes. *J. Geophys. Res.* 110, E12S01.

- Elsgaard, L., et al., 1994. Microbial sulfate reduction in deep-sea sediments at the Guaymas Basin - hydrothermal vent area - Influence of temperature and substrates. *Geochim. Cosmochim. Acta* 58, 3335-3343.
- Elwood Madden, M.E., et al., 2004. Jarosite as an indicator of water-limited chemical weathering on Mars. *Nature* 431, 821-823.
- Encrenaz, T., et al., 2011. A stringent upper limit to SO₂ in the Martian atmosphere. *Astron. Astrophys.* 530, A37.
- Erkaev, N.V., et al., 2014. Escape of the martian protoatmosphere and initial water inventory. *Planet. Space Sci.* 98, 106-119.
- Fairen, A.G., et al., 2009. Stability against freezing of aqueous solutions on early Mars. *Nature* 459, 401-404.
- Farquhar, J., et al., 2000a. Atmospheric influence of Earth's earliest sulfur cycle. *Science* 289, 756-758.
- Farquhar, J., et al., 2007a. Implications of conservation of mass effects on mass-dependent isotope fractionations: Influence of network structure on sulfur isotope phase space of dissimilatory sulfate reduction. *Geochim. Cosmochim. Acta* 71, 5862-5875.
- Farquhar, J., et al., 2007b. Implications from sulfur isotopes of the Nakhla meteorite for the origin of sulfate on Mars. *Earth Planet. Sci. Lett.* 264, 1-8.
- Farquhar, J., et al., 2001. Observation of wavelength-sensitive mass-independent sulfur isotope effects during SO₂ photolysis: Implications for the early atmosphere. *J. Geophys. Res.* 106, 32829-32839.
- Farquhar, J., et al., 2000b. Evidence of atmospheric sulphur in the martian regolith from sulphur isotopes in meteorites. *Nature* 404, 50-52.
- Farrand, W.H., et al., 2009. Discovery of jarosite within the Mawrth Vallis region of Mars: Implications for the geologic history of the region. *Icarus* 204, 478-488.
- Fei, Y., Bertka, C.M., 2005. The interior of Mars. *Science* 308, 1120-1121.
- Fei, Y., et al., 2000. Structure type and bulk modulus of Fe₃S, a new iron-sulfur compound. *Am. Mineral.* 85, 1830-1833.
- Fialips, C.I., et al., 2005. Hydration state of zeolites, clays, and hydrated salts under present-day martian surface conditions: Can hydrous minerals account for Mars Odyssey observations of near-equatorial water-equivalent hydrogen? *Icarus* 178, 74-83.
- Fishbaugh, K.E., et al., 2007. On the origin of gypsum in the Mars north polar region. *J. Geophys. Res.* 112.
- Floran, R.J., Prinz, M., 1978. The Chassigny meteorite: A cumulate dunite with hydrous amphibole-bearing melt inclusions. *Geochim. Cosmochim. Acta* 42, 1213-1229.

- Foley, C.N., et al., 2003. Final chemical results from the Mars Pathfinder alpha proton X-ray spectrometer. *J. Geophys. Res.* 108, 8096.
- Foley, C.N., et al., 2001. Chemistry of Mars Pathfinder samples determined by the APXS, Lunar Planet. Sci. XXXII, Houston, TX, p. 1979.
- Folkner, W.M., et al., 1997. Interior structure and seasonal mass redistribution of Mars from ratio tracking of Mars Pathfinder. *Science* 278, 1749-1752.
- Foster, I.S., et al., 2010. Characterization of halophiles in natural MgSO₄ salts and laboratory enrichment samples: Astrobiological implications for Mars. *Planetary and Space Science* 58, 599-615.
- Franchi, I.A., et al., 1999. The oxygen-isotopic composition of Earth and Mars. *Met. Planet. Sci.* 34, 657-661.
- Frank, K.L., et al., 2015. Key factors influencing rates of heterotrophic sulfate reduction in active seafloor hydrothermal massive sulfide deposits. *Front. Microbiol.* 6, 1449.
- Frankel, C., 1996. *Volcanoes of the Solar System*. Cambridge University Press, Cambridge, UK.
- Franz, H.B., et al., 2013. Mass-independent fractionation of sulfur isotopes during broadband SO₂ photolysis: Comparison between ¹⁶O- and ¹⁸O-rich SO₂. *Chem. Geol.* 362, 56-65.
- Franz, H.B., et al., 2014a. Isotopic links between atmospheric chemistry and the deep sulphur cycle on Mars. *Nature* 508, 364-368.
- Franz, H.B., et al., 2014b. Carbon and sulfur isotopic composition of Yellowknife Bay sediments: Measurements by the Sample Analysis at Mars (SAM) Quadrupole Mass Spectrometer, Lunar Planet. Sci. XLV, The Woodlands, TX.
- Gaillard, F., et al., 2013. Geochemical reservoirs and timing of sulfur cycling on Mars. *Space Sci. Rev.* 174, 251-300.
- Gaillard, F., Scaillet, B., 2009. The sulfur content of volcanic gases on Mars. *Earth Planet. Sci. Lett.* 279, 34-43.
- Gaillard, F., Scaillet, B., 2014. Sulfur outgassing by volcanoes on Mars: What really matters, Workshop of Volatiles in the Martian Interior, Houston, TX, p. 1014.
- Gaillard, F., et al., 2011. Atmospheric oxygenation caused by a change in volcanic degassing pressure. *Nature* 478, 229-232.
- Gaillard, F., et al., 2015. The redox geodynamics linking basalts and their mantle sources through space and time. *Chem. Geol.* 418, 217-233.
- Gao, X., Thiemens, M.H., 1991. Systematic study of sulfur isotopic composition in iron meteorites and the occurrence of excess ³³S and ³⁶S. *Geochim. Cosmochim. Acta* 55, 2671-2679.

- Gao, X., Thiemens, M.H., 1993a. Isotopic composition and concentration of sulfur in carbonaceous chondrites. *Geochim. Cosmochim. Acta* 57, 3159-3169.
- Gao, X., Thiemens, M.H., 1993b. Variations of the isotopic composition of sulfur in enstatite and ordinary chondrites. *Geochim. Cosmochim. Acta* 57, 3171-3176.
- Gellert, R., et al., 2006. Alpha Particle X-Ray Spectrometer (APXS): Results from Gusev crater and calibration report. *J. Geophys. Res.* 111, E02S05.
- Gendrin, A., et al., 2005. Sulfates in martian layered terrains: The OMEGA/Mars Express view. *Science* 307, 1587-1591.
- Gibson, E.K., Jr., 1983. Sulfur in achondritic meteorites. *Proc. Lunar Planet. Sci.* 14, 247-248.
- Gibson, E.K., et al., 1985. Sulfur in achondritic meteorites. *Meteoritics* 20, 503-511.
- Glotch, T.D., et al., 2006. Mineralogy of the light-toned outcrop at Meridiani Planum as seen by the Miniature Thermal Emission Spectrometer and implications for its formation. *J. Geophys. Res.* 111, E12S03.
- Golden, D.C., et al., 2009. Sulfur mineralogy at the Mars Phoenix landing site, Lunar Planet Sci. XL, The Woodlands, TX, p. 2319.
- Gooding, J.L., 1978. Chemical weathering on Mars. *Icarus* 33, 483-513.
- Gooding, J.L., et al., 1990. Volatile compounds in shergottite and nakhlite meteorites. *Meteoritics* 25, 281-289.
- Gooding, J.L., Muenow, D.W., 1986. Martian volatiles in shergottite EETA 79001: New evidence from oxidized sulfur and sulfur-rich aluminosilicates. *Geochim. Cosmochim. Acta* 50, 1049-1059.
- Gooding, J.L., et al., 1991. Aqueous alteration of the Nakhla meteorite. *Meteoritics* 26, 135-143.
- Gough, D.O., 1981. Solar interior structure and luminosity variations. *Solar Phys.* 74, 21-34.
- Gounelle, M., Zolensky, M.E., 2001. A terrestrial origin for sulfate veins in CI1 chondrites. *Met. Planet. Sci.* 36, 1321-1329.
- Greenwood, J.P., et al., 2000. Sulfur isotopic compositions of individual sulfides in martian meteorites ALH 84001 and Nakhla: Implications for crust-regolith exchange on Mars. *Earth Planet. Sci. Lett.* 184, 23-35.
- Gregersen, L.H., et al., 2011. Mechanisms and evolution of oxidative sulfur metabolism in green sulfur bacteria. *Front. Microbiol.* 2, doi: 10.3389/fmicb.2011.00116.
- Gross, J., et al., 2013. Petrography, mineral chemistry, and crystallization history of olivine-phyric shergottite NWA 6234: A new melt composition. *Met. Planet. Sci.* 48, 854-871.
- Grott, M., et al., 2013. Long-term evolution of the martian crust-mantle system. *Space Sci. Rev.* 174, 49-111.

Grott, M., et al., 2011. Volcanic outgassing of CO₂ and H₂O on Mars. *Earth Planet. Sci. Lett.* 308, 391-400.

Grotzinger, J.P., et al., 2005. Stratigraphy and sedimentology of a dry to wet eolian depositional system, Burns formation, Meridiani Planum, Mars. *Earth Planet. Sci. Lett.* 240, 11-72.

Grotzinger, J.P., et al., 2014. A habitable fluvio-lacustrine environment at Yellowknife Bay, Gale Crater, Mars. *Science* 343.

Gulick, V.C., Baker, V.R., 1989. Fluvial valleys and Martian paleoclimates. *Nature* 341, 514-516.

Haberle, R.M., 1998. Early Mars Climate Models. *J. Geophys. Res.* 103, 28467-28480.

Halevy, I., Head, J.W.I., 2014. Episodic warming of early Mars by punctuated volcanism. *Nature Geosci.* 7.

Halevy, I., et al., 2010. Explaining the structure of the Archean mass-independent sulfur isotope record. *Science* 329, 204-207.

Halevy, I., et al., 2007. A sulfur dioxide climate feedback on early Mars. *Science* 318, 1903-1907.

Hartmann, W.K., Neukum, G., 2001. Cratering chronology and the evolution of Mars. *Space Sci. Rev.* 96, 165-194.

Hauber, E., et al., 2011. Very recent and wide-spread basaltic volcanism on Mars. *Geophys. Res. Lett.* 38, L10201.

Haughton, D.R., et al., 1974. Solubility of sulfur in mafic magmas. *Bull. Soc. Econ. Geol.* 69, 451-467.

Head, J.W., et al., 2002. Northern lowlands of Mars: Evidence for widespread volcanic flooding and tectonic deformation in the Hesperian Period. *J. Geophys. Res. Planets* 107, E001445.

Head, J.W., et al., 2006. The Huygens-Hellas giant dike system on Mars: Implications for Late Noachian-Early Hesperian volcanic resurfacing and climatic evolution. *Geology* 34, 285-288.

Henley, R.W., et al., 2015. Porphyry copper deposit formation by sub-volcanic sulphur dioxide flux and chemisorption. *Nature Geosci.* 8, 210-215.

Herd, C.D.K., 2003. The oxygen fugacity of olivine-phyric martian basalts and the components within the mantle and crust of Mars. *Met. Planet. Sci.* 38, 1793-1805.

Herd, C.D.K., et al., 2002. Oxygen fugacity and geochemical variations in the martian basalts: Implications for martian basalt petrogenesis and the oxidation state of the upper mantle of Mars. *Geochim. Cosmochim. Acta* 66, 2025-2036.

Hirschmann, M.M., Withers, A.C., 2008. Ventilation of CO₂ from a reduced mantle and consequences for the early Martian greenhouse. *Earth Planet. Sci. Lett.* 270, 147-155.

- Hoefen, T.M., et al., 2003. Discovery of Olivine in the Nili Fossae Region of Mars. *Science* 302, 627-630.
- Hoefen, T.M., et al., 2000. Unique Spectral Features in Mars Global Surveyor Thermal Emission Spectra: Implications for Surface Mineralogy in Nili Fossae, *AAS*, p. 1118.
- Hogenboom, D.L., et al., 1995. Magnesium sulfate-water to 400 MPa using a novel piezometer: Densities, phase equilibria, and planetological implications. *Icarus* 115, 258-277.
- Hughes, K.A., Lawley, B., 2003. A novel Antarctic microbial endolithic community within gypsum crusts. *Environ Microbiol.* 5, 555-565.
- Hulston, J.R., Thode, H.G., 1965. Variations in the S33, S34, and S36 contents of meteorites and their relation to chemical and nuclear effects. *J. Geophys. Res.* 70, 3475-3484.
- Humayun, M., et al., 2013. Origin and age of the earliest Martian crust from meteorite NWA 7533. *Nature* 503, 513-516.
- Hyde, B.C., et al., 2011. Methods to analyze metastable and microparticulate hydrated and hydrous iron sulfate minerals. *Am. Mineral.* 96, 1856-1869.
- Imae, N., Ikeda, Y., 2007. Petrology of the Miller Range 03346 nakhlite in comparison with the Yamato-000593 nakhlite. *Met. Planet. Sci.* 42, 171-184.
- Imae, N., et al., 2005. Petrology of the Yamato nakhlites. *Met. Planet. Sci.* 40, 1581-1598.
- Irving, A.J., 2017. An up-to-date list of martian meteorites. <http://www.imca.cc/mars/martian-meteorites-list.htm>.
- Janchen, J., et al., 2005. Experimental studies of the water sorption properties of Mars-relevant porous minerals and sulfates, *Lunar Planet. Sci.* XXXVI, p. 1263.
- Jensen, M.L., Nakai, N., 1962. Sulfur isotope meteorite standards, results and recommendations, *Biogeochemistry of Sulfur Isotopes*. NSF Symposium, New Haven, CT.
- Johnson, J.R., et al., 2007. Mineralogic constraints on sulfur-rich soils from Pancam spectra at Gusev crater, Mars. *Geophysical Research Letters* 34.
- Johnson, S.S., et al., 2015. Insights from the metagenome of an acid salt lake: The role of biology in an extreme depositional environment. *PLoS ONE* 10, e0122869.
- Johnson, S.S., et al., 2008. Sulfur-induced greenhouse warming on early Mars. *J. Geophys. Res.* 113, E08005.
- Johnson, S.S., et al., 2009. Fate of SO₂ in the ancient Martian atmosphere: Implications for transient greenhouse warming. *J. Geophys. Res.* 114, E11011.
- Jones, J.H., 1989. Isotopic relationships among the shergottites, the nakhlites, and Chassigny. *Proc. Lunar Planet. Sci.* 19, 465-474.
- Jugo, P.J., 2009. Sulfur content at sulfide saturation in oxidized magmas. *Geology* 37, 415-418.

- Jugo, P.J., et al., 2005. Experimental data on the speciation of sulfur as a function of oxygen fugacity in basaltic melts. *Geochim. Cosmochim. Acta* 69, 497-503.
- Jugo, P.J., et al., 2010. Sulfur K-edge XANES analysis of natural and synthetic basaltic glasses: Implications for S speciation and S content as a function of oxygen fugacity. *Geochim. Cosmochim. Acta* 74, 5926-5938.
- Kamysny, A., Jr., et al., 2014. Multiple sulfur isotopes fractionations associated with abiotic sulfur transformations in Yellowstone National Park geothermal springs. *Geochem. Trans.* 15.
- Kargel, J.S., Lewis, J.S., 1993. The composition and early evolution of Earth. *Icarus* 105, 1-25.
- Karunatillake, S., et al., 2014. Sulfates hydrating bulk soil in the martian low and middle latitudes. *Geophys. Res. Lett.* 41, 7987-7996.
- Kasting, J.F., 1991. CO₂ condensation and the climate of early Mars. *Icarus* 94, 1-13.
- Kemp, A.L.W., Thode, H.G., 1968. The mechanism of the bacterial reduction of sulphate and of sulphite from isotope fractionation studies. *Geochim. Cosmochim. Acta* 32, 71-91.
- Kerber, L., et al., 2015. Sulfur in the early martian atmosphere revisited: Experiments with a 3-D Global Climate Model. *Icarus* 261, 133-148.
- Khan, A., Connolly, J.A.D., 2008. Constraining the composition and thermal state of Mars from inversion of geophysical data. *J. Geophys. Res.* 113, CiteID E07003.
- Khayat, A.S., et al., 2015. A search for SO₂, H₂S and SO above Tharsis and Syrtis volcanic districts on Mars using ground-based high-resolution submillimeter spectroscopy. *Icarus* 253, 130-141.
- King, P.L., et al., 2008. Fe-sulfates in Mars: Considerations for martian environmental conditions, Mars sample return and hazards, Ground truth from Mars: Science Payoff from a Sample Return Mission. LPI, Albuquerque, pp. 46-47.
- King, P.L., et al., 2004. The composition and evolution of primordial solutions on Mars, with application to other planetary bodies. *Geochim. Cosmochim. Acta* 68, 4993-5008.
- King, P.L., McLennan, S.M., 2010. Sulfur on Mars. *Elements* 6, 107-112.
- King, P.L., McSween, H.Y., 2005. Effects of H₂O, pH, and oxidation state on the stability of Fe minerals on Mars. *J. Geophys. Res.* 110.
- Kiseeva, E.S., Wood, B.J., 2013. A simple model for chalcophile element partitioning between sulphide and silicate liquids with geochemical applications. *Earth Planet. Sci. Lett.* 383, 68-81.
- Klingelhofer, G., et al., 2004. Jarosite and hematite at Meridiani Planum from Opportunity's Mossbauer Spectrometer. *Science* 306, 1740-1745.
- Knoblauch, C., Jorgensen, B.B., 1999. Effect of temperature on sulphate reduction, growth rate and growth yield in five psychrophilic sulphate-reducing bacteria from Arctic sediments. *Environ Microbiol.* 1, 457-467.

- Konneke, M., et al., 2013. *Desulfoconvexum algidum* gen. nov., sp. no., a psychrophilic sulfate-reducing bacterium isolated from a permanently cold marine sediment. *Int. J. System. Evol. Microbiol.* 63, 959-964.
- Konopliv, A.S., et al., 2011. Mars high resolution gravity fields from MRO, Mars seasonal gravity, and other dynamical parameters. *Icarus* 211, 401-428.
- Kounaves, S.P., et al., 2010. Soluble sulfate in the martian soil at the Phoenix landing site. *Geophys. Res. Lett.* 37, L09201.
- Kounaves, S.P., et al., 2009. The MECA Wet Chemistry Laboratory on the 2009 Phoenix Mars Scout Lander. *J. Geophys. Res.* 114, E00A19.
- Krasnopolsky, V.A., 2012. Search for methane and upper limits to ethane and SO₂ on Mars. *Icarus* 217, 144-152.
- Krasnopolsky, V.A., et al., 2004. Detection of methane in the martian atmosphere: Evidence for life? *Icarus* 172, 537-547.
- Kress, V.C., Carmichael, I.S.E., 1991. The compressibility of silicate liquids containing Fe₂O₃ and the effect of composition, temperature, oxygen fugacity and pressure on their redox states. *Contr. Min. Petr.* 108, 82-92.
- Labidi, J., et al., 2013. Non-chondritic sulphur isotope composition of the terrestrial mantle. *Nature* 501, 208-212.
- Labidi, J., et al., 2016. Experimentally determined sulfur isotope fractionation between metal and silicate and implications for planetary differentiation. *Geochim. Cosmochim. Acta* 175, 181-194.
- Lamarche-Gagnon, G., et al., 2015. Evidence of in situ microbial activity and sulphidogenesis in perennially sub-0 degrees C and hypersaline sediments of a high Arctic permafrost spring. *Extremophiles* 19, 1-15.
- Lane, M.D., 2007. Mid-infrared emission spectroscopy of sulfate and sulfate-bearing minerals. *Am. Mineral.* 92, 1-18.
- Lane, M.D., et al., 2008. Mineralogy of the Paso Robles soils on Mars. *Am. Mineral.* 93, 728-739.
- Lane, M.D., et al., 2007. Identifying the phosphate and ferric sulfate minerals in the Paso Robles soils (Gusev crater, Mars) using an integrated spectral approach, *Lunar Planet. Sci. XXXVIII*, League City, TX, p. 1338.
- Lapen, T.J., et al., 2010. A younger age for ALH84001 and its geochemical link to shergottite sources in Mars. *Science* 328, 347-351.
- Lauretta, D.S., et al., 1997. Experimental simulations of sulfide formation in the solar nebula. *Science* 277, 358-360.
- Leshin, L.A., Vicenzi, E., 2006. Aqueous processes recorded by Martian meteorites: Analyzing Martian water on Earth. *Elements* 2, 157-162.

- Lever, M.A., et al., 2013. Evidence for microbial carbon and sulfur cycling in deeply buried ridge flank basalt. *Science* 339, 1305-1308.
- Li, C., Ripley, E.M., 2005. Empirical equations to predict the sulfur content of mafic magmas at sulfide saturation and applications to magmatic sulfide deposits. *Mineral. Depos.* 40, 218-230.
- Li, C., Ripley, E.M., 2009. Sulfur contents at sulfide-liquid or anhydrite saturation in silicate melts: empirical equations and example applications. *Econ. Geol.* 104, 405-412.
- Lichtenberg, K.A., et al., 2010. Stratigraphy of hydrated sulfates in the sedimentary deposits of Aram Chaos, Mars. *J. Geophys. Res.* 115, E00D17.
- Lillis, R.J., et al., 2008. Rapid decrease in Martian crustal magnetization in the Noachian era: Implications for the dynamo and climate of early Mars. *Geophys. Res. Lett.* 35, L14203.
- Lin, T.J., et al., 2016. Linkages between mineralogy, fluid chemistry, and microbial communities within hydrothermal chimneys from the Endeavour Segment, Juan de Fuca Ridge. *Geochem. Geophys. Geosys.* 17, 300-323.
- Liu, Y., Wang, A., 2015. Dehydration of Na-jarosite, ferricopiapite, and rhomboclase at temperatures of 50 deg C and 95 deg C: Implications for martian ferric sulfates. *J. Raman Spectrosc.* 46, 493-500.
- Lodders, K., 1998. A survey of shergottite, nakhlite and chassigny meteorites whole-rock composition. *Met. Planet. Sci.* 33, A183-A190.
- Lodders, K., Fegley, B., Jr., 1997. An oxygen isotope model for the composition of Mars. *Icarus* 126, 373-394.
- Lodders, K., et al., 2009. Abundances of the elements in the solar system, In: Trumper, J.E. (Ed.), *Landolt-Bornstein, New Series, Astron. Astrophys.* Springer-Verlag, Berlin, Heidelberg, New York.
- Lorand, J.P., et al., 2012. Metal-saturated sulfide assemblages in NWA 2737: Evidence for impact-related sulfur devolatilization in Martian meteorites. *Met. Planet. Sci.* 47, 1830-1841.
- Lorand, J.P., et al., 2005. Sulfide mineralogy and redox conditions in some shergottites. *Met. Planet. Sci.* 40, 1257-1272.
- Lorand, J.P., et al., 2015. Nickeliferous pyrite tracks pervasive hydrothermal alteration in martian regolith breccia: A study in NWA 7533. *Met. Planet. Sci.*
- Louzada, K.L., et al., 2007. Effect of shock on the magnetic properties of pyrrhotite, the Martian crust, and meteorites. *Geophys. Res. Lett.* 34, L05204.
- MacPherson, G.J., II, T.M.S.R.S.S.G., 2005. The first Mars surface-sample return mission: Revised science considerations in light of the 2004 MER results, Appendix III of *Science Priorities for Mars Sample Return*, p. 68.
- Madden, M.E., et al., 2004. Jarosite as an indicator of water-limited chemical weathering on Mars. *Nature* 431, 821-823.

- Mahaffy, P.R., et al., 2012. The Sample Analysis at Mars Investigation and Instrument Suite. *Space Sci. Rev.* 170, 401-478.
- Mangold, N., et al., 2008. Spectral and geological study of the sulfate-rich region of West Candor Chasma, Mars. *Icarus* 194, 519-543.
- Marion, G.M., et al., 2008. Modeling ferrous-ferric iron chemistry with application to martian surface geochemistry. *Geochim. Cosmochim. Acta* 72, 242-266.
- McAdam, A.C., et al., 2014. Sulfur-bearing phases detected by evolved gas analysis of the Rocknest aeolian deposit, Gale Crater, Mars. *J. Geophys. Res. Planets* 119, 373-393.
- McAdam, A.C., et al., 2016. Reactions involving calcium and magnesium sulfates as potential sources of sulfur dioxide during MSL evolved gas analysis, *Lunar Planet Sci. XLVII*, The Woodlands, TX, p. 2277.
- McCubbin, F.M., et al., 2009. Hydrothermal jarosite and hematite in a pyroxene-hosted melt inclusion in martian meteorite Miller Range (MIL) 03346: Implications for magmatic-hydrothermal fluids on Mars. *Geochim. Cosmochim. Acta* 73, 4907-4917.
- McLennan, S.M., et al., 2014. Elemental geochemistry of sedimentary rocks at Yellowknife Bay, Gale Crater, Mars. *Science* 343.
- McLennan, S.M., et al., 2005. Provenance and diagenesis of the evaporite-bearing Burns formation, Meridiani Planum, Mars. *Earth Planet. Sci. Lett.* 240, 95-121.
- McLennan, S.M., et al., 2010. Distribution of sulfur on the surface of Mars determined by the 2001 Mars Odyssey Gamma-Ray Spectrometer, *Lunar Planet. Sci. XLI*, The Woodlands, TX, p. 1533.
- McLennan, S.M., Grotzinger, J.P., 2008. The Martian surface - Composition, mineralogy, and physical properties, In: Bell, J.F.I. (Ed.), *The sedimentary rock cycle of Mars*. Cambridge University Press, p. 541.
- McLennan, S.M., et al., 2012. Planning for Mars returned sample science: Final report of the MSR End-to-End International Science Analysis Group (E2E-iSAG). *Astrobiology* 12, 175-230.
- McSween, H.Y., 1994. What we have learned about Mars from SNC meteorites. *Meteoritics* 29, 757-779.
- McSween, H.Y., Jr., et al., 1996. QUE 94201 shergottite: Crystallization of a martian basaltic magma. *Geochim. Cosmochim. Acta* 60, 4563-4569.
- McSween, H.Y., Keil, K., 2000. Mixing relationships in the Martian regolith and the composition of globally homogeneous dust. *Geochim. Cosmochim. Acta* 64, 2155-2166.
- Metrich, N., et al., 2009. The oxidation state of sulfur in synthetic and natural glasses determined by X-ray absorption spectroscopy. *Geochim. Cosmochim. Acta* 73, 2382-2399.
- Meyer, C., 2015. *The Martian Meteorite Compendium*.
<http://curator.jsc.nasa.gov/antmet/mmc/index.cfm>.

- Michalski, J.R., Bleacher, J.E., 2013. Supervolcanoes within an ancient volcanic province in Arabia Terra, Mars. *Nature* 502, 47-52.
- Mikouchi, T., et al., 2003. Mineralogy and petrology of Yamato 000593: Comparison with other martian nakhlite meteorites. *Ant. Met. Res.* 16, 34-57.
- Mikouchi, T., et al., 2006. Relative burial depths of nakhlites: An update, *Lunar Planet. Sci.* XXXVII, Houston, TX, p. 1865.
- Ming, D.W., et al., 2014. Volatile and organic compositions of sedimentary rocks in Yellowknife Bay, Gale Crater, Mars. *Science* 343.
- Ming, D.W., et al., 2008. Geochemical properties of rocks and soils in Gusev Crater, Mars: Results of the Alpha Particle X-Ray Spectrometer from Cumberland Ridge to Home Plate. *J. Geophys. Res.* 113, E12S39.
- Ming, D.W., et al., 2006. Geochemical and mineralogical indicators for aqueous processes in the Columbia Hills of Gusev crater, Mars. *J. Geophys. Res.* 111, E02S12.
- Misawa, K., et al., 2003. Crystallization and alteration ages of the Antarctic nakhlite Yamato 00093. *Lunar Planet. Sci.* XXXIV, 1556.
- Mischna, M.A., et al., 2013. Effects of obliquity and water vapor/trace gas greenhouses in the early martian climate. *J. Geophys. Res. Planets* 118, 560-576.
- Morris, R.V., et al., 2006. Mössbauer mineralogy of rock, soil, and dust at Meridiani Planum, Mars: Opportunity's journey across sulfate-rich outcrop, basaltic sand and dust, and hematite lag deposits. *J. Geophys. Res.* 111, E02S13.
- Morris, R.V., et al., 2015. Update on the chemical composition of crystalline, smectite, and amorphous components for Rocknest soil and John Klein and Cumberland mudstone drill fines at Gale crater, Mars, *Lunar Planet. Sci.* XLVI, The Woodlands, TX, p. 1832.
- Morris, R.V., et al., 2000. Mineralogy, composition, and alteration of Mars Pathfinder rocks and soils: Evidence from multispectral, elemental, and magnetic data on terrestrial analogue, SNC meteorites, and Pathfinder samples. *J. Geophys. Res.* 105, 1757-1818.
- Morris, R.V., et al., 2016. Silicic volcanism on Mars evidenced by tridymite in high-SiO₂ sedimentary rock at Gale crater. *Proc. Natl. Acad. Sci.* 113, 7071-7076.
- Murchie, S., et al., 2009a. Evidence for the origin of layered deposits in Candor Chasma, Mars, from mineral composition and hydrologic modeling. *J. Geophys. Res.* 114, E00D05.
- Murchie, S.L., et al., 2009b. A synthesis of Martian aqueous mineralogy after 1 Mars year of observations from the Mars Reconnaissance Orbiter. *J. Geophys. Res. Planets* 114, E00D06.
- Mustard, J.F., Ehlmann, B.L., 2010. Intact stratigraphy traversing the phyllosilicate to sulfate eras at the Syrtis-Isidis contact, Mars, *Lunar Planet. Sci.* XLI, The Woodlands, TX, p. 1533.
- Nachon, M., et al., 2014. Calcium sulfate veins characterized by ChemCam/Curiosity at Gale crater, Mars. *J. Geophys. Res. Planets* 119, 1991-2016.

- Neukum, G., et al., 2004. Recent and episodic volcanic and glacial activity on Mars revealed by the High Resolution Stereo Camera. *Nature* 432, 971-979.
- Newsom, H.E., et al., 1999. Mixed hydrothermal fluids and the origin of the martian soil. *J. Geophys. Res.* 104, 8717-8728.
- Noe Dobrea, E.Z., et al., 2006a. Analysis of a spectrally unique deposit in the dissected Noachian terrain of Mars. *J. Geophys. Res.* 111, E06007.
- Noe Dobrea, E.Z., et al., 2006b. OMEGA analysis of light-toned outcrops in the chaotic terrain of the eastern Valles Marineris region, *Lunar Planet Sci. XXXVII*, Houston, TX, p. 2068.
- Nyquist, L.E., et al., 2001. Ages and geologic histories of martian meteorites. *Space Sci. Rev.* 96, 105-164.
- O'Neill, H.S.C., Mavrogenes, J., 2002. The sulfide saturation capacity and the sulfur content at sulfide saturation of silicate melts at 1400 deg C and 1 bar. *J. Petrol.* 43, 1049-1087.
- Ono, S., et al., 2006. Mass-dependent fractionation of quadruple stable sulfur isotope system as a new tracer of sulfur biogeochemical cycles. *Geochim. Cosmochim. Acta* 70, 2238-2252.
- Orsi, W.D., et al., 2016. Transcriptional analysis of sulfate reducing and chemolithotrophic sulfur oxidizing bacteria in the deep seafloor. *Environ Microbiol. Rep.* 8, 452-460.
- Palme, H., Jones, A., 2003. Solar system abundances of the elements, *Treatise on Geochemistry*, pp. 41-61.
- Palme, H., et al., 1988. Moderately volatile elements, In: Kerridge, J.F., et al. (Ed.), *Meteorites and the Early Solar System*. Univ. Arizona Press, pp. 436-461.
- Pasek, M., et al., 2005. Sulfur chemistry with time-varying oxygen abundance during Solar System formation. *Icarus* 175, 1-14.
- Pavlov, A.A., Kasting, J.F., 2002. Mass-independent fractionation of sulfur isotopes in Archean sediments: Strong evidence for an anoxic Archean atmosphere. *Astrobiology* 2, 27-41.
- Peale, S.J., et al., 1975. Origin of Martian channels: Clathrates and water. *Science* 187, 273-274.
- Peterson, R.C., Grant, A., 2005. Dehydration and crystallization reactions of secondary sulfate minerals found in mine waste: In situ powder diffraction experiments. *Can. Mineral.* 41, 1173-1181.
- Peterson, R.C., et al., 2008. Meridianite: A new mineral species observed on Earth and predicted to exist on Mars. *Am. Mineral.* 92, 1756-1759.
- Peterson, R.C., Wang, R., 2006. Crystal molds on Mars: Melting of a possible new mineral species to create chaotic terrain. *Geology* 34, 957-960.
- Phillips, R.J., et al., 2001. Ancient geodynamics and global-scale hydrology on Mars. *Science* 291, 2587-2591.

- Pollack, J.B., et al., 1987. The case for a warm, wet climate on early Mars. *Icarus* 71, 203-224.
- Postawko, S.E., Kuhn, W.R., 1986. Effect of the greenhouse gases (CO₂, H₂O, SO₂) on Martian paleoclimate. *J. Geophys. Res.* 91, 431-438.
- Poulet, F., et al., 2005. Phyllosilicates on Mars and implications for early martian climate. *Nature* 438, 623-627.
- Ramirez, R.M., et al., 2013. Warming early Mars with CO₂ and H₂. *Nature Geosci.* 7, 59-63.
- Rampe, E., et al., 2016. Mineralogical and geochemical trends in a fluviolacustrine sequence in Gale crater, Mars, Goldschmidt Conf., Japan.
- Rampe, E.B., et al., 2015. Potential cement phases in sedimentary rocks drilled by Curiosity at Gale crater, Mars, Lunar Planet. Sci. XLVI, The Woodlands, TX, p. 2038.
- Rao, M.N., et al., 1999. Martian soil component in impact glasses in a martian meteorite. *Geophys. Res. Lett.* 26, 3265-3268.
- Rao, M.N., et al., 2011. Isotopic evidence for a Martian regolith component in shergottite meteorites. *J. Geophys. Res. Planets* 116, E08006.
- Rao, M.N., et al., 2012. Laboratory shock experiments on basalt - iron sulfate mixes at ~40-50 GPa and their relevance to the martian regolith component present in shergottites, Lunar Planet. Sci. XLIII, The Woodlands, TX, p. 1659.
- Rao, M.N., et al., 2008. The nature of Martian fluids based on mobile element studies in salt-assemblages from Martian meteorites. *J. Geophys. Res.* 113, E06002.
- Rieder, R., 1997. The chemical composition of martian soil and rocks returned by the mobile Alpha Proton X-ray Spectrometer: Preliminary results from the X-ray mode. *Science* 278, 1771-1774.
- Rieder, R., et al., 2004. APXS on Mars: Analyses of soils and rocks at Gusev Crater and Meridiani Planum, Lunar Planet. Sci. XXXV, League City, TX, p. 2172.
- Righter, K., et al., 2009. Experimental evidence for sulfur-rich martian magmas: Implications for volcanism and surficial sulfur sources. *Earth Planet. Sci. Lett.* 288, 235-243.
- Ringwood, A.E., 1979. *On the origin of the Earth and Moon*. Springer Verlag, New York.
- Rivoldini, A., et al., 2011. Geodesy constraints on the interior structure and composition of Mars. *Icarus* 213, 451-472.
- Roach, L.H., et al., 2010. Diagenetic haematite and sulfate assemblages in Valles Marineris. *Icarus* 207, 659-674.
- Robbins, S.J., et al., 2011. The volcanic history of Mars: High-resolution crater-based studies of the calderas of 20 volcanoes. *Icarus* 211, 1179-1203.

- Robinson, B.W., 1993. Sulfur isotope standards, Reference and intercomparison materials for stable isotopes of light elements. IAEA consultants meeting, Vienna.
- Rochette, P., et al., 2005. Matching martian crustal magnetization and magnetic properties of martian meteorites. *Met. Planet. Sci.* 40, 529-540.
- Rouchy, J.-M., Monty, C., 1981. Stromatolites and cryptalgal alminites of Messinian gypsum of Cyprus, In: Monty, C. (Ed.), *Phanerozoic Stromatolites*. Springer, Berlin, pp. 155-178.
- Ruff, S.W., et al., 2006. The rocks of Gusev crater as viewed by the Mini-TES instrument. *J. Geophys. Res.* 111, E12S18.
- Sagan, C., Chyba, C., 1997. The early faint Sun paradox: Organic shielding of ultraviolet-labile greenhouse gases. *Science* 276, 1217-1221.
- Sagan, C., Mullen, G., 1972. Earth and Mars: Evolution of atmospheres and surface temperatures. *Astrophys. J.* 360, 727-736.
- Sagemann, J., et al., 1998. Temperature dependence and rates of sulfate reduction in cold sediments of Svalbard, Arctic Ocean. *Geomicro. J.* 15, 85-100.
- Salle, B., et al., 2004. Laser-induced breakdown spectroscopy for Mars surface analysis: Capabilities at stand-off distances and detection of chlorine and sulfur elements. *Spectrochim. Acta Part B* 59, 1413-1422.
- Sanloup, C., et al., 1999. A simple chondritic model of Mars. *Phys. Earth Planet. Int.* 112, 43-54.
- Sattley, W.M., Madigan, M.T., 2010. Temperature and nutrient induced responses of Lake Fryxell sulfate-reducing prokaryotes and description of *Desulfovibrio lacusfryxellense*, sp. nov., a pervasive, cold-active, sulfate-reducing bacterium from Lake Fryxell, Antarctica. *Extremophiles* 14, 357-366.
- Schrader, C.M., et al., 2011. Ni, S, and Cl in EETA 79001 lithology C, Lunar Planet. Sci. XLII, The Woodlands, TX, p. 2814.
- Schubert, G., Spohn, T., 1990. Thermal history of Mars and the sulfur content of its core. *J. Geophys. Res.* 95, 14095-14104.
- Self, S., et al., 2006. Volatile fluxes during flood basalt eruptions and potential effects on the global environment: A Deccan perspective. *Earth Planet. Sci. Lett.* 248, 518-532.
- Settle, M., 1979. Formation and deposition of volcanic sulfate aerosols on Mars. *J. Geophys. Res.* 84, 8343-8354.
- Shahar, A., et al., 2009. Sulfur isotopic fractionation during the differentiation of Mars. *Geochim. Cosmochim. Acta* 73, A1201.
- Shahar, A., et al., 2015. Sulfur-controlled iron isotope fractionation experiments of core formation in planetary bodies. *Geochim. Cosmochim. Acta* 150, 253-264.

- Shen, Y., et al., 2001. Isotopic evidence for microbial sulphate reduction in the early Archaean era. *Nature* 410, 77-81.
- Shirai, N., Ebihara, M., 2004. Chemical characteristics of an olivine-phyric shergottite, Yamato 980459, *Lunar Planet. Sci. XXXV*, Houston, TX, p. 1511.
- Shooner, F., et al., 1996. Isolation, phenotypic characterization, and phylogenetic position of a novel, facultatively autotrophic, moderately thermophilic bacterium, *Thiobacillus thermosulfatus* sp. nov. *Int. J. System. Bacteriol.* 46, 409-415.
- Siebach, K.L., et al., 2014. Subaqueous shrinkage cracks in the Sheepbed mudstone: Implications for early fluid diagenesis, Gale crater, Mars. *J. Geophys. Res. Planets* 119, 1597-1613.
- Smith, J.V., Hervig, R.L., 1979. Shergotty meteorite: Mineralogy, petrography and minor elements. *Meteoritics* 14, 121-142.
- Sobron, P., et al., 2012. Extraction of compositional and hydration information of sulfates from laser-induced plasma spectra recorded under Mars atmospheric conditions - Implications for ChemCam investigations on Curiosity rover. *Spectrochim. Acta Part B* 68, 1-16.
- Solomon, S.C., et al., 2005. New perspectives on ancient Mars. *Science* 307, 1214-1220.
- Squyres, S.W., 1984. The history of water on Mars. *Ann. Rev. Earth Planet. Sci.* 12, 83-106.
- Squyres, S.W., et al., 2012. Ancient impact and aqueous processes at Endeavour crater, Mars. *Science* 336, 570-576.
- Squyres, S.W., et al., 2006. Rocks of the Columbia Hills. *J. Geophys. Res.* 111, E02S11.
- Squyres, S.W., Kasting, J.F., 1994. Early Mars: How warm and wet? *Science* 265, 744-749.
- Stam, M.C., et al., 2010. Sulfate reducing activity and sulfur isotope fractionation by natural microbial communities in sediments of a hypersaline soda lake (Mono Lake, California). *Chem. Geol.* 278, 23-30.
- Stetter, K.O., 1996. Hyperthermophiles in the history of life, In: Bock, G.R., Goode, J.A. (Eds.), *Evolution of Hydrothermal Ecosystems on Earth (and Mars?)*. CIBA Foundation Symposia, pp. 1-18.
- Stevenson, D.J., 2001. Mars' core and magnetism. *Nature* 412, 214-219.
- Stewart, A.J., et al., 2007. Mars: A new core-crystallization regime. *Science* 316, 1323-1325.
- Stockstill, K.R., et al., 2005. Thermal Emission Spectrometer hyperspectral analyses of proposed paleolake basins on Mars: No evidence for in-place carbonates. *J. Geophys. Res.* 110, E10004.
- Stolper, E., McSween, H.Y., Jr., 1979. Petrology and origin of the shergottite meteorites. *Geochim. Cosmochim. Acta* 43, 1475-1498.

- Sutton, S.R., et al., 2008. Sulfur and iron speciation in gas-rich impact-melt glasses from basaltic shergottites determined by micro-XANES, *Lunar Planet. Sci.* XXXIX, Houston, TX, p. 1961.
- Swayze, G.A., et al., 2008. Discovery of the acid-sulfate mineral alunite in Terra Sirenum, Mars, using MRO CRISM: Possible evidence for acid-saline lacustrine deposits?, AGU Fall Meeting, pp. P44A-04.
- Swindle, T.D., et al., 2000. Noble gases in iddingsite from the Lafayette meteorite: Evidence for liquid water on Mars in the last few hundred million years. *Met. Planet. Sci.* 35, 107-115.
- Szymanski, A., et al., 2010. High oxidation state during formation of Martian nakhlites. *Met. Planet. Sci.* 45, 21-31.
- Tanaka, K.L., et al., 2014. The digital global geologic map of Mars: Chronostratigraphic ages, topographic and crater morphologic characteristics, and updated resurfacing history. *Planet. Space Sci.* 95, 11-24.
- Taylor, J., McLennan, S.M., 2009. Aqueous alteration and martian bulk chemical composition, AGU Fall Meeting, pp. P12A-07.
- Thiemens, M.H., 1999. Mass-independent isotope effects in planetary atmospheres and the early solar system. *Science* 283, 341-345.
- Thiemens, M.H., Heidenreich, J.E.I., 1983. The mass-independent fractionation of oxygen: A novel isotope effect and its possible cosmochemical implications. *Science* 219, 1073-1075.
- Thode, H.G., et al., 1953. Sulphur isotope fractionation in nature and geological and biological time scales. *Geochim. Cosmochim. Acta* 3, 235-243.
- Tian, F., et al., 2010. Photochemical and climate consequences of sulfur outgassing on early Mars. *Earth Planet. Sci. Lett.* 295, 412-418.
- Toon, O.B., et al., 1980. The astronomical theory of climate change on Mars. *Icarus* 44, 552-607.
- Topcuoglu, B.D., et al., 2016. Hydrogen limitation and syntrophic growth among natural assemblages of thermophilic methanogens at deep-sea hydrothermal vents. *Front. Microbiol.* 7, 1240.
- Tosca, N.J., McLennan, S.M., 2006. Chemical divides and evaporite assemblages on Mars. *Earth Planet. Sci. Lett.* 241, 21-31.
- Tosca, N.J., et al., 2005. Geochemical modeling of evaporation processes on Mars: Insight from the sedimentary record at Meridiani Planum. *Earth Planet. Sci. Lett.* 240, 122-148.
- Toulmin, P., III, et al., 1977. Geochemical and mineralogical interpretation of the Viking inorganic chemical results. *J. Geophys. Res.* 82, 4625-4634.
- Treiman, A.H., et al., 1993. Preterrestrial aqueous alteration of the Lafayette (SNC) meteorite. *Meteoritics* 28, 86-97.

- Treiman, A.H., et al., 2016. Mineralogy, provenance, and diagenesis of a potassic basaltic sandstone on Mars: CheMin X-ray diffraction of the Windjana sample (Kimberley area, Gale Crater). *J. Geophys. Res. Planets* 121, 75-106.
- Turchyn, A.V., et al., 2016. Microbial sulfur metabolism evidenced from pore fluid isotope geochemistry at Site U1385. *Global Planet. Change* 141, 82-90.
- Ueno, Y., et al., 2009. Geological sulfur isotopes indicate elevated OCS in the Archean atmosphere, solving faint young sun paradox. *Proc. Natl. Acad. Sci.* 106, 14784-14789.
- Urey, H.C., 1947. The thermodynamic properties of isotopic substances. *J. Chem. Soc.*, 562-581.
- USGS, 2000. New Evidence Suggests Mars Has Been Cold and Dry "Red Planet" Abundant with Green Minerals. <http://speclab.cr.usgs.gov/mars.press.release.10.2000.html>.
- Usui, T., et al., 2012. Origin of water and mantle–crust interactions on Mars inferred from hydrogen isotopes and volatile element abundances of olivine-hosted melt inclusions of primitive shergottites. *Earth and Planetary Science Letters* 357-358, 119-129.
- Vaniman, D., et al., 2012. Ceramic ChemCam calibration targets on Mars Science Laboratory. *Space Sci. Rev.* 170, 229-255.
- Vaniman, D.T., et al., 2008. Salt-hydrate stabilities and Mars sample return missions, Ground Truth from Mars: Science Payoff from a Sample Return Mission. LPI, Albuquerque, pp. 103-104.
- Vaniman, D.T., et al., 2004. Magnesium sulphate salts and the history of water on Mars. *Nature* 431, 663-665.
- Vaniman, D.T., et al., 2014. Mineralogy of a mudstone at Yellowknife Bay, Gale Crater, Mars. *Science* 343.
- Vaniman, D.T., Chipera, S.J., 2006. Transformations of Mg- and Ca-sulfate hydrates in Mars regolith. *Am. Mineral.* 91, 1628-1642.
- von Paris, P., et al., 2013. N₂-associated surface warming on early Mars. *Planet. Space Sci.* 82, 149-154.
- Wacey, D., et al., 2011. Earliest microbially-mediated pyrite oxidation in ~3.4 billion-year-old sediments. *Earth Planet. Sci. Lett.* 301, 393-402.
- Wadhwa, M., 2001. Redox state of Mars' upper mantle and crust from Eu anomalies in shergottite pyroxenes. *Science* 291, 1527-1530.
- Wallace, D., Sagan, C., 1979. Evaporation of ice in planetary atmospheres: Ice-covered rivers on Mars. *Icarus* 39, 385-400.
- Wallace, P., Carmichael, I.S.E., 1992. Sulfur in basaltic magmas. *Geochim. Cosmochim. Acta* 56, 1863-1874.

- Walton, E.L., et al., 2010. Martian regolith in Elephant Moraine 79001 shock melts? Evidence from major element composition and sulfur speciation. *Geochim. Cosmochim. Acta* 74, 4829-4843.
- Wang, A., et al., 2013a. The preservation of subsurface sulfates with mid-to-high degree of hydration in equatorial regions on Mars. *Icarus* 226, 980-991.
- Wang, A., et al., 2011. Stability of Mg-sulfates at 10 deg C and the rates of dehydration/rehydration processes under conditions relevant to Mars. *J. Geophys. Res.* 116, E12006.
- Wang, A., et al., 2006a. Sulfates on Mars: A systematic Raman spectroscopic study of hydration states of magnesium sulfates. *Geochim. Cosmochim. Acta* 70, 6118-6135.
- Wang, A., et al., 2009. Phase transition pathways of the hydrates of magnesium sulfates in the temperature range 50 deg C to 5 deg C: Implication for sulfates on Mars. *J. Geophys. Res.* 114, E04010.
- Wang, A., et al., 2006b. Sulfate deposition in subsurface regolith in Gusev crater, Mars. *J. Geophys. Res.* 111, E02S17.
- Wang, A., et al., 2016. Setting constraints on the nature and origin of the two major hydrous sulfates on Mars: Monohydrated and polyhydrated sulfates. *J. Geophys. Res. Planets* 121, 678-694.
- Wang, A., Ling, Z.C., 2011. Ferric sulfates on Mars: A combined mission data analysis of salty soils at Gusev crater and laboratory experimental investigations. *J. Geophys. Res.* 116, CiteID E00F17.
- Wang, A., Zhou, Y., 2014. Experimental comparison of the pathways and rates of the dehydration of Al-, Fe-, Mg-, and Ca-sulfates under Mars relevant conditions. *Icarus* 234, 162-173.
- Wang, C., et al., 1991. Phase equilibria of liquid Fe-S-C-ternary. *ISIJ Intl.* 11, 1292-1299.
- Wang, T., et al., 2007. Dehydration of iron(II) sulfate heptahydrate. *Thermochim. Acta* 462, 89-93.
- Wang, Y., et al., 2013b. Composition of Mars constrained using geophysical observations and mineral physics modeling. *Phys. Earth Planet. Int.* 224, 68-76.
- Wang, Z., Becker, H., 2017. Chalcophile elements in Martian meteorites indicate low sulfur content in the Martian interior and a volatile element-depleted late veneer. *Earth Planet. Sci. Lett.* 463, 56-68.
- Wanke, H., 1981. Constitution of terrestrial planets. *Phil. Trans. R. Soc. Lond. A* 303, 287-302.
- Wanke, H., Dreibus, G., 1988. Chemical composition and accretion history of terrestrial planets. *Phil. Trans. R. Soc. Lond. A* 325, 545-557.

- Wanke, H., Dreibus, G., 1994. Chemistry and accretion history of Mars. *Phil. Trans.: Phys. Sci. Eng.* 349, 285-293.
- Wasson, J.T., Kallemeyn, G.W., 1988. Compositions of chondrites. *Phil. Trans. R, Soc. Lond. A* 325, 535-544.
- Wentworth, S.J., Gooding, J.L., 1994. Carbonates and sulfates in the Chassigny meteorite: Further evidence for aqueous chemistry on the SNC parent planet. *Meteoritics* 29, 860-863.
- Wentworth, S.J., Gooding, J.L., 1996. Water-based alteration of the martian meteorite, QUE 94201, by sulfate-dominated solutions, *Lunar Planet. Sci. XXVII*, p. 1421.
- Wentworth, S.J., McKay, D.S., 1999. Weathering and secondary minerals in the Nakhla meteorite, LPSC XXX, Houston, TX, p. 1946.
- Wentworth, S.J., et al., 2000. Weathering and secondary minerals in the martian meteorite Shergotty, *Lunar Planet. Sci. XXXI*, Houston, TX, p. 1888.
- Werner, S.C., 2009. The global martian volcanic evolutionary history. *Icarus* 201, 44-68.
- Wiens, R.C., et al., 2013. Pre-flight calibration and initial data processing for the ChemCam laser-induced breakdown spectroscopy instrument on the Mars Science Laboratory rover. *Spectrochim. Acta Part B* 82, 1-27.
- Wilson, L., et al., 2001. Evidence for episodicity in the magma supply to the large Tharsis volcanoes. *J. Geophys. Res. Planets* 106, 1423-1433.
- Wilson, S.A., Bish, D.L., 2011. Formation of gypsum and bassanite by cation exchange reactions in the absence of free-liquid H₂O: Implications for Mars. *J. Geophys. Res. Planets* 116, E09010.
- Wilson, S.A., Bish, D.L., 2012. Stability of Mg-sulfate minerals in the presence of smectites: Possible mineralogical controls on H₂O cycling and biomarker preservation on Mars. *Geochim. Cosmochim. Acta* 96, 120-133.
- Winter, J.D., 2001. *An Introduction to Igneous and Metamorphic Petrology*. Prentice Hall, Upper Saddle River, NJ.
- Wiseman, S.M., et al., 2010. Spectral and stratigraphic mapping of hydrated sulfate and phyllosilicate-bearing deposits in northern Sinus Meridiani, Mars. *J. Geophys. Res.* 115, E00D18.
- Woese, C.R., et al., 1991. Archaeal phylogeny - Reexamination of the phylogenetic position of *Archaeoglobidus-fulgidus* in light of certain composition-induced artifacts. *Syst. Appl. Microbiol.* 14, 364-371.
- Wong, A.-S., Atreya, S.K., 2003. Chemical markers of possible hot spots on Mars. *J. Geophys. Res.* 108.
- Wong, A.S., et al., 2005. Correction to and updated reaction in "Chemical markers of possible hot spots on Mars". *J. Geophys. Res.* 110, E10002.

- Wray, J.J., et al., 2011. Columbus crater and other possible groundwater-fed paleolakes of Terra Sirenum, Mars. *J. Geophys. Res.* 116, E01001.
- Wray, J.J., et al., 2009. Diverse aqueous environments on ancient Mars revealed in the southern highlands. *Geology* 37, 1043-1046.
- Xu, W., Parise, J.B., 2009. $(\text{H}_3\text{O})\text{Fe}(\text{SO}_4)_2$, A new phase formed by dehydrating rhomboclase, *Lunar Planet. Sci.* XL, The Woodlands, TX, p. 1816.
- Xu, W., et al., 2008. Relative humidity-induced production of ferricopiapite and rhomboclase from ferric sulfate anhydrate: X-ray diffraction studies under controlled conditions, *Lunar Planet. Sci.* XXXIX, League City, TX, p. 1391.
- Yen, A.S., et al., 2016. Cementation and aqueous alteration of a sandstone unit under acidic conditions in Gale crater, Mars, *Lunar Planet. Sci.* XLVII, The Woodlands, TX, p. 1649.
- Yen, A.S., et al., 2005. An integrated view of the chemistry and mineralogy of martian soils. *Nature* 436, 49-54.
- Yoder, C.F., et al., 2003. Fluid core size of Mars from detection of the solar tide. *Science* 300, 299-303.
- Yoder, C.F., Standish, E.M., 1997. Martian precession and rotation from Viking lander range data. *J. Geophys. Res.* 102, 4065-4080.
- Young, R.E., Schubert, G., 1974. Temperatures inside Mars: Is the core liquid or solid? *Geophys. Res. Lett.* 1, 157-160.
- Yung, Y.L., et al., 1997. CO_2 greenhouse in the early Martian atmosphere: SO_2 inhibits condensation. *Icarus* 130, 222-224.
- Zipfel, J., et al., 2000. Petrology and chemistry of the new shergottite Dar al Gani 476. *Met. Planet. Sci.* 35, 95-106.
- Zolotov, M.Y., 2003. Martian volcanic gases: Are they terrestrial-like?, *Lunar and Planetary Science XXXIV*, Houston, TX, p. 1795.
- Zolotov, M.Y., Shock, E.L., 2005. Formation of jarosite-bearing deposits through aqueous oxidation of pyrite at Meridiani Planum, Mars. *Geophys. Res. Lett.* 32.